A PROANGIOGENIC STRATEGY TO PROMOTE DIABETIC WOUND CLOSURE

LIM SHENG JIE NATALIE

(B.Eng, (Hons), NUS)

A THESIS SUBMITTED

FOR THE DEGREE OF DOCTOR OF PHILOSOPHY

DEPARTMENT OF BIOMEDICAL ENGINEERING

NATIONAL UNIVERSITY OF SINGAPORE

2016

Supervisors:
Associate Professor Michael Raghunath, Main Supervisor
Professor Casey Chan, Co-Supervisor
Assistant Professor Toh Yi-Chin, Co-Supervisor

Examiners:
Associate Professor Martin Lindsay Buist
Associate Professor Phan Toan Thang
Professor Zee Upton, Institute of Medical Biology (IMB), A*STAR

Declaration

I hereby declare that this thesis is my original work and it has been written by me in its entirety. I have duly acknowledged all the sources of information which have been used in the thesis. This thesis has also not been submitted for any degree in any university previously.

_____

Lim Sheng Jie Natalie

8th June 2017

Acknowledgements

I am eternally grateful to God & Blessed Virgin Mary for all the graces. To my advisors A/Prof. Michael Raghunath, Prof. Casey Chan, Asst Prof. Toh Yi-Chin; as well as A/Prof. Martin Buist, the Tissue Modulation Lab members and my family: I am deeply appreciative of your ceaseless encouragements and guidance through the peaks and valleys in my dissertation. For assistance in animal work, I thank Dr. Koh Jun Jia, Dr. Bibay Jan Irving Antonio and Dr. Timothy Chua Teck Chiew (Biological Resource Centre (BRC), A*STAR), Dr. Adeline Sham and Stella Chee (Department of Biomedical Engineering (BME), NUS). I am grateful to Sarah Zulkifli (Institute of Medical Biology (IMB), A*STAR) for help in image acquisition and also to the Advanced Molecular Pathology Laboratory (IMCB, A*STAR) for help in paraffin sectioning and immunostainings. For the many spontaneous and insightful discussions, I am deeply thankful for Prof. Birgitte Lane, Prof. Zee Upton, Dr. David Leavesley (IMB), Prof. Keith Harding (School of Medicine, Cardiff University), Prof. Ge-Ruowen (Dept. Biological Science, NUS), Prof. Evelyn Yim (BME), Dr. Lim Sei Hien (Singapore-MIT Alliance for Research & Technology (SMART)), Prof. Toan Thang Phan (School of Medicine, NUS), Lim Fui Ping (School of Medicine, NUS), Dr. Alvin Chua (Burns Centre, Singapore General Hospital), and Dr. Priscilla Peh (BME, NUS). This dissertation could not be completed without equipment support from BME, BRC, IMB, IMB microscopy unit, Roger Kamm's group (BioSyM SMART), NUS Tissue Engineering Program (Life Sciences Institute) and funding support from NUS research scholarship, NUS Faculty Research Committee grant and BMRC grant SPF2013/004 to Michael Raghunath.

Publications and Conferences

Publications:

1. Rashid R*, **Lim NS*,** Chee SM, Png SN, Wohland T, Raghunath M. (2014) Novel use for polyvinylpyrrolidone as a macromolecular crowder for enhance extracellular matrix deposition and cell proliferation. *Tissue Engineering Part C* Methods 20(12):994-1002

   (*** Both authors contributed equally**)

2. Peh P***, Lim NS*,** Blocki A, Chee SM, Park HC, Liao S, Chan C*, Raghunath M.* (2015). Simultaneous Delivery of Highly Diverse Bioactive Compounds from Blend Electrospun Fibers for Skin Wound Healing. Bioconjug Chem. 2015 Jul 15;26(7):1348-58

   (*** Both authors contributed equally**)

Work in this thesis is published under

3. **Lim, NS**, Sham, A., Chee, S. M. L., Chan, C. and Raghunath, M. (2016), Combination of ciclopirox olamine and sphingosine-1-phosphate as granulation enhancer in diabetic wounds. Wound Rep and Reg. doi:10.1111/wrr.12463

Conferences:

1. **Lim NS,** Lim SH, Kamm RD, Chan C, Raghunath M. *Strategy to Enhance Angiogenesis: A Prolyl Hydroxylase Inhibitor and Lysophospholipid Approach.* **Keystone Symposia: Metabolism and Angiogenesis**, 16-21 March 2014, Whistler, Canada. (Poster presentation)

2. **Lim NS,** Lim SH, Sham AW, Chee SM, Kamm RD, Chan C, Raghunath M. *Advanced Wound Care Strategy to Enhance Angiogenesis combining a Proly Hydroxylase Inhibitor with Lysophospholipid.* **UK-Singapore Skin Research Symposium,** 11-14 March 2015, Biopolis, SIngapore (Oral & Poster Presentation)

3. **Lim NS,** Lim SH, Sham AW, Chee SM, Kamm RD, Chan C, Raghunath M. *Advanced Wound Care Strategy to Enhance Angiogenesis combining a Proly Hydroxylase Inhibitor with Lysophospholipid*. **Biomedical Engineering Society (Singapore) 9th Scientific Meeting (BES9SM),** 16 May 2015, Hwa Chong Institution, Singapore. (Oral presentation, Gold award)

4. Peh P, **Lim NS**, Blocki A, Chee SM, Liao S, Chan C, Raghunath M. *Bioactive Scaffold-Stem Cell Strategy for Treatment of Acute Full Thickness Skin Wounds*. **4th Termis World Congress**, 8-11 September 2014, Boston, MA, USA (Poster Presentation)

5. **Lim NS,** Lim SH, Sham AW, Chee SM, Kamm RD, Chan C, Raghunath M. *Advanced Wound Care Strategy to Enhance Angiogenesis combining a Proly Hydroxylase Inhibitor with Lysophospholipid.* **4th Termis World Congress**, 8-11 September 2014, Boston, MA, USA (Poster Presentation)

6. **Lim NS**, Sham AW, Chee SM, Chan C, Raghunath M. *A diabetic rodent model with humanized wound contraction and wound depth variation.* **Singapore International Conference on Skin Research**, 18-21 April 2016, Biopolis, Singapore (Poster Presentation)

Table of Contents

Summary

The aim of this dissertation is to repurpose two drugs 1) antifungal ciclopirox olamine (CPX) and 2) lysophospholipid sphingosine-1-phosphate (S1P) as a proangiogenic combination to promote diabetic skin wound contraction. Contraction involves the pulling of perilesional skin into the wound to reduce wound area. Here, forces driving contraction arises from the compaction of collagen fibers in the granulation tissue and this process requires a robust angiogenesis. In diabetics, both angiogenesis and wound contraction are diminished leading to impaired wound healing. To emulate this pathology and to address it pharmacologically, I developed a wound healing model in the diabetic Zucker fatty rat and topically treated it with CPX+S1P. Using *in vitro* approaches, I demonstrated that CPX+S1P upregulates a crucial driver of angiogenesis, hypoxia-inducible factor-1, in endothelial cells. Injection of CPX+S1P into subcutaneously implanted sponges in experimental rats showed, in an additive manner, a fivefold increase in endothelial infiltration and lectin-perfused vessel length. Further, I developed a splinted diabetic rodent model to achieve low wound contraction rates that are characteristic for the healing mode of diabetic ulcers in humans. I discovered specific dorsal sites that allowed for incremental full thickness excisional wound depths from 1 mm (superficial) to 3 mm (deep). This enabled me to reduce wound contraction from 51% in superficial wounds to 8% in deep wounds. While the effects of topical gel treatment of CPX+S1P were masked by the rodent-characteristic dominant contraction in superficial wounds, they became clearly evident in deep diabetic wounds. Here, a fivefold increase of functional large vessels resulted in

accelerated granulation tissue formulation, accompanied by a 40% increase of compacted thick collagen fibres. This was associated with substantially reduced matrix metalloproteinase-3 and -13 expression. These findings translated into a fivefold increase in granulation-driven contraction, promoting diabetic wound closure. With CPX and S1P analogues already in clinical use, their combination presents an attractive proangiogenic treatment to be repurposed to promote healing of diabetic wounds.

List of Abbreviations

2-OG	2-Oxoglutarate
α-SMA	Alpha smooth muscle actin
AGEs	Advanced glycation end products
ANG	Angiopoietin
APMA	Aminophenylmercuric Acetate
ATP	Adenosine triphosphate
ATPase	Adenosine triphosphatase
bFGF	Basic fibroblast growth factor
bHLH	Basic helix-loop-helix
CAD	C-terminal transactivation domain
CBP	CREB-binding protein
c-MET	Hepatocyte growth factor receptor
CPX	Ciclopirox Olamine
CPX+S1P	Combination of Ciclopirox Olamine and Sphingosine-1-phosphate
DCCT	Diabetes complications and control trial
DLL	Delta-like 4
ECs	Endothelial cells
ECM	Extracellular matrix
EGF	Epidermal growth factor
EGM	Endothelial growth factor media-2
eNOS	Endothelial nitric oxide synthase
FIH	Factor inhibiting HIF-1
FITC	Fluorescein isothiocyanate
FDA	Food and Drug Administration
HBO	Hyperbaric oxygen therapy
HIF-1	Hypoxia-inducible factor-1
HIF-1α	Hypoxia-inducible factor-1 alpha
HRE	Hypoxia responsive elements
HUVECs	Human umbilical vein endothelial cells
IGF	Insulin-like growth factors

Km	Michaelis constant
micro-CT	Microcomputed tomography
MMP	Matrix metalloproteinase
mTOR	Mechanistic target of rapamycin
NF-κB	Nuclear factor kappa-light-chain-enhancer of activated B cells
NPWT	Negative pressure wound therapy
ODD	Oxygen-dependent degradation
p42/44 MAPK	p42/44 mitogen-activated protein kinase
PAS	PER(Period circadian protein)-ARNT(aryl hydrocarbon receptor nuclear translocator protein) – SIM(single-minded protein)
PDGF-BB	Platelet derived growth factor BB
PHD	Prolyl-4-hydroxylases
pO_2	Partial pressure of oxygen
PVA	Polyvinyl alcohol
pVHL	von Hippel Lindau protein
ROS	Reactive oxygen species
RECA-1	Rat endothelial cell antigen-1
S1P	Sphingosine-1-phosphate
S.C.	Subcutaneous
TGF- β	Transforming growth factor-β(1)
TUNEL	Terminal deoxynucleotidyl transferase dUTP nick end labeling
USH	Ultrasound Healing therapy
VEGF	Vascular endothelial growth factor
ZDF	Zucker Diabetic Fatty

List of Figures

List of Tables

Chapter 1

Research Strategy

1.1 Goal: Accelerate diabetic wound closure

Diabetes (Diabetes mellitus) is a metabolic syndrome characterized by a chronic elevation of blood glucose levels, rising beyond 130 mg/dL after 8 hours of fasting [1]. This metabolic syndrome arises from defects in insulin action, insulin secretion from pancreatic beta cells or both [2]. Since the early 1960s, diabetes has been well established to impair skin wound closure [3-5]. Prolonged impairment in wound closure (i.e., ulcer) is an avenue for infection leading to cellulitis, myositis, abscesses, necrotizing fasciitis, septic arthritis, tendinitis, and osteomyelitis [8]. Consequently, foot ulcers are a major risk factor for diabetes-related amputations [9,10],with a lower leg lost to diabetes globally every 20 seconds [11]. As the prevalence of diabetes is set to increase globally from 8.3% of the population in 2013 to 9.9% by 2030, diabetes-related amputations are predicted to rise [11]. Unfortunately, a simple normalization of blood glucose levels alone is insufficient to reverse the long-term side effects of diabetes including impaired skin wound closure [6,7]. Thus the goal of this study is to develop an adjuvant therapy to accelerate diabetic wound closure.

1.2 Focus: Increase wound contraction

Wound closure depends on two mechanisms: (1) re-epithelialization and (2) contraction [12]. Re-epithelialization refers to the migration of epidermal cells to cover the denuded epithelial area [28]. Contraction reduces the area needed for re-epithelialization by pulling perilesional skin into the wound (§2.1). While being

aware that both mechanisms are impaired in chronic wounds [13,28], I have chosen to focus on promoting contraction under diabetes.

The contribution of contraction to wound closure depends on regional human anatomy. It ranges from 21% on the forearm [14,15] to 90% in regions with less tight fastening to underlying structures such as the trunk or perineum [16]. In humans, wound contraction is principally driven by the compaction of collagen fibers in the granulation tissue [17]. This process crucially depends on a robust formation of new blood vessels (angiogenesis) in the granulation tissue. Angiogenesis accounts for up to 60% of the granulation tissue mass [18], with vessel densities exceeding that of uninjured tissues by more than 3-fold [19]. This initially overshooting angiogenesis ensures cellular traffic, delivery of nutrients and oxygen required for collagen synthesis and maturation, and also aerobic respiration to generate ATP to drive the contraction and compaction of collagen fibers by fibroblasts.

Diabetic wounds typically exhibit a low angiogenic response [2]. This in part explains their impaired granulation tissue formation and consequently impaired wound contraction [13,20]. Thus to accelerate granulation formation and contraction, I developed a proangiogenic drug strategy.

1.3 Proangiogenic Drug Strategy: CPX+S1P

To develop a proangiogenic strategy (Figure 1.1), I first identified major inhibitors of angiogenesis in diabetic wounds (§2.4). These are:

(i) high reactive oxygen species (ROS) levels;

(ii) high advanced glycation end products (AGEs) levels;

(iii) low hypoxia-inducible factor 1 (HIF-1) activity;

(iv) high matrix metalloproteinase (MMP) levels; and

(v) low sphingosine-1-phosphate (S1P) levels.

To overcome these angiogenic inhibitiors, a review of the literature suggests a combination of divalent metal chelators and S1P supplementation might hold promise (§2.4). In addition, a laboratory colleague Lim Sei Hien, recently discovered that ciclopirox olamine (CPX), a divalent metal chelator, in combination with S1P (CPX+S1P) synergistically increases endothelial sprouting *in vitro* (§2.6.2) [21]. Both drugs are also clinically available. CPX is a FDA-approved topical anti-fungal agent while S1P's analogue is FDA-approved as an oral treatment for multiple sclerosis. Here drug repurposing and drug synergy is an attractive translational strategy for diabetic wound treatment.

1.4 Formulating hypotheses

To date, it remains unknown if CPX+S1P is able to:

(i) hyperinduce the angiogenic master regulator, hypoxia inducible factor (HIF-1) (§2.3.4);

(ii) potentiate angiogenesis *in vivo*; or

(iii) increase diabetic wound contraction.

Accordingly, I formulated three hypotheses (§2.7); namely:

(1) CPX+S1P potentiates HIF-1 activity *in vitro;*

(2) CPX+S1P potentiates angiogenesis *in vivo;* and

(3) CPX+S1P increases diabetic wound contraction.

1.4.1 Methodology to test Hypothesis 1

To assess if CPX+S1P potentiates HIF-1 activity *in vitro* (§3.1), I assessed the protein expression of **(i) HIF-1 upstream regulators** (HIF-1α, phosphorylated p42/44 MAPK) and **(ii) HIF-1 downstream targets** (VEGF, c-MET, eNOS) in monolayer culture of human endothelial cells. Their protein expression were compared among mono and combinatory treatments of CPX and S1P.

1.4.2 Methodology to test Hypothesis 2

To assess if CPX+S1P potentiates angiogenesis *in vivo* (§3.2), I adopted a well-established subcutaneous rodent sponge implantation model and intradermally injected the drugs into the sponge over 2 weeks. Thereafter I assessed **(i) endothelial infiltration** and **(ii) functional vessel length** in the sponge. These effects were compared among mono and combinatory treatments of CPX and S1P.

1.4.3 Methodology to test Hypothesis 3

To assess if CPX+S1P increases diabetic wound contraction, I develop a full-thickness skin excision diabetic rodent model that exhibits low skin wound contraction (§3.3, Figure 1.1). Rodents unlike humans have an innate ability for extensive wound contraction due to the presence of a subcutaneous *panniculus carnosus* muscle and loose attachment of the dermis, making the skin extremely mobile. This limits the options to assess pharmacological treatments to improve granulation-driven wound contraction as in human skin. To develop a low contraction wound model, I exploited the presence of a dorsal fat pad in the Zucker diabetic fatty rat which allows for wound depth increment from ~1 mm (superficial wound) to ~3 mm (deep wound). This approach was combined with two existing humanized contraction techniques i.e., wound edge splinting and excision of *panniculus carnosus*. CPX+S1P was then topically delivered to superficial and deep wounds in a carboxymethylcellulose gel every alternate day over a month. Thereafter I assessed the following parameters against the placebo gel treatment:

(i) wound closure and contraction;

(ii) collagen deposition and collagen fiber thickness;

(iii) MMP-3 and MMP-13 protein expression;

(iv) functional vessel density and size; and

(v) myofibroblast presence (α-SMA protein expression).

1.5 Research Strategy Flowchart

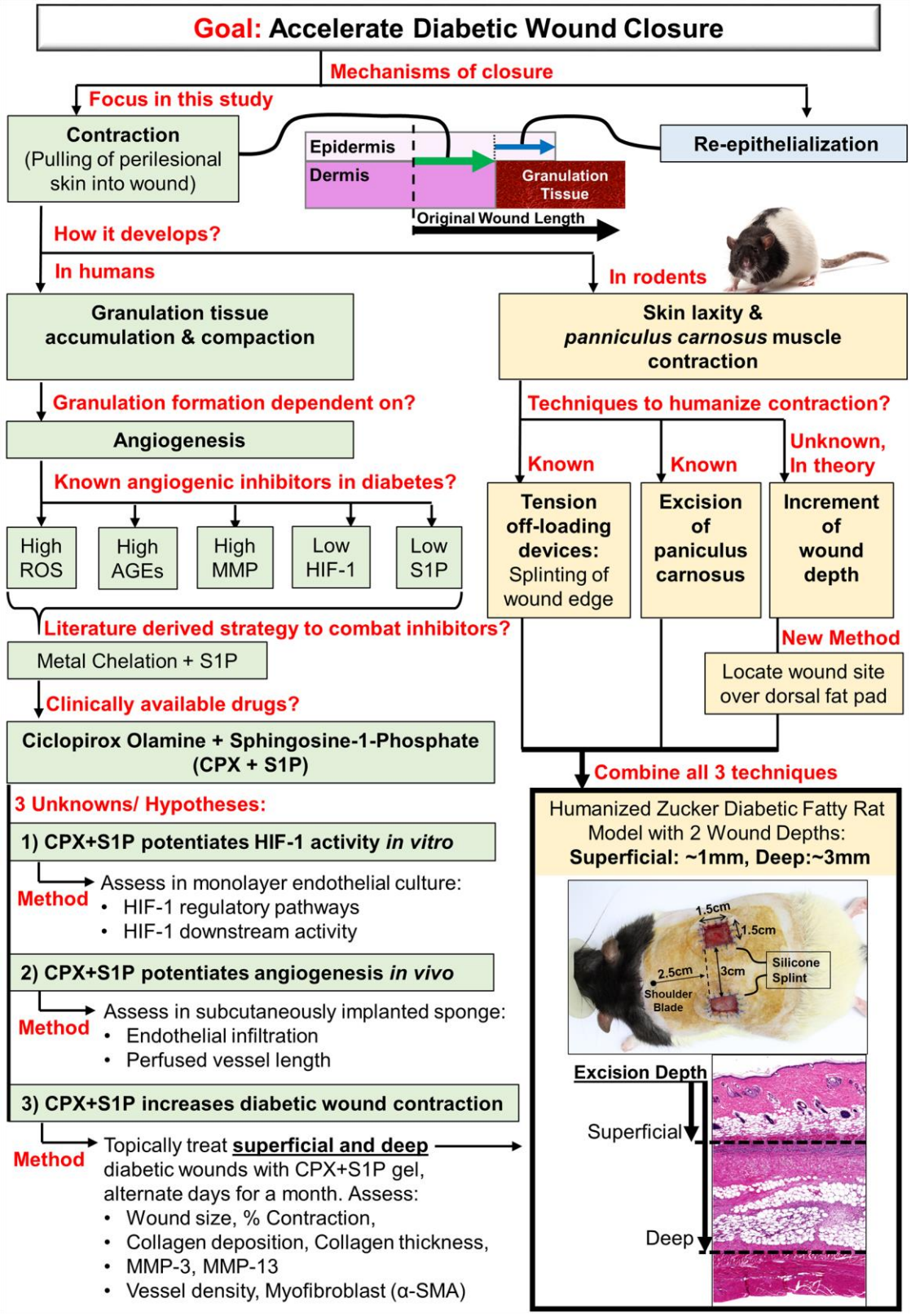

Figure 1.1 Research strategy flowchart.

Chapter 2

Literature Review

2.1 Wound closure mechanisms

2.1.1 Basic structure of skin

Skin, in the strictest sense, refers to the layer of epidermis and dermis [22], but at times, the layer of subcutaneous fat directly attached to the dermis has also been considered to be a component of skin [22] (Figure 2.1). The outermost layer of skin is the epidermis. It is thin and avascular, being made up of four main layers of keratin producing cells called keratinocytes [23]. The epidermis is separated from the underlying dermis by the dermal epidermal junction also known as the basement membrane. At this junction, the downward rete ridges from the epidermis interlocks with the upward ridges from the dermis anchoring the epidermis to the dermis, preventing their sliding motion [23].

The thickest layer of the skin is the dermis. Its thickness ranges from 2 mm to 4 mm in humans, being anatomically site dependent [23]. Unlike the epidermis, the dermis comprises mainly of extracellular matrix (ECM) and is sparsely populated by cells. The primary cell type in the dermis is the fibroblast, which synthesises and remodels the major dermal ECM components: collagen types I and III (which occur in a proportion of 4:1) and elastin [24]. The dermis is further subdivided into two layers, the papillary dermis and the reticular dermis. The papillary dermis is thin and highly vascular, having finger-like projections into the epidermis [23]. The reticular dermis is thick, comprising of 80% of the dermis. Here sweat glands, nerves, hair follicles and blood vessels are surrounded by collagen bundles. Collagen is the major structural protein in skin, forming 75%

of the skin's total dry weight. It gives the skin its tensile strength and anchors the skin to the subcutaneous tissue beneath [23].

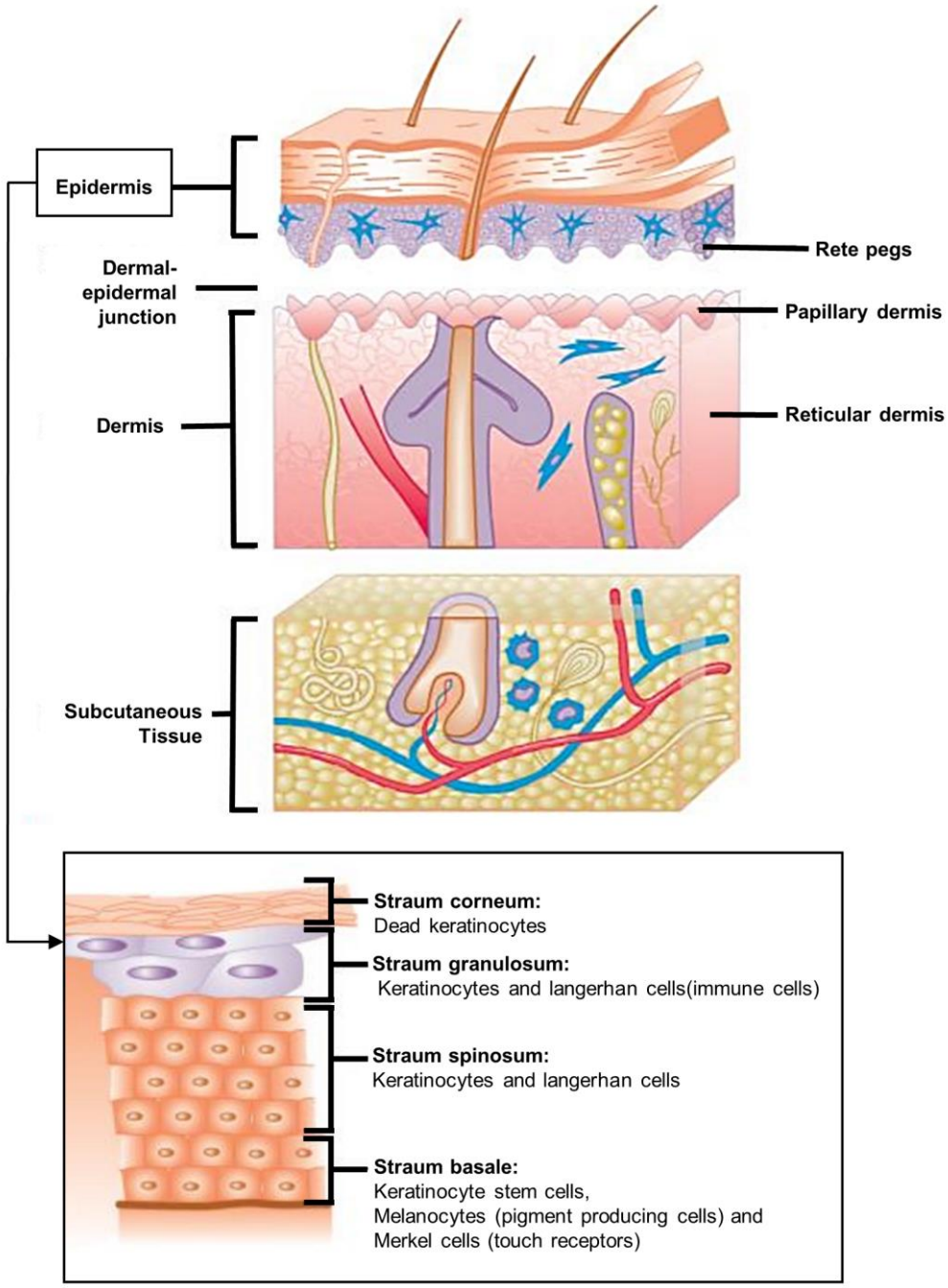

Figure 2.1 The basic structure of skin. (*Figure adapted from Baranoski S. (2010)* [23]*. Copyright © 2010 F.A. Davis. Note: Names of epidermal cell types were added to F.A. Davis's figure)*

2.1.2 Full-thickness wound closure mechanisms

Full-thickness wounds, such as diabetic foot ulcers [25], involve the destruction of both the epidermis and the dermis layers. At times, full-thickness wounds extend to the destruction of underlying subcutaneous fat and connective tissue [12]. This is in contrast to a partial-thickness wound, wherein the tissue destruction extends into but not through the dermis. Full-thickness wound closure can be macroscopically identified by the disappearance of light-reflecting new stroma that fills the wound bed (i.e., granulation tissue), and the replacement of a non-reflecting fully epithelialized surface (Figure 2.2) [15]. This process occurs through through two mechanisms: **(i) re-epithelialization** and **(ii) contraction** [15] (Figure 2.2).

As this dissertation focuses on developing an adjuvant therapy that accelerates contraction in diabetic full-thickness skin wounds, I will briefly introduce re-epithelialization and then delve into the development of wound contraction.

Re-epithelialization involves a lateral migration of epithelial cells, mainly keratinocytes, to resurface the wound. In a non-chronic wound, this process usually begins within 24 hours after injury and can be identified by the thickening of epidermis immediately adjacent to the wound edge [24]. Here keratinocytes at the wound edge lose their firm attachment to the underlying dermis, and begin to migrate laterally across the wound while fixed keratinocytes near the wound edge proliferate rapidly and appear to migrate by moving over one another in a leapfrog fashion until the defect is bridged [26,27]. For a detailed review on

reepithelialisation mechanism, I refer the reader to a comprehensive review by Pastar et al. (2014) [28].

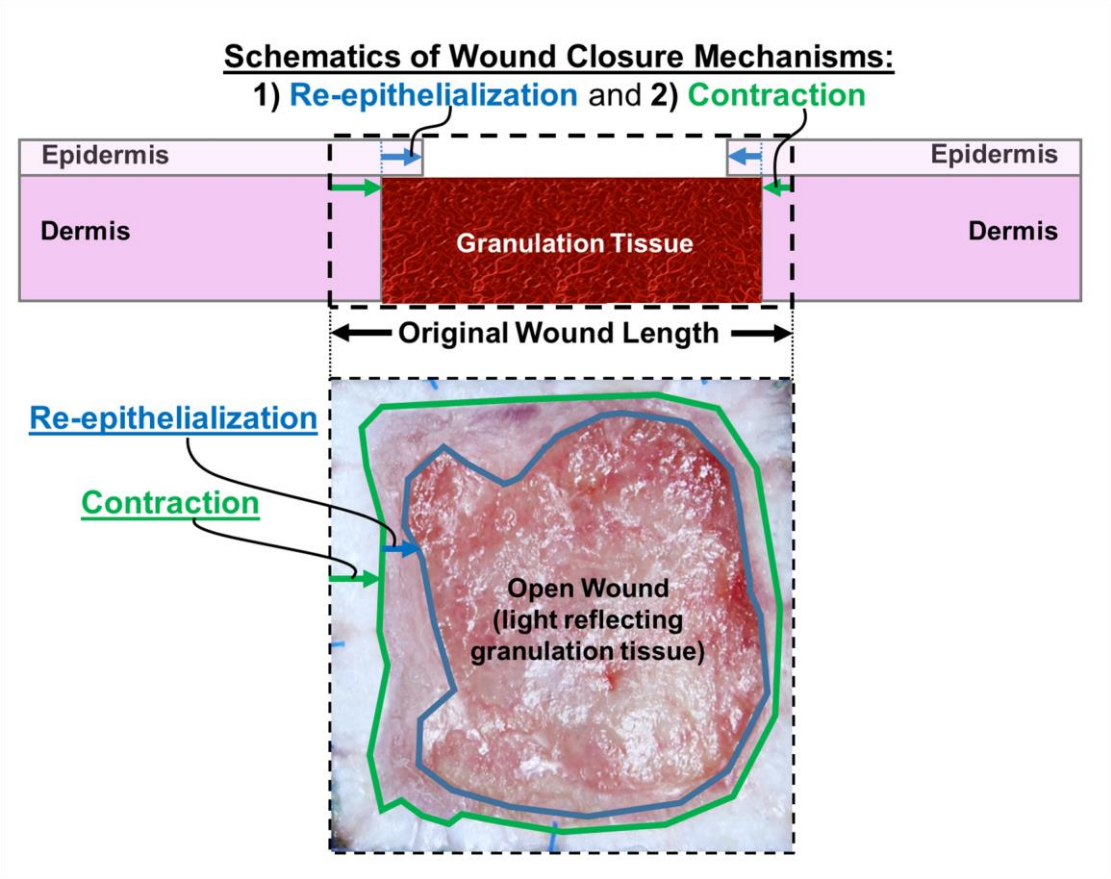

Figure 2.2 Full-thickness skin wound closure mechanisms. Cross-section schematics (top) and macroscopic plan view (bottom) of wound closure. Blue line in macroscopic image denotes the re-epithelialized front and the green line denotes the contraction front.

Contraction, on the other hand, refers to the pulling of perilesional skin towards the centre of the wound (Figure 2.2) [15]**.** In humans, contraction develops as collagen fibers in the granulation tissue is compacted generating a force that pulls the perilesional skin into the wound [17]. Wound contraction can be distinctly observed approximately 4 days post-injury and is usually complete by 12-15 days after wounding [29-31]. It contributes to ~21% to 37% of wound closure area in the adult human forearm [14,15,32], increasing to ~90% in the

trunk and perineum regions where skin is not tightly bound down to underlying structures [16]. Contraction is undesirable when it results in scar “contracture” which pulls deeper tissues, not only skin, toward the injury site, deforming facial features and limiting the excursion of joints. Nonetheless, contraction plays a crucial role in full-thickness skin wounds wherein a large amount of tissue is destroyed, leaving a gap which cannot be approximated [12]. Contraction also aids in reducing the area for re-epithelization [33].

2.2 Development of wound contraction

Wound contraction is widely accepted to occur during granulation tissue development, requiring [34,35]:

(i) fibroblast infiltration and proliferation,

(ii) collagen synthesis and deposition,

(iii) myofibroblast contractile forces, and

(iv) fibroblast tractional forces.

Importantly, these events are intimately supported by a robust development of blood vessels (angiogenesis) in the granulation tissue.

2.2.1 Angiogenesis in granulation tissue

The granulation tissue begins to form approximately 3 days post-injury [36]. It consists of cellular elements including fibroblasts, inflammatory cells, along with abundant new capillaries embedded in a loose extracellular matrix of mainly

fibrous collagen (type I, III and IV) enriched in proteoglycans, glycosaminoglycans, and noncollagenous proteins [24]. Here neovessels account for ~60% of the early granulation mass [18] with vessel density exceeding that of uninjured tissues by more than 3-fold [19]. The delivery of oxygenated blood gives newly formed translucent granulation tissue its bright red colour, which is a predictive index for the subsequent healing of chronic wounds [37-40]. As 98% of wound oxygen is consumed by neutrophils to kill bacteria [41], the initially overshooting angiogenesis ensures the delivery of oxygen and cellular traffic, required for collagen synthesis and maturation, and also aerobic respiration to generate ATP which powers the mechanobiological activity of fibroblasts during contraction and compaction of collagen fibers.

2.2.2 Fibroblast infiltration and proliferation

With the concurrent increase in angiogenesis, fibroblasts begin to accumulate in the granulation tissue, accounting for ~30 to 40% of the early wound cells [42]. Fibroblasts are typically identified by their spindle-like morphology and a positive expression of vimentin, an intermediate filament in mesenchymal cells [43]. Fibroblasts not only originate from resident fibroblasts in the adjacent non-wounded dermis [44,45], but also arises from blood vessels. This was first observed by Geoffrey Hadfield (1963) in granulation tissue of rodent wounds ~3 days post-wounding. Here vessels were seen widely dilated, with fibroblastic cells in the perivascular sheaths leaving the vascular plexus and migrating into the wound stroma [46]. Subsequent studies identified that these fibroblast-like cells are pericytes, fibrocytes, adventitial cells and bone marrow mesenchymal

stem cells [47,48]. These fibroblasts of heterogenous origins rapidly proliferate in the presence of growth factors and cytokines secreted by platelets, macrophages, lymphocytes and endothelial cells (ECs) [44]. The activity of many of these growth factors e.g. platelet-derived growth factor (PDGF), Insulin growth factor 1 (IGF-1), transforming growth factor beta 1 (TGF- β1) rely on redox-signaling [49,50] which is supported by an oxygenated blood supply.

2.2.3 Collagen synthesis and deposition by fibroblasts

In early granulation tissues, fibroblasts synthesise fine and randomly oriented collagen type III fibrils, increasing the synthesis of collagen type I fibrils as the granulation tissue matures [24]. Importantly, the conditions for collagen synthesis and maturation can only proceed if oxygen is available to be incorporated into the structure of nascent collagen by the enzymes prolyl 4-hydroxylase, lysyl hyroxylase and lysyl oxidase [51]. During collagen synthesis, prolyl hydroxylase inserts an oxygen atom into selected prolines of procollagen peptides, converting them to hydroxyprolines. This allows for collagen to be exported extracellularly. Thereafter lysyl hyroxylases hydroxylate lysines in the collagen molecule to cross-link collagen monomers into collagen fibrils. Lysines that become stable covalent links in the collagen structure are further condensed by lysyl oxidases to polymerize collagen.

With oxygen-dependent enzymes required for collagen synthesis and maturation, it is thus not surprising that the rate of collagen deposition is proportional to the wound oxygen tension (pO_2) [52]. Here collagen deposition

is 0 when $pO_2 = 0$, at half-maximal when $pO_2 = 25$ mmHg and at maximal velocity when pO_2 exceeds 200 mmHg [51]. In ischemic diabetic wounds, pO_2 ranges only beween 4 to 11 mmHg [53], correlating to the sparse collagen deposition in the wound [54]. As such, the intially overshooting angiogenesis is critical to support collagen deposition in the granulation tissue.

2.2.4 Differentiation of fibroblasts into myofibroblasts

Approximately 5 days post-wounding, fibroblasts begin to develop a contractile phenotype by differentiating into smooth muscle-like fibroblasts called myofibroblasts [55], reaching a maximal density between day 16 and day 31 [56]. The contribution of myofibroblasts to contraction was first discovered by Gabbiani and colleagues in 1971 [57]. They were found to differentiate upon exposure to transforming growth factor-β(1) (TGF-β) or a high matrix elastic modulus beyond ~20,000Pa [55,58]. Interestingly, proliferating ECs support this differentiation by secreting connective tissue growth factor [35,59,60] which activate the downstream TGF-β effect in fibroblasts [61-64].

Compared to fibroblasts, myofibroblasts have a more extensive network of cytoplasmic stress fibers with large focal adhesion sites [65]. These cytoplasmic stress fibers are made up of microfilaments; actin and myosin II, wherein the predominant actin form is α-smooth muscle actin (α-SMA). α-SMA is frequently used to discriminate myofibroblasts from fibroblasts; and has been found *in vitro* to confer a 2-fold increase in cell contractility compared to α-SMA negative fibroblasts [35]. Interestingly, a recent study by James Tomasek's group have

also indicated that the α-SMA negative fibroblasts can also upregulate other muscle actin isoforms to increase their contractile ability upon exposure to TGF-β [66].

Importantly, the sliding action of actin–myosin filaments is crucial in generating tension in collagen fibrils [35]. Myofibroblasts can adopt a combination of i) strong and far-ranging isometric contractions to shorten the fibril, and also ii) weak but repetitive subcellular contractions to straighten out the slack region of the fibrils [67]. These locally contracted fibrils can be proteolytically processed and/or stabilised by addition of new extracellular matrix (ECM) and crosslinks [67]. Once remodelled, the fibres can again bear mechanical load and myofiroblast are able to re-spread. This ultimately results in stabilised granulation matrix contraction, which is in contrast to the reversible and short-lived contraction of striated smooth muscles [17].

To a great degree, this cellular contractile event is supported by a robust delivery of oxygenated blood supply. Aerobic cellular respiration generates abundant adenosine triphosphate (ATP) needed for sustained myosin ATPase (adenosine triphosphatase) activity [17]. As such, the lack of oxygen was demonstrated by Boris Hinz's group to result in the reversible disassembly of α-SMA from stress fibers [68], compromising the contractile activity of myofibroblast.

2.2.5 Fibroblast tractional forces

Another mechanism by which the granulation matrix is condensed is through fibroblast tractional forces [17]. Here tractional forces are likened to that of a moving thread on the military tank; whereby collagen sites attached to the surface of the fibroblast are pulled over that surface [69]. This tractional force is driven by the oxygen-dependent rapid sliding and relaxation of actin-myosin cytoskeleton microfilaments [17]. Here, fibroblasts do not buckle/contract. Instead, they adopt an elongated shape to minimize flexibility in order to translocate collagen fibrils [70]. As the collagen fibrils are rapidly translocated over the cell surface, they come into contact with other collagen fibrils and self-assemble into an ordered cross-striated structure. The aforementioned oxygen-dependent enzyme, lysyl oxidase, then progressively compacts collagen fibers by eliminating water between fibrils [17].

2.2.6 Wound contraction terminates

The concerted events of

i) fibroblast infiltration and proliferation,
ii) collagen synthesis and deposition,
iii) myofibroblast contractile forces, and
iv) fibroblast tractional forces,

result in the compaction of granulation matrix. This provides a driving force that pulls the perilesional skin into the centre of the wound (contraction). It is thus presumed that wound contraction terminates with a reduced effectiveness of

forces generated by (myo)fibroblasts [71]. Here the increasing collagen interconnectivity and fibril stability, renders collagen translocation less susceptible by the fibroblast [70]. Also as angiogenesis decreases in mature granulation tissues, the population of fibroblasts and myofibroblasts decreases by apoptosis [70,72]. Ultimately, the granulation tissue is replaced by a collagen-rich scar tissue wherein collagen fibers are spatially oriented in the axis of (myo)fibroblasts (along which mechanical force develops).

Having understood that angiognesis is crucial in wound contraction, but yet impaired in diabetes; it follows then that a proangiogenic strategy would be required to accelerate diabetic wound contraction.

2.3 Process of sprouting angiogenesis

2.3.1 Basic structure of blood vessels

Angiogenesis refers to the blood vessel outgrowth from pre-existing ones. The smallest blood vessels are known as capillaries. Capillaries consist of a single layer of cells called endothelial cells (ECs) which are in direct contact with blood. ECs are connected to another EC via tight junctions. This junction regulates paracellular permeability [73]. Surrounding the ECs are mural cells such as vascular pericytes which provide vascular stability [74] (Figure 2.3). ECs together with mural cells synthesize extracellular matrix (ECM) such fibronectin, collagen IV and laminin to create a surrounding basement membrane needed

for structural and organizational stability [75]. Larger vessels have additional muscular layers constituting the vessel wall, such as the tunica media, and an outer connective tissue layer called the tunica adventitia containing nerves to regulate the vascular tone [76].

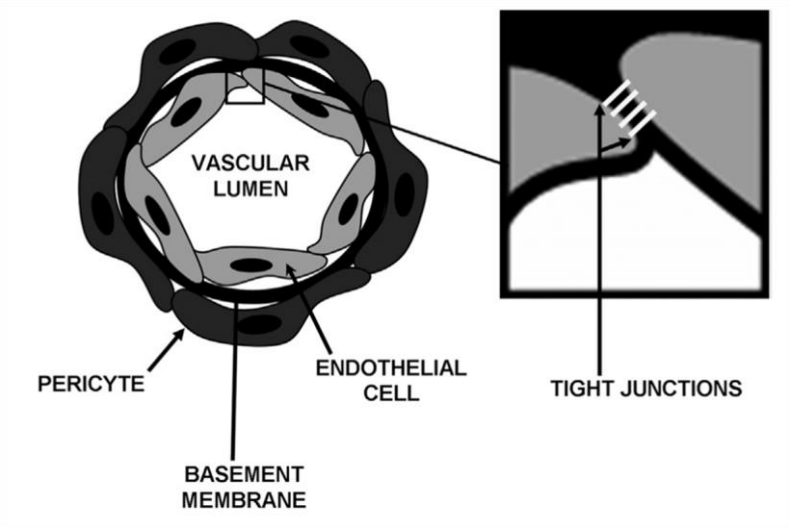

Figure 2.3 Structure of capillary. *(Figure reprinted from Garcia-Mendina et al. (2014)* with permission [74]*. Copyright © 2014 Elsevier.)*

2.3.2 Sprouting versus splitting angiogenesis

There are two processes of vessel outgrowth from a pre-existing vessel: 1) splitting or 2) sprouting [77]. Sprouting has been far better understood, being first described by Ausprunk and Folkman in 1977 [78], while splitting was discovered more than a decade later by Burri and Tarak in 1990 [79]. Sprouting angiogenesis, as the name implies, is characterized by sprouts of ECs which grow towards an angiogenic stimulus. Sprouting angiogenesis can therefore add blood vessels to portions of tissues previously devoid of blood vessels [77].

Splitting angiogenesis, on the other hand, occurs when opposing vessel walls cave into the lumen of a capillary and establish a zone of contact called transcapillary pillars (Figure 2.4). Mural cells invade these pillars and lay down collagen fibers to increase the girth of the pillars. This results in a further increase in capillaries from an existing capillary bed, without a corresponding increase in the number of endothelial cells [80]. The control of its process still remains poorly understood as laborious methods are required to prove the presence of splitting, which involve determining the frequency of tissue pillars from scanning electron micrographs of vascular casts [77].

Figure 2.4 Sequence of events in splitting angiogenesis. (*Figure reprinted from Djonov et al. (2003)* with permission [81]*. Copyright © 2003 Springer-Verlag.)*

In the context of full-thickness skin wounds, the vascular network in the dermis and subcutaneous tissue is lost. As such the sprouting process plays a more relevant role as pre-existing vessels may not be present within the wound site. The following section thus reviews the sprouting process.

2.3.3 Overview of sprouting angiogenesis

Sprouting angiogenesis occurs typically in response to hypoxia. It occurs via a fixed sequence of events [82,83] (Figure 2.5):

(i) Selection of sprouting ECs

(ii) Sprout outgrowth and guidance

(iii) Sprout fusion and lumen formation, and

(iv) Perfusion and maturation

2.3.4 Tissue hypoxia drives sprouting

Under normoxia blood vessels are maintained in a quiescent state, controlled by a fine balance of pro-angiogenic and anti-angiogenic signals. However when a tissue becomes hypoxic (i.e., typically below venous pO_2 (40 mmHg or ~6%) [84]), cells within the tissue secrete angiogenic cytokines such as VEGF, tipping the balance in favor of angiogenesis. In granulation tissues hypoxia occurs approximately 2 to 4 days post-wounding [84,85]. Hypoxia was first discovered by Remensnyder et al. in 1968 to correlate strongly with the level of angiogenesis in wounded tissues of the cremaster muscle of rats [85]. Depending on the magnitude of hypoxia, cells can either undergo cell death or induce an adaptive survival response through the activation of the master regulator of oxygen homeostasis, transcriptional factor hypoxia-inducible factor-1 (HIF-1). As HIF-1 activity is central to the development of angiogenesis, the following section is thus dedicated to its explanation in full detail.

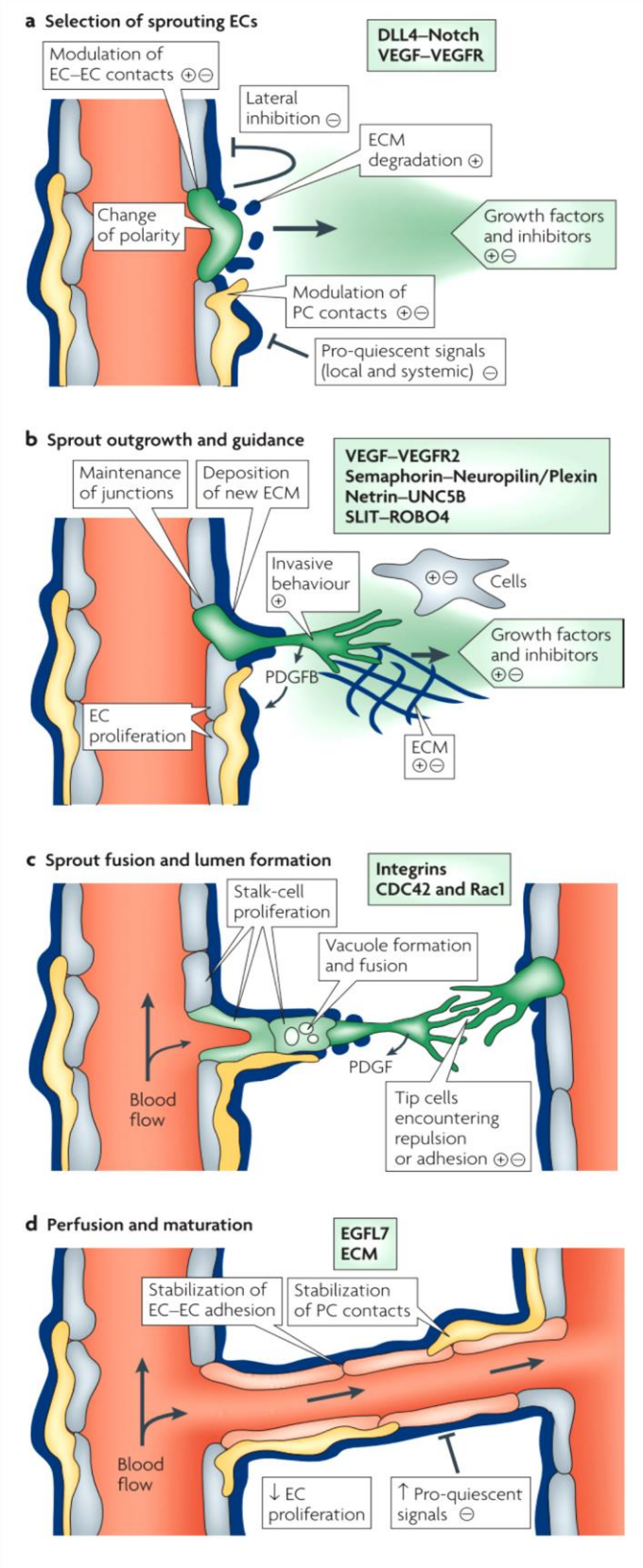

Figure 2.5 Sequence of events in sprouting angiogenesis. (Reprinted from Adam et al. (2007) with permission [82]. Copyright © 2007 Nature Publishing Group.

2.3.4.1 HIF-1 structure and function

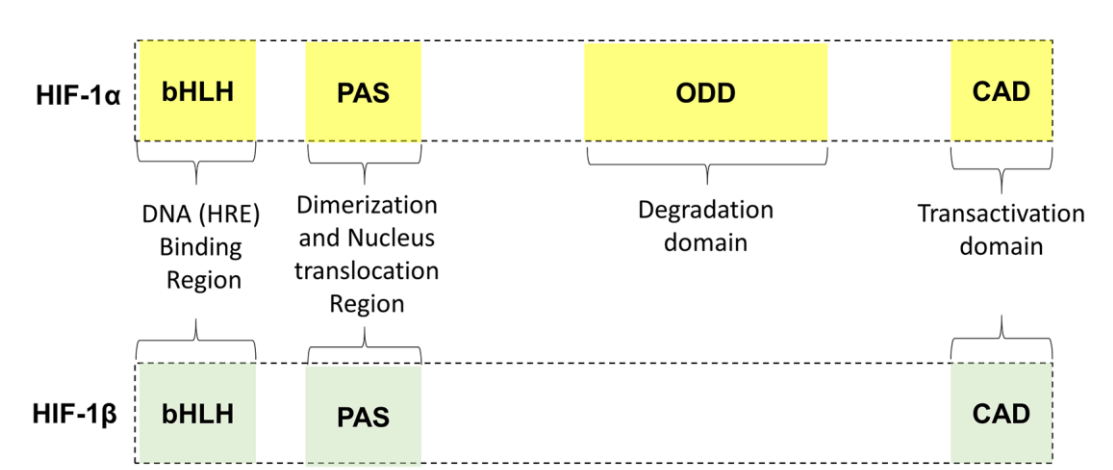

Figure 2.6 Basic structure of HIF-1

The transcriptional factor HIF-1 was first identified by Semenza and Wang in 1992 [86]. It is found ubiquitously expressed in mammalian cells, existing as a heteroduplex with an alpha subunit and a beta subunit [87]. The beta subunit is usually present in excess, while the alpha subunit is the limiting factor in the creation of a functional dimer [88].

The N-terminus of the HIF-1α and HIF-1β polypeptide contains a basic helix-loop-helix domain (bHLH) and a PER-ARNT-SIM domain (PAS) (Figure 2.6). Here the bHLH domain binds to specific DNA sequences (5'-RCGTG-3') called Hypoxia Responsive Elements (HRE) [89]. The PAS domain, on the other hand, is involved in the heterodimerization of the alpha and beta subunits; and also their translocation into the nucleus [90,91].

Both HIF-1α and HIF-1β polypeptides also contain a C-terminal transactivation domain (CAD). CAD recruits HIF-1's transcriptional co-activators, CREB-

binding protein (CBP) and p300. Importantly, this recruitment regulated by the enzyme Factor Inhbiting HIF-1 (FIH) [92]. The HIF-1α polypeptide in particular, contains an additional oxygen-dependent degradation (ODD) domain. This domain, regulated by a class of enzymes: prolyl-4-hydroxylases (PHD), determines the degradation of HIF-1α [93].

Both PHD and FIH enzymes are highly sensitive oxygen sensors [94], with an oxygen affinity (Km :90 - 250μM) lower than that of oxygen tensions in tissues [95]. Here the activity of PHD and FIH is mainly governed by 3 cofactors [96]:
(i) dioxygen (O_2),
(ii) 2-oxoglutarate (2-OG; a citric acid cycle intermediate), and
(iii) ferrous iron (Fe^{2+}).

When all 3 cofactors are present under normoxia, PHD and FIH actively repress HIF-1 activation (Figure 2.7). PHD hydroxylates the ODD domain, enabling the von Hippel Lindau protein (pVHL) to bind to HIF-1α thus ubiquitinating it. This results in its proteasomal degradation. Concurrently, FIH hydroxylates the CAD domain to prevent the recruitment of transcriptional co-activators CBP-p300. This inhibits HIF-1 transcription.

Under hypoxia or in the absence of any cofactor, PHD and FIH are inactive and thus do not repress HIF-1 activity (Figure 2.7). The unhydroxylated ODD domain allows HIF-1α to escape proteolysis and accumulate in the cytoplasm. The stable HIF-1α then translocates into the nucleus, dimerizing with HIF-1β to forming the HIF-1 heterodimer. The unhydroxylated CAD domains of HIF-1

allows for transcriptional co-activators CBP/p300 to be recruited [97]. This HIF-1 heterodimer complex then binds to HRE, upregulating the transcription of numerous HIF-1 target genes related to angiogenesis, vasomotor regulation, growth and apoptosis, migration, energy metabolism, matrix function, hormonal regulation and transcriptional regulation [98,99].

In endothelial cells (ECs), HIF-1 activation upregulates approximately 245 gene probes with at least a 1.5 fold increase; and it also concurrently downregulates 325 gene probes by at least 1.5 fold [100]. Figure 2.8 provides an overview of some of the well-known HIF-1 target genes upregulated in ECs [100,101]. Among the various HIF-1 angiogenic targets, vascular endothelial growth factor-A (VEGF-A) has been the indisputable angiogenic stimulant for the selection of sprouting ECs.

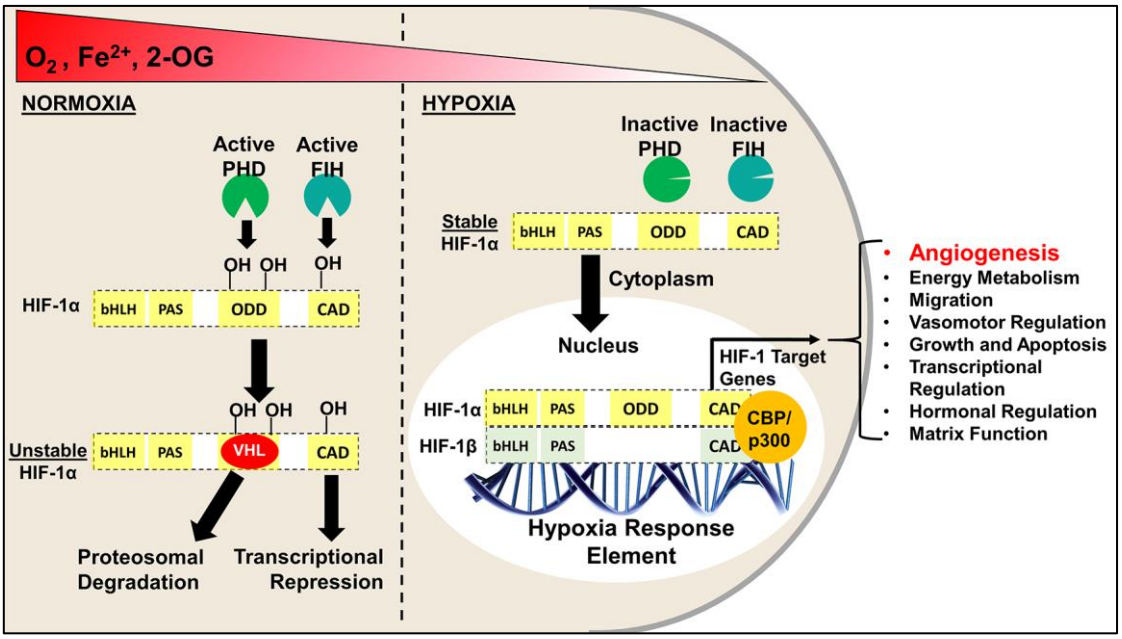

Figure 2.7 Intracellular pathways involved in the oxygen dependent regulation of HIF-1α and the transcription of HIF-1 target genes in a cell.

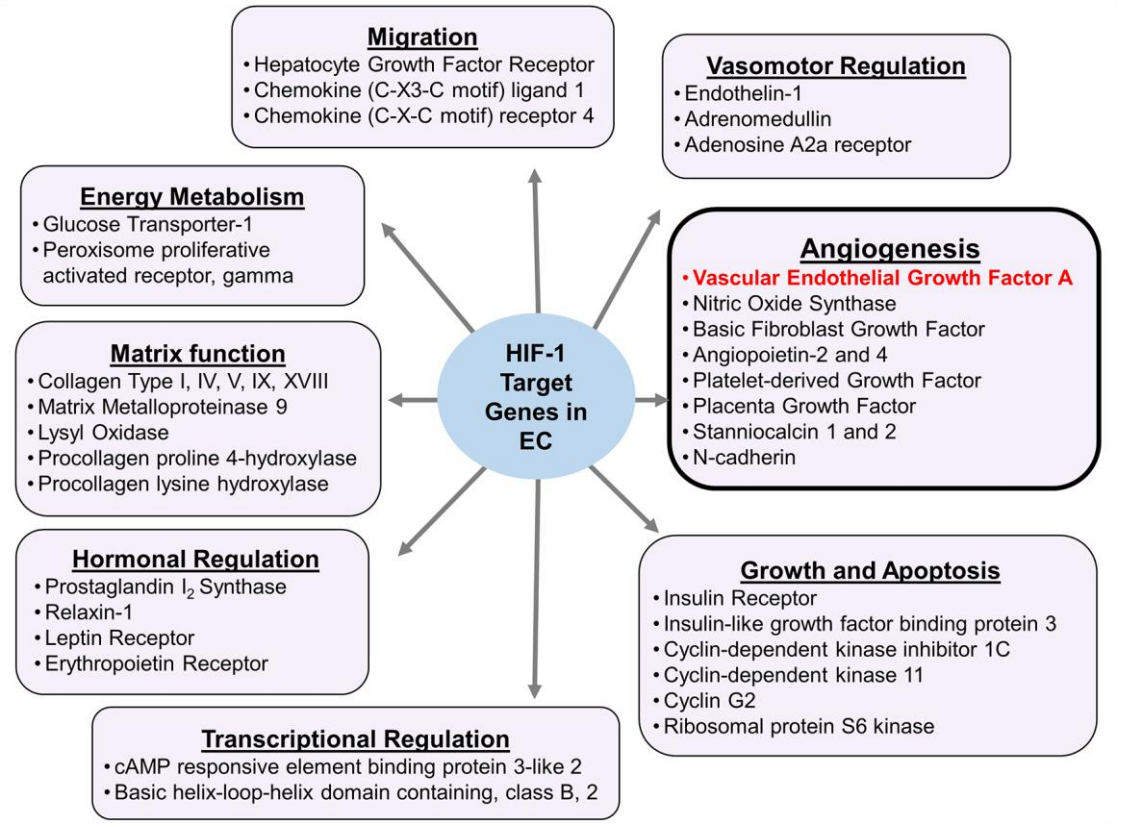

Figure. 2.8 A list of some known direct transcriptional target genes of HIF-1 upregulated in endothelial cells, categorized based on their functions [100,101].

2.3.5 Selection of sprouting ECs with VEGF-A

VEGF-A was first discovered by Dvorak and colleagues in 1983 [102]. It was found to be absent in normal skin but strongly upregulated upon injury, correlating temporally and spatially with the proliferation of new blood vessels [36,103]. In 1996, Carmeliet and colleagues demonstrated that the loss of a single VEGF-A allele results in defective vascular development and early embryonic lethality [104]. And to date, there does not appear to be redundant growth factor mechanisms that can replace the role of VEGF-A in angiogenesis [105]. Other proangiogenic growth factors such as platelet derived growth factor B (PDGF-B), basic fibroblast growth factor (bFGF), angiopoietin (ANG), transforming growth factors, apelin, and insulin-like growth factors (IGF) serve to complement or coordinate VEGF-A signalling rather than function as independent regulators of EC proliferation, migration and survival [106].

In hypoxic tissues, parenchymal cells such as dermal fibroblasts are major producers of VEGF-A [107]. Upon HIF-1 activation they upregulate VEGF secretion by approximately 10-fold [21], inducing a VEGF-A microgradient towards the surrounding “mother” vessel. Here quiescent ECs expose to the highest VEGF-A concentration are selected as tip cells for sprouting [83]. Tip cells upregulate Delta-like 4 (DLL) signalling molecule expression and extend numerous filopodia into surrounding ECM in search of angiogenic cues [83]. They have an increased glycolytic activity and adopt a migratory phenotype, with limited proliferative capacity, navigating at the forefront of endothelial sprouts [83].

2.3.6 Sprout outgrowth and guidance

As tip cells emigrate from the “mother” vessel, they secrete matrix metalloproteinases (MMP) to breakdown the basement membrane, EC-mural cell adhesions and surrounding extracellular matrix (ECM). MMP exposes cryptic proangiogenic integrin binding sites in the ECM, releases ECM-bound angiogenic growth factors such as VEGF-A, bFGF, IGF [108] and also anti-angiogenic molecules to prevent inappropriate sprouting and coordinate branching. MMP regulation is essential for sprouting, given that excessive degradation of the ECM leaves too little matrix support for the branch to sprout [83].

In order for the sprout to elongate, proliferation of ECs are necessary. As such, not all ECs exposed to paracrine VEGF-A will become migratory tip cells. ECs that acquire the tip cell phenotype, secrete DLL to activate Notch signalling in neighbouring ECs [83]. This suppresses the VEGF receptor 2 expression in neighbouring ECs, rapidly dampening their sensitivity to paracrine VEGF-A [109]. These cells thus adopt a stalk cell phenotype, producing fewer filopodia and are more proliferative following closely behind a tip cell.

As endothelial sprouts elongate along the VEGF-A gradient, they transit into a region of hypoxia, being further away from the “mother vessel”. To support their metabolic requirements, the ECs’ HIF-1 activity is upregulated. This results in an increase in glycolysis, ATP production [100] and it also induces a VEGF-A autocrine loop to maintain EC proliferation and motility under hypoxia [110].

2.3.7 Sprout fusion and lumen formation

Tip cells from two or more sprouts converge and fuse at the source of paracrine VEGF-A secretion. Multiple intracellular vacuoles then begin to form in the stalk cells. These vacuoles merge to create a continuous lumen for perfusion [82]. Here the size of the lumen depends on VEGF-A levels, with larger lumens form under higher VEGF-A exposure [111].

2.3.8 Perfusion and maturation

Up till this point, VEGF-A has been effective in developing newly formed immature vessels. Nonetheless, high concentrations of VEGF-A induces tortuous and leaky vessels [112]. This observation led to VEGF's initial designation as the vasopermeability factor [102,113]. A functional vessel network requires synergism among various angiogenic growth factors. Here HIF-1 activated ECs release PDGF-B [114] to recruit mural cells for the rebuild of the endothelial basement membrane [83,115]. Platelets also release sphingosine-1-phosphate (S1P) [116] to increase actin lamellipodia assembly and N-cadherin trafficking to the ablumenal side of the ECs [83,117]. Collectively, these events strengthens the EC-pericyte contacts, promoting endothelial tight junctional integrity for a functional vessel network. As local tissues receive adequate perfusion, hypoxia level decreases. Correspondingly, the HIF-1 activity in parenchymal cells and ECs are reduced, and VEGF-A levels returns to normal. The stalk and tip cells return to their quiescent phenotype and the process of sprouting angiogenesis is now terminated.

2.4 Inhibitors of angiogenesis in diabetes

ECs are of key importance to the tight regulation of molecular and cellular exchanges between the interstitial fluid and the bloodstream [420]. They do so by modifying the cell surface expression of adhesion molecules, such as integrins and selectins, and regulate molecular exchanges through paracellular gaps by acting on intercellular adhesion molecules from the cadherin, occluding and junctional adhesion molecule families [420]. Unlike other cell types, ECs are particularly susceptible to intracellular hyperglycemia as they are unable to efficiently reduce their expression of glucose transporters in the face of high blood glucose levels [121,122]. Intracellular hyperglycemia increases the expression of endothelial adhesion molecules [421], promoting the tethering, rolling and adhesion of circulating inflammatory cells to the endothelium. As inflammatory cells infiltrate and accumulate in the interstitial fluid, they release excessive pro-inflammatory cytokines that further disrupt EC-EC tight junctions [422] causing vessels to become leaky. In addition, inflammatory cells release excessive proteases that degrade extracellular matrices and growth factors; and release excessive reactive oxygen species (ROS) that induce cell death. Here chronic inflammation coupled with the glycation of proteins contribute to a reduction in vessel density and an increase in vessel permeability in diabetic wounds [118, 119].

This section provides a discussion on the perturbations of five biofactors which are herein termed as angiogenic inhibitors:

(i) high reactive oxygen species (ROS) levels;

(ii) high advance glycated end products (AGEs) levels;

(iii) low hypoxia-inducible factor-1 (HIF-1) activity;

(iv) high matrix metalloproteinases (MMP) levels; and

(v) low sphingosine-1-phosphate (S1P) level.

Importantly, these angiogenic inhibitors are not mutually exclusive and would need to be concurrently addressed to promote a functional vasculature in diabetic wounds. In the course of the discussion, I will highlight a proangiogenic strategy, involving divalent metal chelation and S1P supplementation to combat these angiogenic inhibitors.

2.4.1 Angiogenic inhibitor: High levels of ROS

The first major angiogenic inhibitor in diabetics is the elevated level of reactive oxygen species (ROS) present in endothelial cells (ECs) [120]. An increase in intracellular glucose, results in an increased glucose oxidation in the Kreb's cycle. This generates a large number of electron donors such as NADH and $FADH_2$, which donates their electrons rapidly across mitochondrial membrane protein complexes [121]. But as these protein complexes are unable to cope with the high influx of electrons, the excess electrons are instead donated to molecular oxygen generating ROS such as superoxides. The mitochondrial isoform of the enzyme superoxide dismutase degrades this oxygen free radical to hydrogen peroxide, which can be further converted to various other forms of ROS by an iron-catalysed Haber-Weiss reaction (Figure 2.9) [121,123].

A low level of ROS acts as signaling molecules in the regulation of fundamental cell growth and adaptation responses. However as ROS rises beyond the cell's antioxidant capacity, it damages DNA, resulting in cellular senescence and apoptosis [124]. Moreover a high level of ROS induces EC membrane lipid peroxidation and decreases nitric oxide synthesis [124]. This loss of endothelial nitric oxide results in dysfunctional vasodilation, increased platelet aggregation, increased inflammation and increased endothelial permeability (reviewed in Van den Oever et al. (2010)) [124].

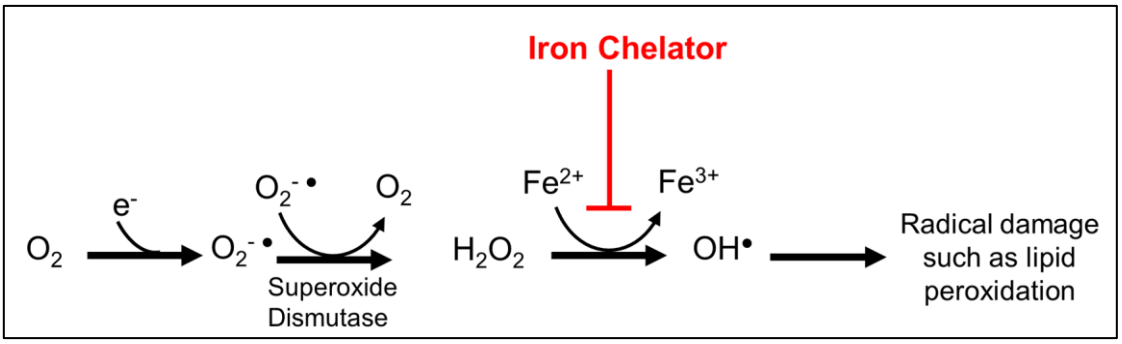

Figure 2.9 Generation of ROS catalysed by iron [123]. ($OH^\bullet$: hydroxyl radical)

Iron chelators reduce ROS

Strategies that supress ROS include the use of iron chelators [123], free radical scavengers (e.g. Vitamin E) and antioxidant enzymes (e.g. superoxide dismutase). Iron chelation, in particular, has been thought to be particularly useful for diabetics as they typically exhibit elevated serum ferritin levels compared to nondiabetics [125,126]. In 2009, Geoffrey Gurtner's group demonstrated *in vitro* that the iron chelator, deferoxamine, effectively reduces ROS production levels in ECs cultured under hyperglycemia [127]. Subsequently, they delivered an intraperitoneal injection of deferoxamine in an

ischemic dorsal skin flap of diabetic mice and found it effective in reducing necrosis while promoting angiogenesis [128]. Takuji Nakashima's group also discovered that the iron chelator Ciclopirox Olamine (CPX) could dose-dependently scavenge ROS released from inflammatory cells [129]. In 2011 Michael Longaker's team topically applied CPX in diabetic murine wounds and showed that it did indeed promote endothelial cell infiltration [130]. Cumulative evidence thus support iron chelators as an effective proangiogenic strategy to suppress ROS in diabetic wounds.

2.4.2 Angiogenic inhibitor: High levels of AGEs

The second major angiogenic inhibitor in diabetics is an elevated level of advanced glycation end-products (AGEs). In particular, AGEs present in the diabetic skin tissue correlate closely with the severity of microvascular complications [124,131]. Compared to nondiabetics, diabetics have an approximately 5-fold increase in AGE-serum peptides [132]. Here AGEs are formed through a non-enzymatic glycosylation process where excess glucose attaches to free amino groups on proteins to form an Amadori product (Figure 2.10a). The Amadori product rearranges into highly reactive intermediates with dicarbonyl groups (such as deoxyglucosone, glyoxal and methylglyoxal) which are capable of physically crosslinking proteins, DNA or lipids to form various AGEs products (Figure 2.10b) [133,134]. Similar to ROS, the formation of AGEs is catalysed by transitional metal ions; wherein the oxidation and reduction of metal ions drive the vicious cycle of dicarbonyl AGE precursor and ROS formation (Figure 2.11) [135-137].

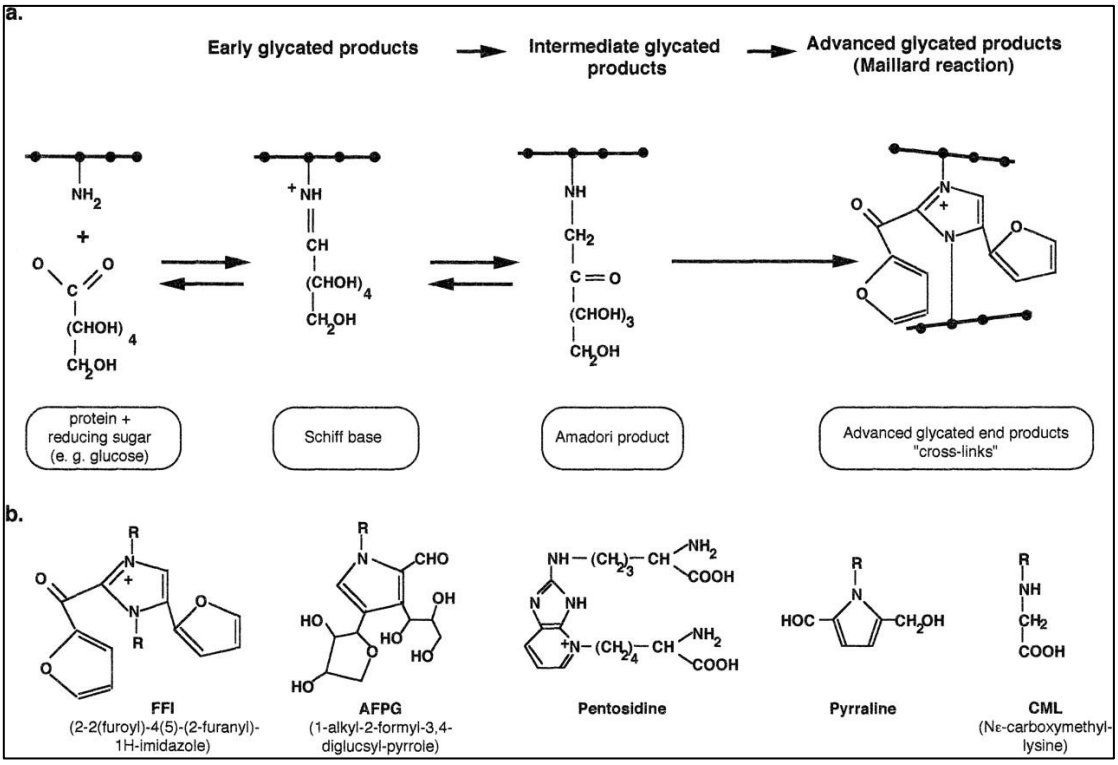

Figure 2.10 (a) AGEs formation: Glucose condenses with amino groups to form reversible Schiff base adducts. Intramolecular rearrangements results in Amadori products which upon further rearrangements, dehydration and condensation reactions result in irreversible AGEs. **(b)** Various structures of AGEs. *(Figure reprinted from Bierhaus et al. with permission* [136] *Copyright © 1998 Oxford University Press.)*

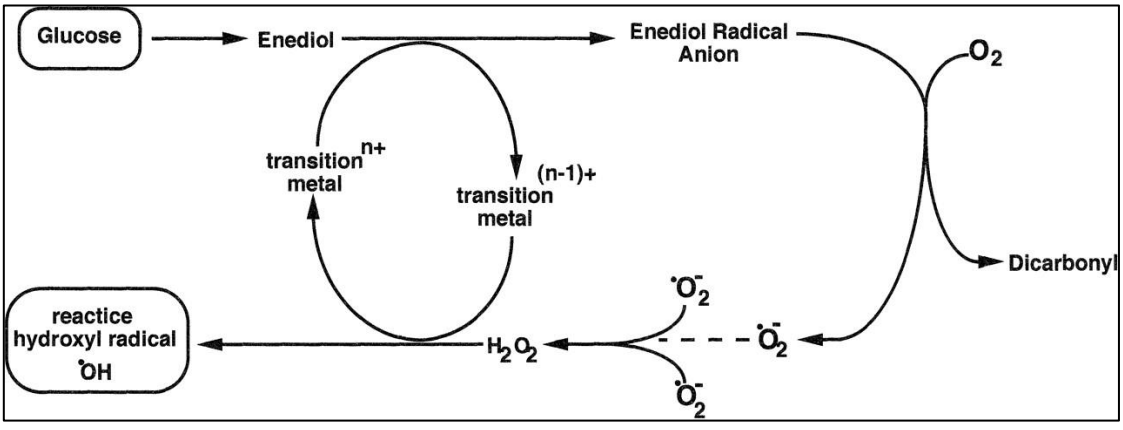

Figure 2.11 Vicious cycle of transition metal-driven ROS formation (hydroxyl radicle) and AGE precursor formation (dicarbonyl compounds). *(Figure repprinted from Bierhaus et al. with permission* [136] *Copyright © 1998 Oxford University Press.)*

AGEs chemically modify and cross link tissue proteins, lipids, and DNA. This affects their structure, function and turnover, contributing to a gradual decline in endothelial function [124]. In particular, AGE-modified proangiogenic growth factors have an attenuated downstream signalling response [138-142]. When injected in nondiabetic animals, AGE-modified proangiogenic growth factor attenuate angiogenesis compared to the unglycated form [143]. In addition, AGEs reduce the rate of collagen polymerisation [144] and decrease collagen's affinity for proteoglycans [124]. This in part contributes to an increase in endothelial permeability and a decrease in endothelial matrix elasticity [124,145]. AGEs also increase the expression of endothelial adhesion molecules, which in turn promotes the interaction of the endothelium with inflammatory cells [144].

Metal chelators reduce AGEs

Strategies to decrease AGEs include the use of AGEs-inhibitors and AGEs-breakers. AGEs-inihibitors, such as aminoguanidine and pyridoxamine, were proposed to trap reactive dicarbonyl intermediates, while AGEs-breakers such as alagebrium, phenacylthiazolium and phenacyldimethylthiazolium bromide were proposed to cleave AGEs dicarbonyl cross-links in tissue proteins [146]. Nonetheless their mechanism of action remains poorly understood.

Cumulative evidence by John Baynes's group indicated that both AGEs-breakers and AGEs inhibitors in fact shared a similar working mechanism i.e., metal chelation [137,146]. AGE inhibitors displayed weak to potent copper

chelating activity while AGE-breakers had extremely strong potent copper chelating activity to inhibit metal-catalysed oxidation reactions involved in AGE formation [146]. In 2010, Yukio Fujiwara's group discovered that an oral delivery of a non-specific metal chelator, citric acid, prevented AGEs formation in the eye lens of diabetic Wistar rats [147].

These metal chelating AGE-inhibitors and AGE-breakers have also been reported to be effective in promoting functional blood vessel development in various diabetic models. In 1999, Teixeira et al. found that an intraperitoneal treatment of the AGE-inhibitor aminoguanidine in diabetic rats promoted pericytes and vascular cell infiltration into subcutaneously implanted sponge granuloma [148,149]. The same aminoguanidine was later found to be effective in reducing skin flap necrosis in diabetic rats [150]. The AGE-breaker phenacylthiazolium was found by Daniel Herion's group to improve endothelium-dependent dilation in a mesenteric ischemia diabetic rodent model [151], while Bruce Wolffenbuttel's group also demonstrated that the AGE-breaker alagebrium reversed carotid artery stiffness in diabetic rats [152]. Cumulative evidence thus indicate that metal chelators are effective in suppressing the anti-angiogenic effects of AGEs.

2.4.3 Angiogenic inhibitor: Low HIF-1 activity

The third major angiogenic inhibitor in diabetics is low hypoxia-inducible factor-1 (HIF-1) activity [153,154]. The transcriptional factor HIF-1 is an upstream regulator of numerous target proteins involved in angiogenesis (§2.3.4). Its impaired activity has been attributed to a particular AGEs precursor – methylglyoxal [155]. Methylglyoxal forms stable adducts with HIF-1's subunit – HIF-1α, and impairs its activity in three ways. Firstly, it reduces HIF-1α's capacity for heterodimerization with HIF-1β. Secondly, it increasing HIF-1α's degradation by promoting HIF-1α's association with heat shock protein 40/70 [155]. Thirdly it covalently modifies HIF-1's transcription co-activator p300 thereby suppressing HIF-1's transcriptional activity [156]. Collectively, these effects attenuate various HIF-1 downstream gene expressions (e.g. VEGF, bFGF, eNOS and glycolytic enzymes), reducing the migration of endothelial cells (ECs) [94,128,153,156-158].

Iron chelation reverses HIF-1 activity impairment

To increase HIF-1 activity, iron chelators have been proposed. Here iron chelators work via a two-pronged approach. Firstly, it curtails methylglyoxal formation as iron is a catalyst for methylglyoxal AGEs precursor formation [128] . Secondly, it inhibits HIF-1α subunit degradation [159] as Fe^{2+} is a cofactor for prolyl hydroxylases that continuously earmark the HIF-1α for proteasomal degradation. Cumulative evidence have demonstrated the angiogenic efficacy of iron chelators in treating both diabetic and nondiabetic wounds (Table 1).

Table 1. Iron chelators in wound healing models.

Iron Chelator	Specificity (IC_{50})* [94]	Animal Model (References)	Delivery/ Dose	Results
Desferrioxamine	8–10μM	Dorsal full-thickness skin excision diabetic mice [127,154]	Topical 1mM Alternate day	**Increased:** • Wound closure • HIF-1α • EC infiltration • Granulation • Receptors (CXCR4, C-Kit, Tie-2) • VEGF
		Ischemic skin flap diabetic mice [128]	Intra-peritoneal (Dose unclear)	**Increased:** • EC infiltration • VEGF **Reduced:** • Flap Necrosis
Hydralazine	Unknown	S.C sponge nondiabetic mice [160]	Intravenous 5 mg/kg Daily	**Increased:** • EC infiltration
Ethyl 3,4-dimethyl benzoate	330 μM	S.C sponge nondiabetic mice [161]	Intradermal 360 mg/ml Alternate day	**Increased:** • EC infiltration
Ciclopirox Olamine (FG-2229)	1 μM	Dorsal full-thickness skin excision diabetic mice [130,161]	Topical 50mM Alternate day	**Increased:** • Wound closure • HIF-1α • EC infiltration • Cellularity
TM 6008	0.57 μM	S.C sponge nondiabetic mice [162]	Intradermal 50 μg Alternate day	**Increased:** • EC infiltration • Haemoglobin content
L-Mimosine	455 μM	S.C sponge nondiabetic mice [161]	Intradermal 15 mg/ml Alternate day	**Increased:** • EC infiltration

*Specificity (IC_{50}) for prolyl hydroxylase (PHD) or Factor Inhibiting HIF-1 (FIH).

(S.C. refers to subcutaneous)

2.4.4 Angiogneic inhibitor: High MMP levels

The fourth angiogenic inhibitor in diabetics is the overexpression of matrix metalloproteinases (MMPs). MMPs are a group of zinc- or calcium-dependant proteolytic enzymes, which are collectively endowed with the capability of degrading all extracellular matrix (ECM) proteins [163]. MMPs play an important role in angiogenesis by (i) degrading vascular basement membrane and ECM components to allow detachment of pericytes and endothelial cell (ECs) migration; (ii) localizing MMP-2 to the invading edge of EC to aid migration; (iii) exposing cryptic integrin binding sites from cleaved ECM molecules; and (iv) releasing and activating angiogenic growth factors stored in the ECM [169].

In normal physiological angiogenesis there exists a tightly-controlled balance between MMP activity and MMP inhibitors (reviewed in Rundhaug (2005)) [169]. However in diabetic wounds this balance is perturbed, with overexpression of collagenases; MMP-1 (65-fold), MMP-8 (2-fold) and gelatinases; MMP-2 (6-fold) and MMP-9 (14-fold) compared to nondiabetic traumatic wounds [164]. Moreover, MMP elevation in diabetics exists even prior to wounding [165]. Such prolonged overactivity of MMP often results in ‘off target’ destruction of ECM proteins, proangiogenic growth factors and their ligand binding domains [170]. In human chronic wound fluid, a 30-fold increase in total MMP activity is associated with a proportionate increase in epidermal growth factor degradation [171]. Diabetics also typically exhibit elevated levels of collagen degradation as evidenced by an increase urinary hydroxyproline content [172]. This increase in collagen degradation releases abundant anti-angiogenic collagen chain fragments such as endostatin, tumstatin, arrestin and canstatin. Exposure to

these anti-angiogenic fragments induces EC apoptosis and inhibits VEGF and bFGF-induced EC migration [169,173].

Zinc chelators reduces MMP activity

The pathophysiological pathway of the elevated MMPs in diabetics remains unclear. Recent evidence suggests a possible link between high ROS and high MMPs levels mediated by the transcription factor NF-κB [166-168]. Current efforts to downregulate MMP activity include the use of small-molecule mimics of MMP substrates combined with a hydroxamic acid zinc-binding group that chelates the catalytic Zn^{2+} ion (reviewed in Jacobsen et al. (2010)) [174]. These inhibitors are potent, inhibiting all MMP subtypes. However the broad spectrum MMP inhibitor (ilomastat) was first tested in nondiabetic models of rodent, porcine and human wounds. The result was a delay in wound closure [175-177]. Some thus assumed that broad inhibition of MMP may also be detrimental for diabetic wound healing [177], and began designing specific MMP inhibitors [174]. In 2015, Mayland Chang's group found that selectively inhibiting gelatinases (MMP-2 and MMP-9) and membrane type MMP-14 enhanced angiogenesis and wound closure in diabetic murine wounds [178]. Nonetheless, it is not known if a broad spectrum of MMP inhibition does indeed result in reduced efficacy in diabetic wound healing compared to specific MMP inhibition.

2.4.5 Angiogneic inhibitor: Low S1P levels

The fifth angiogenic inhibitor is a low plasma level of lysosphingolipid: sphingosine-1-phosphate (S1P). S1P was discovered in 1991 by Sarah Spiegel's group [180]. It is intracellularly derived from the phosphorylation of sphingosine, a cell membrane lipid molecule [181]. It can be exported extracellularly and carried in the blood plasma by high-density lipoprotein (HDL) and albumin [116,182]. Recent evidence indicates that diabetic HDL with a higher content of S1P exerts vasculoprotective effects as a form of the body's compensatory mechanism to prevent or delay diabetic complications [179]. Here severe diabetics were found to exhibit a reduced HDL-S1P level compared to early stage diabetics [179]. Nonetheless, its pathophysiological pathway remains unclear. Some evidence suggests a high ROS levels as a cause, degrading a key enzyme involved in S1P synthesis i.e., sphingosine kinase 1 [197]. Other evidence indicates an association between AGEs and S1P levels [198].

The vasculoprotective effects of S1P are exerted through G-protein coupled S1P receptors [183]. ECs express three G-protein coupled S1P receptor subtypes: S1P1, S1P2, and S1P3 [184]. S1P1 and S1P3 has been proposed to be the major receptors mediating angiogenesis [185,186], while the role of S1P2 in angiogenesis remains unclear as conflicting studies indicate both proangiogenic and anti-angiogenic effects of S1P2 [187,188]. Histological analysis of S1P1 knockout mice revealed that S1P1 signalling is not essential for EC differentiation, proliferation, migration or tube formation [189]. However

its deficiency resulted in defective migration of mural cells (vascular smooth muscle cells and pericytes) around nascent blood vessels leading to severe haemorrhaging and death *in-utero* [189,190]. Numerous studies have also established that S1P1 signalling enhances actin lamellipodia, actin assembly, vascular endothelial cadherin-containing adheren junctions between EC-EC and also N-cadherin-dependent junctions between EC-pericytes [189,191-195]. S1P1 activation also enhances the EC-EC adheren junctions by suppressing the expression of endothelial adhesion molecules [420]. Its suppression reduces the interaction between inflammatory-cells with the endothelium; and hence there will be less infiltration of inflammatory cells and consequently less proinflammatory cytokines, which is a major cause for EC-EC tight junction disruption.

As mentioned above, S1P is not necessary for EC migration. However, its presence accelerates EC migration which is mediated through both S1P1 and S1P3 signalling [186]. S1P3 signalling also promotes vasodilation by increasing EC nitric oxide production [196].

S1P supplementation promotes functional non-leaky vasculature

Current evidence indicates that direct supplementation of S1P or its synthetic analogue, FTY720 is efficacious in promoting functional non-leaky vasculature. In nondiabetic mice, Timothy Hla's group reported that oral delivery of FTY720 effectively reversed VEGF-induced vasculature permeability [200]. In diabetic rats, intraperitoneal injection of FTY720 (1mg/kg) was also seen to reverse the

permeability of inter-endothelial clefts and albuminal surface in the cardiac microvasculature [201]. *In vitro*, FTY720 blocked VEGF-induced internalization of VE-cadherin to promote EC-EC tight junctions formation, and augmented endothelial barrier transmonolayer electrical resistance in a hyperglycaemic EC culture [191]. In diabetic mice, Yoshinao Soma's group reported that topical delivery of 100 µM S1P increased angiogenesis and wound closure [199].

2.4.6 Proangiogenic strategy: Metal chelation + S1P

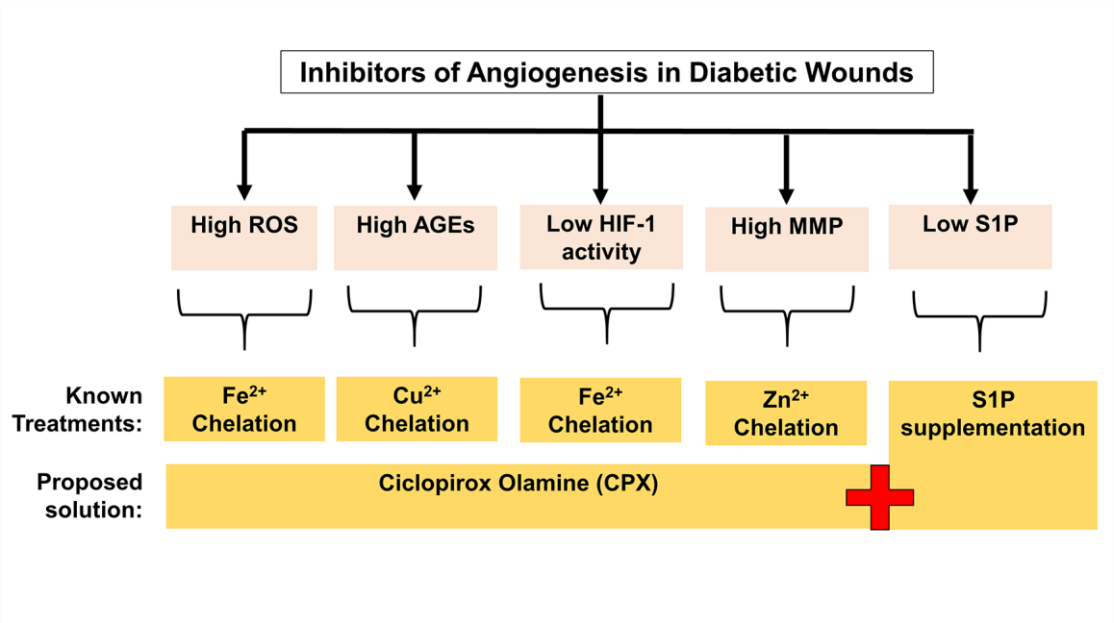

Figure 2.12 Summary of angiogenic inhibitors and treatments

To conclude §2.4, the current literature indicates that: (i) high ROS, (ii) high AGE, (iii) high MMP, (iv) low HIF-1 activity and (v) low S1P are major angiogenic inhibitors in diabetics (Figure 2.12). Accordingly, I have identified that metal (iron, copper, zinc) chelation is a common solution to tackle causes (i) to (iv). This treatment has an added utility in diabetics as they typically exhibit elevated serum levels of zinc, copper, and iron [125,202]. To tackle cause (v), a direct

supplementation of S1P was seen to be effective. **Thus the literature suggests that combination of a broad spectrum metal chelator and S1P would be a good proangiogenic strategy in diabetic wounds.**

2.5 In the market: FDA-approved proangiogenic drugs

FDA, the drug regulatory agency for the largest current pharmaceutical market in the world, has approved three groups of adjuvant proangiogenic therapies for diabetic wound healing: (i) biological matrices, (ii) modalities and (iii) drugs [203]. The clinical efficacy of all three groups of adjuvant proangiogenic therapies has been comprehensively reviewed by Greer and colleagues [205], and the consensus remains that there is no gold standard adjuvant treatment for diabetic wound closure; wherein the treatment is easy to apply and remove, causes no pain, is cost effective, has no complications, and allows for universally complete healing outcomes under various patient parameters [206]. Under drug therapies, only two proangiogenic drugs have been approved: (i) platelet-derived growth factor-B homodimer (PDGF-BB) and (ii) platelet rich plasma gel (PRP) [204]. In this section, I discuss the efficacy of both these proangiogenic drugs. A discussion on the efficacy of biological matrices and modalities can be found in Appendix A.

2.5.1 Recombinant platelet-derived growth factor-BB

Recombinant PDGF-BB (generic name: Becaplermin, trade name: Regranex, Systagenix Wound Management Inc., Gargrave, UK) was the first proangiogenic drug approved by FDA in 1998 for diabetic ulcers. PDGF-BB is a hypoxia-inducible factor-1 (HIF-1) downstream growth factor (Figure 2.8) that supports neovessel stabilization by recruiting mural cells to induce functional anastomoses (§2.3.8). It also promotes fibroblast proliferation [207]. When topically applied onto diabetic murine and human wounds [211-213], PDGF-BB accelerated angiogenesis, granulation tissue formation, wound contraction and re-epithelialization [208-210]. Nonetheless, it has not been equivocally translated into daily practice [8]. Clinical results from more than 7000 patients revealed a modest 10% increase in the rate of diabetic healing with PDGF-BB [214], with some trials indicating that recombinant PDGF-BB was was only as effective as that of standard care or moist treatment with sodium carboxymethylcellulose gel [205]. The lack of efficacy is believed to be contributed by high levels of MMP in wound fluids, which rapidly degrades PDGF-BB [8]. Increasing its dosage to compensate for high degradation rates poses a risk of skin malignancy [215,216]. In 2008, FDA issued a black box warning following a post-market epidemiologic study linking the use of more than three tubes of Becaplermin to a fivefold increased risk of mortality in patients with a history of malignancy [217]. In 2012, Becaplermin was withdrawn from the European Union market [218].

2.5.2 Platelet rich plasma gel

Autologous platelet rich plasma gel (PRP) (AutoloGel System, Cytomedix Inc, Rockville, MD) is the second proangiogenic drug that the FDA approved in 2007 for diabetic ulcers. PRP contains a high concentration of platelets in a small volume of plasma. It works by the degranulation of the α-granules in platelets, which releases proangiogenic growth factors such as PDGF, TGF-β, VEGF, EGF and IGF [219]. PRP is derived from a two-step process: (1) centrifugation of whole blood from the patient to separate the plasma from red blood cells; and (2) centrifugation of plasma to separate PRP from platelet-poor plasma [219]. Hereafter, PRP is activated with thrombin or calcium to result in a gelatinous platelet gel [219]. Upon activation, α-granules secrete proangiogenc factors with more than 95 percent of the presynthesized growth factors secreted within 1 hour [220]. Following this initial burst release, platelets continue to synthesize and secrete additional proteins for the balance of their lives (5 to 10 days) [220].

When used in various diabetic animal models of hind-limb ischemia [221] and full-thickness wounds [222], PRP was efficacious in promoting angiogenesis and wound closure. However, its efficacy remains debatable in clinical studies [205, 223-224]. When compared against saline gel, PRP significantly decreased the diabetic ulcer size [224]. However this did not translate into a significant increase in the mean time to healing, nor an increase in percentage of ulcers healed [205,224]. Interestingly, Kakagia et al. highlighted that PRP's efficacy in decreasing diabetic ulcer size was significantly potentiated when combined with a protease-modulating biomaterial [225]. It thus becomes clear that future

successful treatments will require strategies that concurrently address the multi-factorial dysfunctions in the diabetic wound environment.

2.5.3 A need for a new proangiogenic drug approach

In summary, the current clinical approach in directly delivering a single or a combination of angiogenic growth factors for diabetic wound healing faces several major limitations. Firstly, supraphysiological doses of growth factors are required for efficacy due to (i) the short serum half-life of growth factors [226], (ii) the failure to supress overactive protease activity, and (iii) the failure to reverse an impaired HIF-1 activity (a major driver for pro-angiogenic stimulants). Secondly, the high doses required for efficacy leads to an increase risk of malignancy. Thirdly, delivery of single angiogenic growth factors may be insufficient for a mature and functional vascular network and can in some cases result in deregulated proliferation of ECs forming haemangiomas and vascular lacunae [227].

My proposed proangiogenic strategy involves combining metal chelation and sphingosine-1-phosphate (S1P). As discussed in §2.4.6, this strategy seeks to address the multifactorial angiogenic inhibitors in the diabetic wound environment. Here metal chelation aborogates the need for supraphysiological doses of growth factors by (i) suppressing matrix metalloproteinases (MMP) activity to reduce growth factor degradation, and (ii) reversing the impaired HIF-1 activity to induce physiological release of a variety of proangiogenic

stimulants. Complementarily, S1P supplementation promotes a mature and functional vascular network.

2.6 Drug repurposing and synergy approach

2.6.1 Background

The high research and development costs are not unique to the field of wound repair [230]. Despite the billions of dollars poured in by pharmaceutical companies yearly for *de novo* drug discovery, very few drugs tested enter the market [230]. In fact, there has been a paucity in FDA's new drug approval over the last 10 years [228,229] (Figure 2.13). If the new drug successfully emerges from regulatory channels and clinical trials, time becomes the enemy [230]. Here, the process of acquiring adequate data to support drug approval typically requires 10 to 15 years. By then patent protection can lapse and generic competitors begin to take a large portion of the market share [230, 231]. At the end of the process, the high pricing of new drugs become a financial constraint for caregivers. Thus to reduce the cost, reduce the time-frame for drug approval and to increase success rates, drug repurposing and drug synergy approaches are favoured [232].

Drug repurposing is a process of finding new uses of existing drugs. Here drug repurposing leverages on established clinical drug libraries of pharmacology, formulation development, potential toxicity and bulk manufacturing process to shave off substantial risks, costs and several years for translation [232].

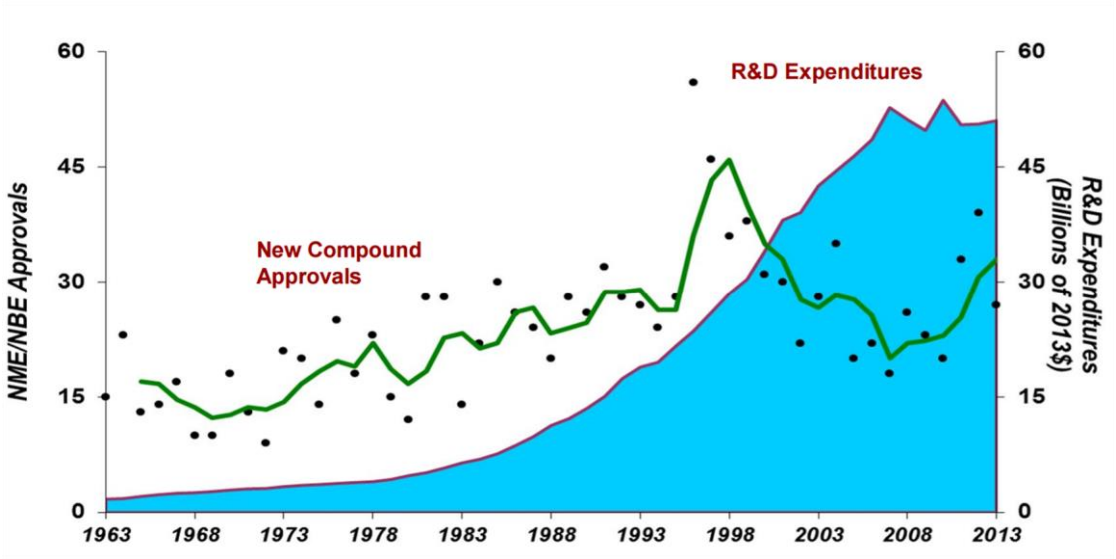

Figure 2.13 Paucity in new molecular entity (NME)/ new biological entity (NBE) approvals despite rising research and development (R&D) expenditures. (*Figure reprinted with permission from Tufts CSDD; PhRMA, 2014 Industry Profile* [228]. *Copyright © 2014 Tufts CSDD.)*

Drug synergy, on the other hand, involves the identification of drug pairs that creates a greater effect than the sum of the individual drug's effect [233]. Here drug synergy can result when one drug's action helps another drug's availability in the target cells, either by increasing the second drug's entry to the cell or by decreasing the second drug's degradation [234]. Drug synergy can also occur when drugs target the products of genes that act in parallel pathways. Although *in vitro* identification of drug synergy is rare (4–10%) [235], various methods to predict synergistic drug combinations have been developed. They include network analysis of expression profiles, clustering of chemogenomic profiles of drug perturbations [236] and screening of drugs in three-dimensional microfluidics devices [21].

2.6.2 Repurposing and sprouting synergy of CPX and S1P

A three-dimensional microfluidic platform that screens angiogenic drugs which induces endothelial cell (EC) sprouting was established in 2013 by Roger Kamm's group (Singapore MIT Alliance for Research and Technology) [21]. In their platform (Figure 2.14), human umbilical vein ECs and IMR-90 fibroblast are separated by a collagen channel. ECs are allowed to sprout through the collagen gel towards the microgradient of angiogenic factors released by fibroblasts. Fibroblasts, on the other hand, are encapsulated in alginate beads unable to migrate into the collagen gel. Using this platform, a colleague in my lab assessed the efficacy of EC sprouting under mono or combinatory treatment of drugs: ciclopirox olamine (CPX) and sphingosine-1-phosphate (S1P).

Here S1P and CPX are clinically used for different purposes. S1P is a lysophospholipid whose analogue (Fingolimod, code name FTY720) has been FDA-approved as an oral drug for multiple sclerosis since 2010 [237]. CPX is an off-patent synthetic antifungal drug discovered in the late 1960s [238]. It has been FDA-approved in multiple anti-fungal topical formulations as 0.8% CPX (Batrafen®) for skin and shampoo and 8% CPX in nail lacquer [239]. CPX is highly lipophilic, penetrating the deep layers of the skin easily and can be safely eliminated in the form of glucuronides [238]. Importantly, CPX is a metal chelator. It chelates divalent metal cations (Mg^{2+}, Ca^{2+}, Cu^{2+}, Fe^{2+}, Zn^{2+} and Mn^{2+}) with high affinity [240]. In 2003, CPX was serendipitously identified by Roger Wenger's group [241] as an inhibitor of HIF-1α degradation by chelating Fe^{2+}, a cofactor for the prolyl and arginyl hydroxylases that continuously earmark the

HIF-1α subunit for proteasomal degradation. They further demonstrated CPX's angiogenic effect in a chick embryo chorioallantoic membrane assay [241].

As an extension to their findings, my lab discovered that the combination of CPX and S1P potentiated the number of sprouting ECs and its sprout length [21,242]. Of the maximal sprout length formed, S1P alone increased sprout length by ~150 µm as compared to control, while CPX alone increased sprout length by ~60 µm as compared to control (Figure 2.14). Notably, their combination increased sprout length by ~290 µm, which exceeds the effects of either agent alone or their additive effects (e.g., 150 µm + 60 µm = 210 µm, which is less than 290 µm). This demonstrates a synergistic angiogenic effect. Moreover under confocal microscopy, the sprouts growing towards the encapsulated fibroblast were found to exhibit lumina of approximately 30 µm in diameter (Figure 2.15).

Since no other metal chelator has been reported to synergistically promote endothelial sprouting with S1P, I have thus decided to use the combination of CPX and S1P as a proangiogenic strategy for diabetic wound healing.

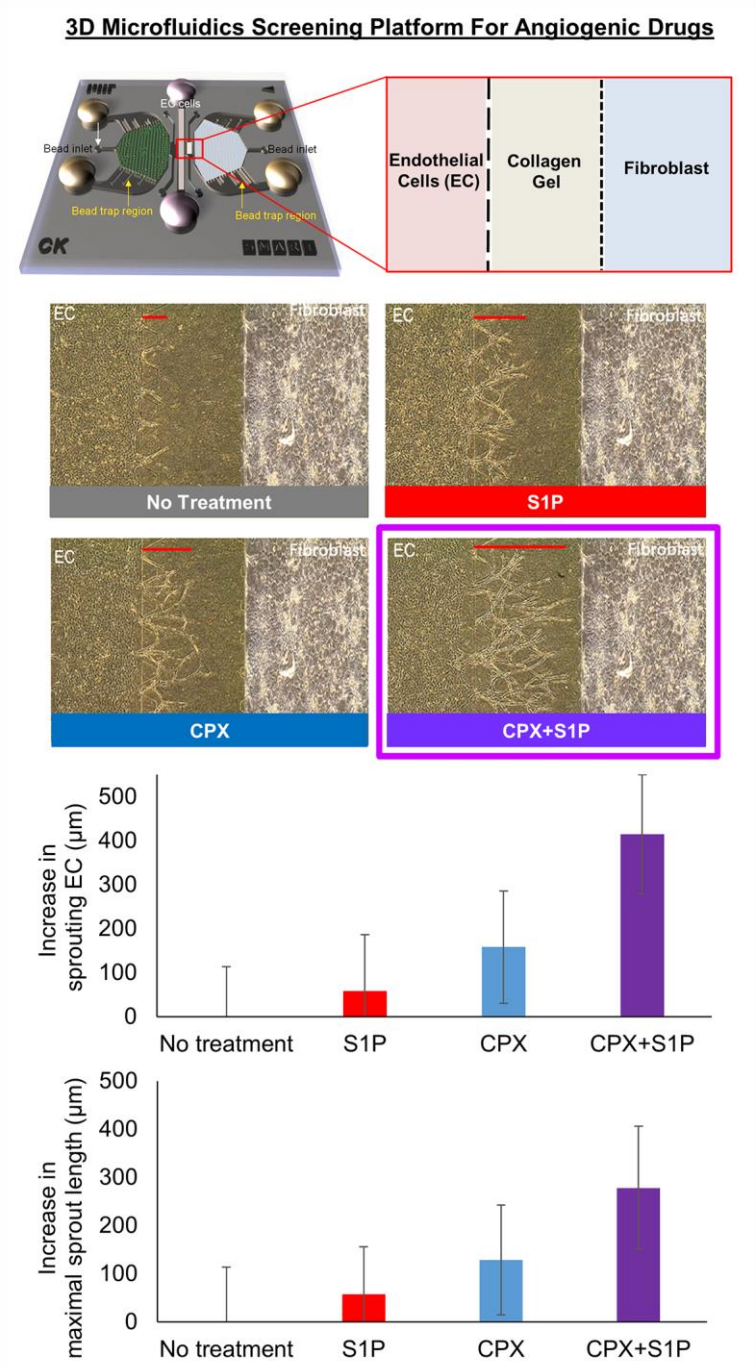

Figure 2.14 In a 3D microfluidics platform, 8 µM CPX+ 250 nM S1P synergistically increased human umbilical vein endothelial cell (HUVECs) infiltration and sprout length in the presence of fibroblasts (IMR-90). HUVECs seeded in the left channel, sprout through a collagen gel towards IMR-90 cells trapped within the right channel. Horizontal red bars, in the bright field images, represent EC sprout length. *(Figures compiled from Lim et al.* [21] *)*

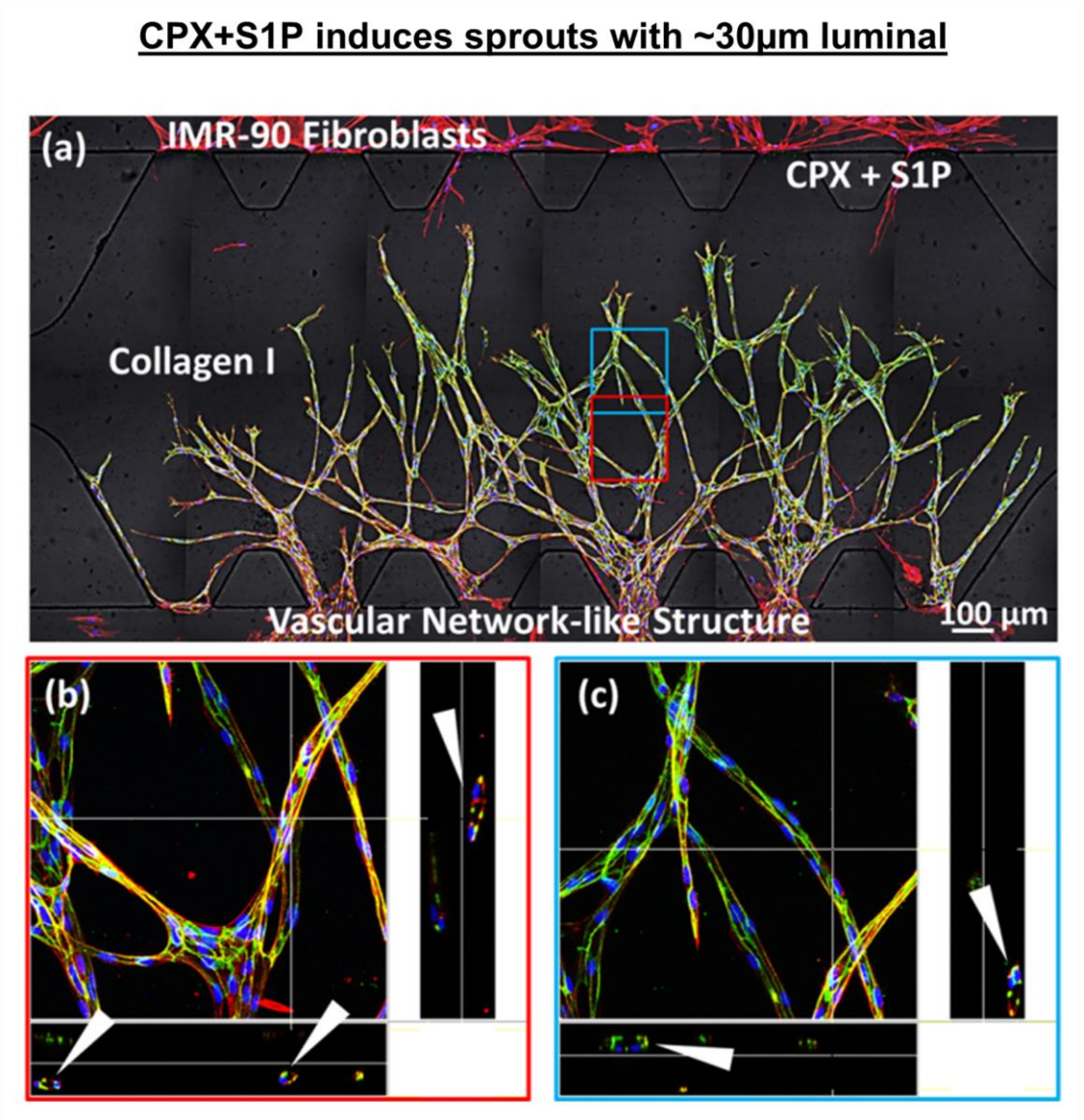

Figure 2.15 In combination, CPX and S1P induced vascular network structure with defined lumina. (a) Stitched; (b) and (c) sectioned 20x confocal image of CPX+S1P induced vascular network stained with Hoechst (blue), phalloidin actin (red) and VE-cadherin (green) shows sprouts that anastomose. White arrows indicate lumina of endothelial sprouts with diameters of ~30 µm. *(Figure reproduced from Lim et al.* [21] *with permission from The Royal Society of Chemistry).*

Chapter 3

Methods and Materials

3.1 Hypothesis 1:

CPX+S1P potentiates HIF-1 activity *in vitro*

3.1.1 Rationale for assessing HIF-1 activity in endothelial cells

Hypothesis 1 seeks to assess if CPX+S1P potentiates HIF-1 activity *in vitro.* Here I have chosen to use endothelial cells (ECs), more specifically human umbilical vein ECs (HUVECs), as the *in vitro* cell type to be assessed. Compared to other cell types like fibroblasts, ECs are not known to be the biggest producers of angiogenic growth factors [21]. Nonetheless their autocrine production of proangiogenic stimulants are vital for angiogenesis. In 2004, Tang et al. ablated HIF-1α in murine ECs to disrupt their autocrine production of vascular endothelial growth factor-A (VEGF-A) [110]. They demonstrated i*n vivo* that this ablation inhibited EC proliferation, chemotaxis and extracellular matrix penetration inspite of exposure to VEGF-A [110]. Morever HIF-1α's ablation in EC impaired murine wound closure [110]. In 2006, Calvani et al. discovered that the HIF-1α-induced bFGF autocrine loop in ECs was necessary for the survival and sprouting of hypoxic ECs [101]. Overexpressing HIF-1α in ECs was separately shown *in vitro* to potentiate its invasion into an environment with abundant proangiogenic growth factors [100].

In Hypothesis 1, I assessed the HIF-1 activity in ECs under an exposure to mono and combinatory treatment of CPX and S1P. Here HIF-1's activity is assessed through a two-pronged approach. Firstly, through the upregulation of two of HIF-

1’s upstream activators: (i) HIF-1α and (ii) phosphorylated p42/44 MAPK [243,244]. Secondly, through the upregulation of three of HIF-1’s downstream angiogenic targets [245]: (i) VEGF-A, (ii) c-MET (Hepatocyte growth factor receptor) and (iii) eNOS (endothelial nitric oxide synthase).

3.1.2 Culturing HUVECs

Primary human umbilical vein endothelial cells (HUVECs) were kindly provided by Dr. Jerry Chan (KK Hospital, Singapore), harvested in accordance with Domain Specific Review Board of National Healthcare Group. HUVECs were plated in cell culture flasks precoated with 50 µg/ml rat tail collagen I solution (BD Biosciences, San Jose, CA) in 0.02 M acetic acid (VWR, Radnor, PA) and maintained in endothelial growth medium (EGM; Lonza, Walkersville, MD) until 80% to 90% confluent. HUVECs were used at passage 5 to 6.

3.1.3 Preparation of CPX and S1P solution

10 mM ciclopirox olamine (CPX) (Sigma, St. Louis, MO) stock solution was prepared in dimethyl sulfoxide and diluted to 1- 40 µM working solution in culture media. S1P powder (Sigma) was dissolved in methanol:water (95:5) at 0.5 mg/ml under sonication. Solvent was evaporated at 55°C in a water bath to render a thin film of S1P to be stored at -20°C [21]. 4 mg/ml of fatty acid-free bovine serum albumin (Sigma) in phosphate-buffered saline was the diluent to make a 125 µM S1P stock [21]. The final S1P concentration in the culture media was 0 - 0.2 µM.

3.1.4 Immunoblotting

80 000 HUVECs were seeded into 6-well plates (Greiner Bio-One, Frickenhausen, Germany) in EGM (Lonza) and allowed to adhere for 24 hours. Thereafter EGM was removed, cells were washed with Hanks' balanced salt solution (Thermo Fisher Scientific) and then treated with 0 – 40 µM CPX or 0 - 0.2 µM S1P in endothelial basal media (Lonza) supplemented with 5% FBS (Thermo Fisher Scientific) at 37°C with 5% CO_2. The HUVEC monolayer was lysed 1 to 8 hours after treatment with 100 ul of sodium dodecyl sulfate (SDS) sample buffer containing the phosphatase inhibitors aprotinin, leupeptin, and pepstatin at 10 µg/mL each (R&D Systems, Minneapolis, MN). Protein concentration was determined by Bradford assay (Thermo Fisher Scientific) and 20 µg of total protein per sample was loaded into 10 % resolving / 3 % stacking or 12 % resolving / 5 % stacking SDS PAGE gels, electrophoresed and transferred to nitrocellulose membranes (Biorad, Hercules, CA) for 1 hour at 100 V. Membranes were blocked with 5% bovine serum albumin and incubated with primary rabbit polyclonal antibodies: HIF-1α (1:1000 dilution, GeneTex, Irvine, CA), VEGF-A (1:500 dilution, Abcam, Cambridge, MA), c-MET (1:1000 dilution,Thermo Fisher Scientific), eNOS (1:1000 dilution, Cell Signalling, Danvers, MA, USA), phosphorylated p42/44 MAPK (1:1000 dilution, Cell Signalling) and primary mouse monoclonal antibody β-Actin (1:2000 dilution). Secondary antibodies goat anti-rabbit HRP and goat anti-mouse HRP (1:2000 dilution) were from Dako (Agilent, Santa Clara, CA). Bound antibodies were detected with Supersignal West Pico or Femto Chemiluminescent substrate

(Thermo Fisher Scientific). Chemiluminescence was quantified using ChemiDoc XRS (Biorad).

3.2 Hypothesis 2:

CPX+S1P potentiates angiogenesis *in vivo*

3.2.1 Rationale for using sponge implant model

Hypothesis 2 seeks to assess if CPX+S1P potentiates angiogenesis *in vivo*. There are variety of *in vivo* angiogenic models which has been well reviewed by Staton et al. (2009) [251]. Their advantages and limitations are highlighted in Table 2. The choice *in vivo* model should be one that reflects reality, where reality is defined in terms of applicability to patient treatments and the relevance to the site of evaluation [305]. The 'gold standard' angiogenic model is often cited as the corneal assay system [305], because angiogenesis occurs in an apparently neutral site and its response is easily documented throughout the induction period. Nonetheless, the concept of 'neutral' is paradoxical as blood vessels normally do not grow in this avascular site and the cornea is a 'privileged site' i.e., protected from circulating cells, rapid immune reactions and many serum components [305]. Hence the angiogenic response in the cornea would be different from 'non-privileged sites' like the skin.

There are two *in vivo* models which are relevant for skin wound angiogenesis: (i) the dorsal wound chamber and (ii) the subcutaneous sponge implantation.

Both models allow for serial drug administrations (topical/ intra-dermal injection). I have chosen the subcutaneous sponge implantation over the dorsal wound chamber as it provides an experimental environment of defined dimensions where only new vessels and not existing vessels can be measured and it is also technically less demanding. Since 1951, when sponge implantation was first established by Grinlay and Waugh, many angiogenic compounds have been developed from this model [247-248].

There are a variety of subcutaneously implanted sponges. They include stainless steel mesh chambers, hollow chambers with porous walls and synthetic sponge matrix (polyvinyl alcohol (PVA), cellulose acetate, polyester and polyurethane) implants [306]. These sponges induce a foreign tissue reaction which allow for a rapid deposition of connective tissue around the sponge, creating an artificial tissue space into which plasma infuses and a fibrin clot is which is subsequently replaced by granulation tissue [249,250].

Various angiogenic parameters can be measured from the sponge granulation tissue [306]. They include (i) the endothelial fractional area, (ii) the fraction of EC immunoreactive for proliferating cell nuclear antigen, (iii) the rate of blood flow measured by ^{133}Xe clearance, (iv) the leakiness of vessels measured by fluorescein dye diffusion, (v) the amount of functional vessels measured by haemoglobin levels in the sponge, (vi) the length of functional vessel measured by FITC-isolectin perfused length and (vii) the levels of angiogenic stimulants from sponge exudates.

In Hypothesis 2, I assessed angiogenesis in a subcutaneously implanted PVA sponge under a mono or combinatory intradermal injection of CPX and S1P. Here angiogenesis is determined using two parameters: (i) EC infiltration, and (ii) functional vessel length. ECs are identified with an endothelial cell specific antibody, while functional vessels are identified by isolectin tail-vein perfusion [252-254].

Table 2. *In vivo* angiogenesis assays [251, 305]

Model	Overview	Advantages	Disadvantages
Subcutaneous (S.C.) sponge implantation [307] (done on rats/mice)	Drugs injected into S.C implanted sponges (polymer/ steel/ matrigel). Vessels in bisected sponges immunostained and quantified after 1-3 weeks.	• Simple and fast procedure. • Measurement of new, not existing vessels. • Allows serial application. • Other parameters of granulation tissue can be assessed. • Radioactive tracer clearance allows study of blood flow.	• Angiogenic responses varies widely depending on implant size, structure, porosity, composition and implant site. • Foreign body giant cells secrete angiogenic cytokines which may mask effects of test substance.
Chicken embryo chorioallantoic membrane (CAM) [308]	Drugs released from disc implants on CAM or injected intravenously or intra-allantoically. CAM vessels examined via image analysis or colorimetric detection methods after 1-3days.	• Immunotolerant. • Simple and fast procedure. • Inexpensive. • Allows serial application.	• Large number of eggs required for consistency. • Dramatic heterogeneity of the vasculature & difficult to distinguish new from existing vessels. • Growth of new blood vessels on CAM almost 2D • Cells responding are embryonic. • Diffusion of drugs and growth factors compromised by membrane's peripheral location. • Non-mammalian system.

Model	Overview	Advantages	Disadvantages
Corneal Angiogenesis [309] (done on rabbits guinea pigs, rats and mice)	Drugs released from pellet implanted in cornea pocket. Alternatively, tumour fragments implanted in cornea pocket and drugs topically applied. Cornea vessels examined with colorimetric detection methods.	• Avascular cornea allows real time monitoring of vessel formation. • Allows serial application.	• Technically demanding in small corneas. • Angiogenic process differs between vascular and avascular tissues.
Dorsal skin fold chamber [310] (done on rabbits, mice, rats and hamsters)	Drug solutions are topically introduced into skin chamber. Chamber made by sandwiching extended double layer of dorsal skin with two symmetrical frames. Thereafter, one layer of dorsal skin is completely removed, exposing the other layer, and chamber is cover slipped. Vessels examined by trans illumination and epi-illumination techniques.	• Chambers do not provoke angiogenesis or granulation tissue formation. • Allows repeated intravital microscopic microcirculatory studies in unanaesthetized animals over 3–4 weeks. • Allows analysis of identical blood vessels over time. • Allows analysis of vessel diameter, density, permeability, blood flow.	• Technically demanding.

Model	Overview	Advantages	Disadvantages
Zebrafish Embryo [311]	Drugs added into rearing water or injected into embryo yolksacs. Intersegmental vessels in transparent embryos examined with low-power microscope.	• Inexpensive. • Large-scale screening.	• Non-mammalian system.
Angiomouse [312]	Drugs systemically or locally delivered into implanted tumours that express green fluorescence protein. Fluoresence stero microscopy images vessels as dark networks against against fluorescent background.	• Allows for real time non-invasive quantification of vessel density and length.	• Sensitivity compromised as fluorescence absorbed by surrounding tissues.

3.2.2 PVA sponge implant model

11 Male Sprague-Dawley rats (~300 g) were anesthetized with 2-3% isofurane and 1 litre per minute oxygen. Using standard aseptic procedures, four subcutaneous pockets were prepared in the dorsum of each rat by blunt dissection through 1.5 cm incisions; pockets were positioned in a 3 cm x 3 cm square configuration, with one pocket at each corner (Figure 3.1). A single saline soaked PVA scaffold (1 x 1 x 0.5 cm) (Merocel, Medtronic, CT) was inserted into each subcutaneous pocket, and incisions were closed with interrupted sutures. Analgesic buprenophrine (0.05 mg/kg) and antibiotics enrofloxacin (5mg/kg) was subcutaneously given over 5 days.

7 days post-implantation, 200 µl of drug solution was injected into the center of each implanted sponge. All four sponges in each rat were injected with the same drug. The drug treatments were: (1) Control (vehicle): 4 mg/ml Fatty-acid free rat serum albumin with 1% dimethyl sulfoxide in saline solution; (2) Vehicle plus CPX (0.01 mM, 0.1 mM, 1 mM); (3) Vehicle plus S1P (0.001 mM, 0.01 mM, 0.1 mM); (4) Vehicle plus CPX (0.1 mM) plus S1P (0.01mM). Drugs were injected on alternate days over a 14-day period. On the day of harvest 1 ml of 0.5 µg/µl of fluorescein isothiocyanate (FITC)-tagged isolectin from *Bandeira simplicifolia* (reconstituted in saline containing 1 mM calcium chloride) was injected through the tail vein. 20 min post-injection, the rats were euthanized with carbon dioxide. Sponges were explanted, bisected and frozen-embedded for cryosectioning. All animal experiments were reviewed and approved by the Institutional Animal

Care and Use Committee of the Biomedical Research Committee (BRC IACUC, protocol number 140929).

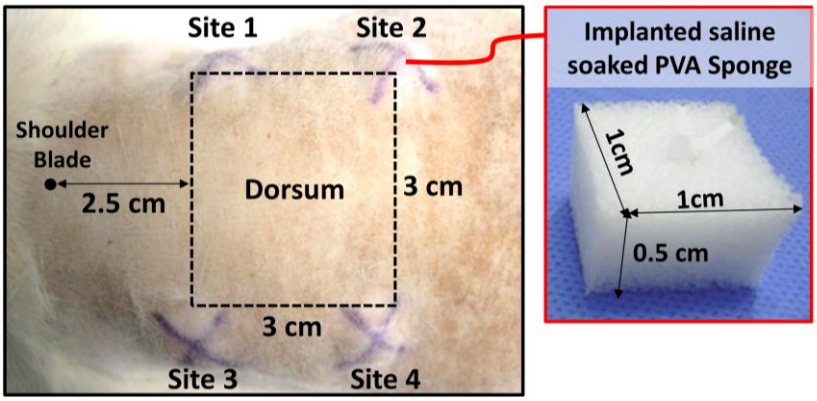

Figure 3.1 Schematic illustration of 4 sites on the dorsum of a rat, where saline soaked PVA sponges were subcutaneously implanted.

3.2.3 Immunohistochemistry for excised PVA sponges

PVA samples were cryosectioned at 2 µm or 50 µm thickness (for confocal imaging) and fixed in ice-cold acetone for 20 minutes. After blocking non-specific binding with 5% BSA and 10% goat serum (Dako), endothelial cell infiltration into the sponges was assessed with a mouse monoclonal antibody against rat endothelial cell antigen-1 (RECA-1) at 1:50 dilution (16 hours, Hycult Biotech, Uden, The Netherlands) and a secondary Alexa Fluor 594-conjugated goat anti-mouse antibody, cross adsorbed against rat IgG at 1:400 dilution (1 hour, Thermo Fisher Scientific). FITC-isolectin-perfused vessels were visualised with rabbit monoclonal anti-FITC at 0.005 mg/mL (16 hours, Thermo Fisher Scientific) and a secondary Alexa Fluor 488-conjugated goat anti-rabbit antibody at 1:400 dilution (1 hour, Thermo Fisher Scientific). Cell nuclei were stained with 0.5 mg/mL DAPI in PBS. 40x magnification images were captured using Zeiss LSM 510 laser scanning confocal system (Zeiss, Goettingen,

Germany) while 4x and 20x magnification images were captured with Olympus IX31 microscope (Tokyo, Japan).

3.2.4 Morphometric analysis of vessel length and EC infiltration

Analysis of RECA-1 positive immunostained areas (20x magnification field of view) and FITC-isolectin perfused vessel length (40x magnification field of view) was performed using ImageJ software. To measure the perfused vessel length of sprouts, 3D confocal images of FITC-isolectin staining were projected onto a 2D plane and processed as previously reported by my lab [21]: enhancing contrast, despeckling, smoothening through Gaussian blur, converting to binary image, threshold and skeletonizing with the Image J plugin: AnalyzeSkeleton.

3.3 Hypothesis 3:

CPX+S1P increases diabetic wound contraction

3.3.1 Rationale for using female Zucker Diabetic Fatty Rats

Hypothesis 3 seeks to assess if CPX+S1P increases diabetic wound contraction in an animal model. Pigs are considered to have the most translational utility due to their similar histological and biochemical properties to human skin [261]. They are similar to human skin in terms of: thickness; having follicular structures that extend deeply into the dermis; well-developed rete ridges and dermal

papillary bodies; epidermal turnover time; abundant subdermal adipose tissue; vascular plexus; and dermal collagen arrangement [261]. However, their high cost for upkeep and difficulties in handling has favoured the routine use of smaller rodent/murine models.

Type 2 diabetic rodent model chosen

In this Hypothesis, I have chosen a type 2 diabetic rodent model, reflective of the current global situation where 85 - 90 % of diabetics are type 2 diabetic [313]. Type 2 diabetes is characterised by insulin resistance and at times may be accompanied by a low insulin production. This is in contrast to type 1 diabetes which is solely characterised by a low insulin production. Table 3 provides a list of the currently available models for type 2 diabetes.

Obese Type 2 Zucker diabetic fatty (ZDF) female rats chosen

Animal models of type 2 diabetes can be divided into two groups: obese and nonobese [314]. As type 2 diabetes in humans is closely associated to obesity, I elected to use an obese strain [314]. Obesity in animals can be induced either through genetic and/or dietary means. Monogenic models of obesity arising from a defective leptin signalling are commonly used in type 2 diabetes research. The leptin hormone induces satiety. Thus a leptin receptor mutation, exhibited in ZDF rats, results in hyperphagia and subsequent obesity [255]. In female obese ZDF rats, induction of diabetes also requires a high fat diet [256]. Here the normal lab diet (on a caloric basis usually around 26% protein, 63% carbohydrate and 11% fat) is replaced with a a diet where the number of calories from fat is increased substantially (around 58% of energy derived from fat)

[314]. A high fat diet induces lipotoxicity of pancreatic beta cells and skeletal muscle cells, which in turn supresses insulin secretion and cellular glucose uptake, elevating blood glucose levels [257, 258]. Not all strains of diabetic animal models develop diabetic complications [314]. Here I chose ZDF rats as they are well-established [255,259,260] to exhibit typical diabetic humans traits of hypertension, neuropathies, nephropathies, polyuria, polydipsy, dysfunctional vasodilation [315–317], leaky vessels [318], impaired angiogenesis [319] and impaired wound closure [20]. In particular the female ZDF rats were chosen over the males as they were recently reported to exhibit a more severe wound healing impairment than their male counterparts [20]. Females are reported to exhibit a more severe reduction in granulation tissue formation and elevated levels of wound matrix metalloproteinases (MMP-3, MMP-13) [20]. To date, the exact mechanism of this gender bias in wound healing is not known.

Differences between human and rodent skin

There are several differences between human and rodent skin which are highlighted in Table 4. A striking difference lies in their mechanism of wound closure. Unlike humans which heal by both contraction and re-epithelialization, loose-skin rodents heal mainly by extensive contraction. Thus the next section is dedicated to discussing techniques to limit extensive wound contraction in rodents.

Table 3. Animal models of type 2 diabetes

Etiology	Obese	Non-Obese
Spontaneous or Genetically derived	**MOUSE** • *ob/ob* [320] • *db/db* [321] • Kuo Kondo [322] • Yellow KK obese [323] • New Zealand obese [324] • NONcNZo10 [325] • M16 [326] • Tsumara Suzuki obese [327] **RAT** • Male Zucker diabetic fatty [328] • Otuska Long Evans Tokushima fatty [329] • James C Russel/LA corpulent [330] • Spontaneously hypertensive rat/NIH-corpulent [331] **PIG** • Female Yucatan minipigs [332]	**MOUSE** • Non-obese C57BL/6 Akita mutant [343] • Alloxan Sensitive/Lt [344] **RAT** • Cohen diabetic [345] • Goto-Kakizaki [346] • Torri [347]
Diet/Nutrition	**MOUSE** • Spiny [333] • C57/BL 6J [334] **RAT** • Israeli Sand [335] • Female Zucker diabetic fatty [256] • Ctenomys talarum [336] **MONKEY** • Obese rhesus monkey [337]	-Nil-
Chemically induced	**MOUSE** • Goldthioglucose treated obese [338] **PIG** • Micro-pig [339]	**MOUSE/RAT** • Alloxan treated [348] • Streptozotocin treated [349]

Etiology	Obese	Non-Obese
Surgically induced	**RAT** • Ventromedial hypothalamus lesioned dietary obese [340]	**ANIMALS** • Partial pancreatectomized [350]
Genetically Modified (Transgenic/ Knockout)	**MOUSE** • β_3 receptor knockout [341] • Uncoupling protein (UCP1) knockout [342]	**MOUSE** (mainly) • Transgenic/ knockout of genes implicated in insulin resistance (IRS-1 [351] , IRS-2, [352] GLUT-4 [353]), lipid and glucose metabolism (PPARs) [354], and insulin secretion (GLUT-2 [355], Glucokinase [356], IGF-1R [357]) **RAT** • Human islet amyloid polypeptide transgenic [358]

Table adapted from Chatzigeorgiou et al. (2009) [262] with permission.

Table 4. Differences between human and murine/rodent skin

Traits	Human	Rodent/ Mouse
Hair Cycle	Highly variable, region-dependent	~3 weeks
Epithelial architecture	Rete ridges present	No rete ridges
Apocrine sweat glands	Present in axilla, inguinal, and perianal skin regions	Not present
Biomechanical properties	Thick, relatively stiff, adherent to underlying tissues	Thin, compliant, loose
Hypodermal thickness	Less variable	Hair cycle-dependent
Subcutaneous muscle layer	Present only in neck region as platysma	Present throughout as panniculus carnosus
Major method of wound healing	Contraction and re-epithelialization	Extensive contraction

Table adapted from Wong et al. (2011) [263].

3.3.2 Techniques to limit extensive contraction in rodents

Unlike humans, rodents have (i) a loosely organized subdermal fascial plane, and (ii) a thin sheet of striated muscle lying between the subcutaneous fat and dermal layer called the *panniculus carnosus*. Upon injury, this rodent anatomy permits an extensive pulling of perilesional skin into the wound, limiting the wound volume for granulation tissue accumulation. Hence modeling human granulation tissue-driven contraction using loose-skinned rodents poses a challenge [264]. Current efforts to overcome extensive contraction in loose-skin animals are discussed in Table 5. They include the use of (i) wound sites with firmly anchored skin and (ii) tension off-loading devices.

I have chosen to combine three surgically simple techniques of (i) wound margin splinting, (ii) wound depth increment and (iii) *panniculus carnosus* excision to achieve low wound contraction rates, characteristic of human diabetic ulcers. The technique of wound margin splinting was first used in the 1960s. Splinting offloads tensile forces generated within and around the wound site [265,266] and has been well-established to promote granulation tissue-driven contraction [265-267]. The second technique of wound depth increment has not been demonstrated *in vivo* to attenuate contraction. Nonetheless, a recent mathematical modelling study supports this notion [269]. It is also well accepted that deeper wounds delay granulation tissue formation; as such wound depth has been a crucial predictive index for diabetic foot ulcer healing [268,270]. To allow for wound depth variation, I have identified a dorsal fat pad in ZDF rats and located the wound site over it.

Table 5. Techniques to limit extensive wound contraction in animals [264,271]

Techniques	Model	Limitations
Wound sites with firmly anchored skin	**Rabbit ear** [359] (Removal of skin and underlying perichondrium.)	Healing in the absence of an underlying vascularized soft connective tissue. Granulation tissue composition can vary with different wound ground.
	Murine Cranial Excision [360] (Removal of skin from crown down to calvarial periosteum.)	
	Murine tail excision [361] (Circumferential removal of skin collar from ~2-3cm fom tail base.)	
Tension off-loading devices	**Wound margin splinting** (Doughnut shaped splints made from silicone [362]/ steel washers [363]/ PDMS [364] fixated on perilesional wound by gluing and suturing.)	Mutilation of soft splints with self-grooming. Require rat jackets and secure bandage. Increase tensile forces around the wound site, may counteract fibrosis and scarring.
	Distraction device [365] (Screw-driven retractor with teeth projecting into the wound margin retracts the wound over a period of time.)	Alter mechanical environment.
	Wound chamber [366] (A pair of metal rings clamped together to enclose a skin fold in which one side of the fold includes a full-thickness excisional wound that has a transparent glass or plastic window.)	Implant exerts a pro-inflammatory response. Surgically demanding technique. May damage perilesional vasculature and upset angiogenic growth factor balance. Alter mechanical environment.

3.3.3 Creating a moist wound healing environment with topical gel

In Hypothesis 3, I sought to create a moist wound healing environment which is a standard of care for chronic wound treatment [272]. A moist wound healing environment is more likely to promote wound healing and autolytic debridment as compared to a dry environment [272]. Here I prepared a topical aqueous-based gel treatment using sodium carboxymethylcellulose, a natural cellulose derivative that is widely used in FDA-approved wound healing gels such as becalpermin [273]. The treatment gel contained 2% w/v sodium carboxymethylcellulose (Aquasorb A-500, Ashland, KY), 4 mg/ml fatty acid free rat serum albumin, 1% dimethyl sulfoxide with 0.1 mM CPX and 0.01 mM S1P. The placebo/control gel treatment excluded CPX and S1P. To remove air bubbles, both gel types were centrifuged under vacuum for 5 minutes.

3.3.4 Creating a full-thickness excisional wound

15 eight-week old female obese Zucker diabetic fatty (ZDF) rats (Charles River Laboratories, Boston, MA) were randomly divided into three groups: (1) nondiabetic ZDF rats treated with control gel, (2) diabetic ZDF rats treated with control gel, and (3) diabetic ZDF rats treated with CPX+S1P gel. Nondiabetic rats were maintained on standard laboratory chow while diabetic rat groups were fed with a 48% kcal high fat diet (D12468, Research Diets Inc., NJ) *ad libitum* to induce diabetes. Rats were considered diabetic when non-fasting glucose levels exceeded 160 mg/dl (9 mmol/L).

Pre-surgery procedures

Pre-surgery procedures were done in a laminar flowhood (Figure 3.2). Rats 18- to 20-weeks old were anesthetized with inhalant isoflurane (1.5%) with 2 litres per minute of oxygen and placed over a heating pad. Ophthalmic ointment was applied. Analgesic (meloxicam: 4 mg/kg), antibiotics (enrofloxacin 5mg/kg) and 4 ml of saline were subcutaneously injected. The dorsal fur was shaved (Oster Golden A5 Clipper; size 50 blade) and treated with a depilatory cream (90 seconds; Veet, Reckitt Benckiser, Slough, United Kingdom) to remove remaining fur. Remnants of the depilatory cream were removed with a wet gauze. The dorsum of the rats was disinfected with 70% ethanol.

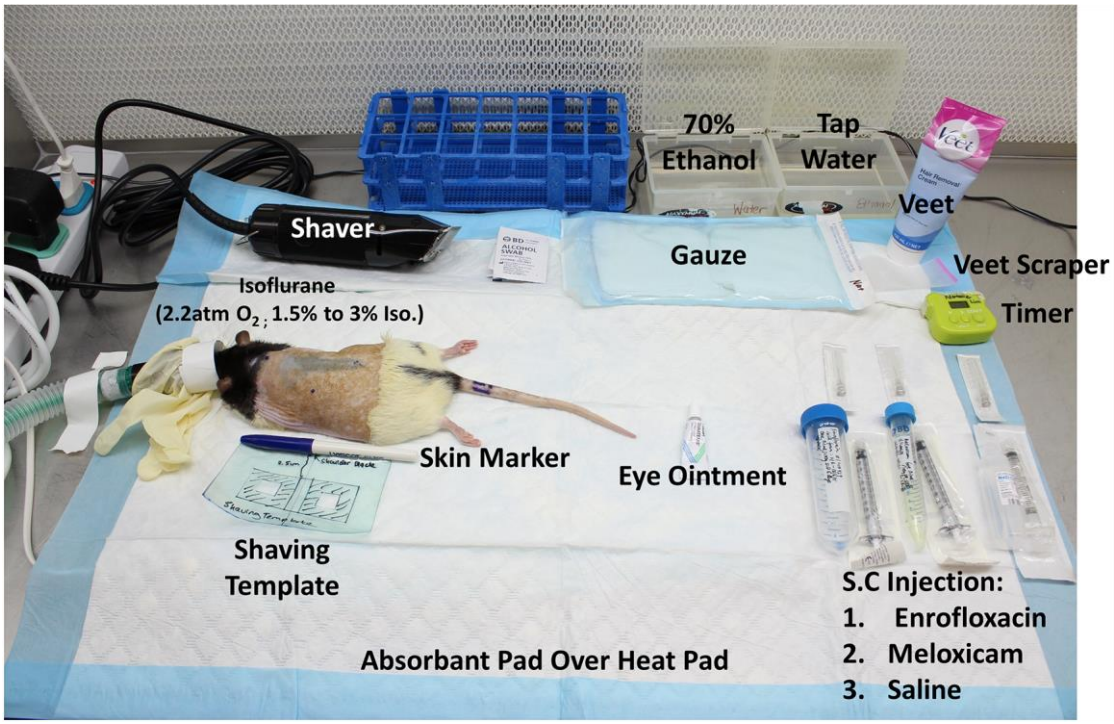

Figure 3.2 Pre-surgery setup in a laminar flow hood.

Surgical procedure: Wound depth increment

The surgical procedures were performed in a biosafety cabinet (Figure 3.3), located in proximity to a surgical side table (Figure 3.4). Rats were laid on a heating pad and continued to receive inhalant isoflurane (1.5%) with 2 litres per minute of oxygen. A sterile drape (Halyard Health, Alpharetta, GA) was overlaid on the dorsum of the rat. The dorsum of the rat was disinfected with povidone-iodine and 70% ethanol.

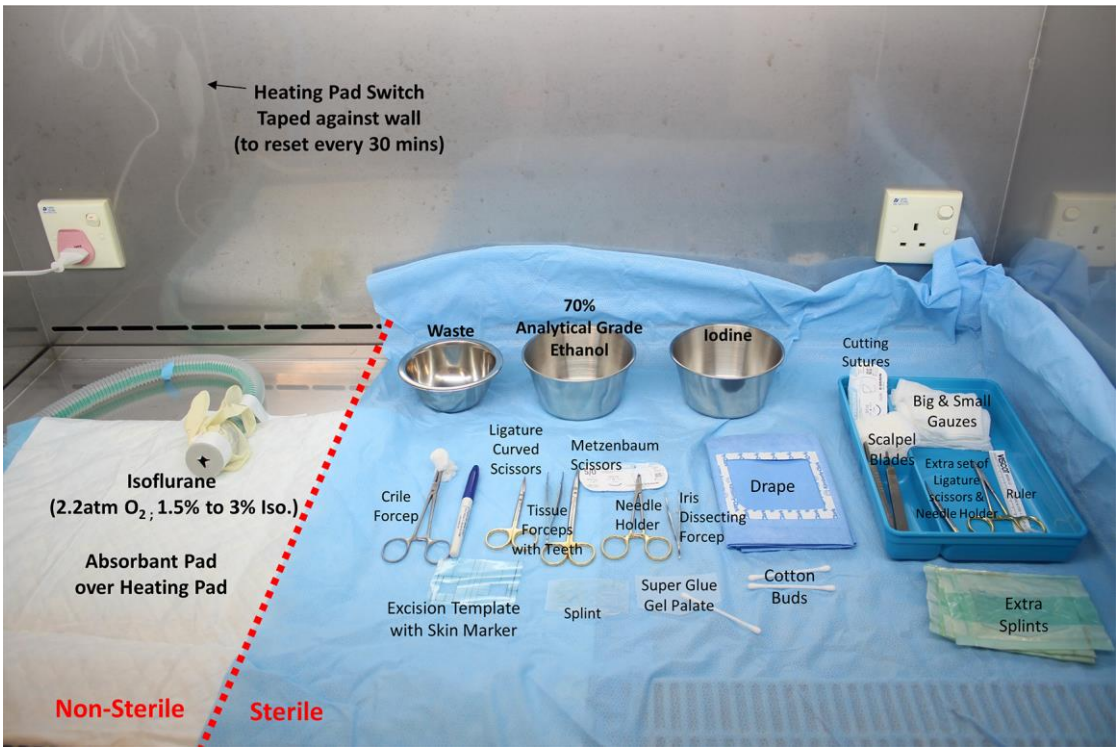

Figure 3.3 Surgery setup in a biosafety cabinet

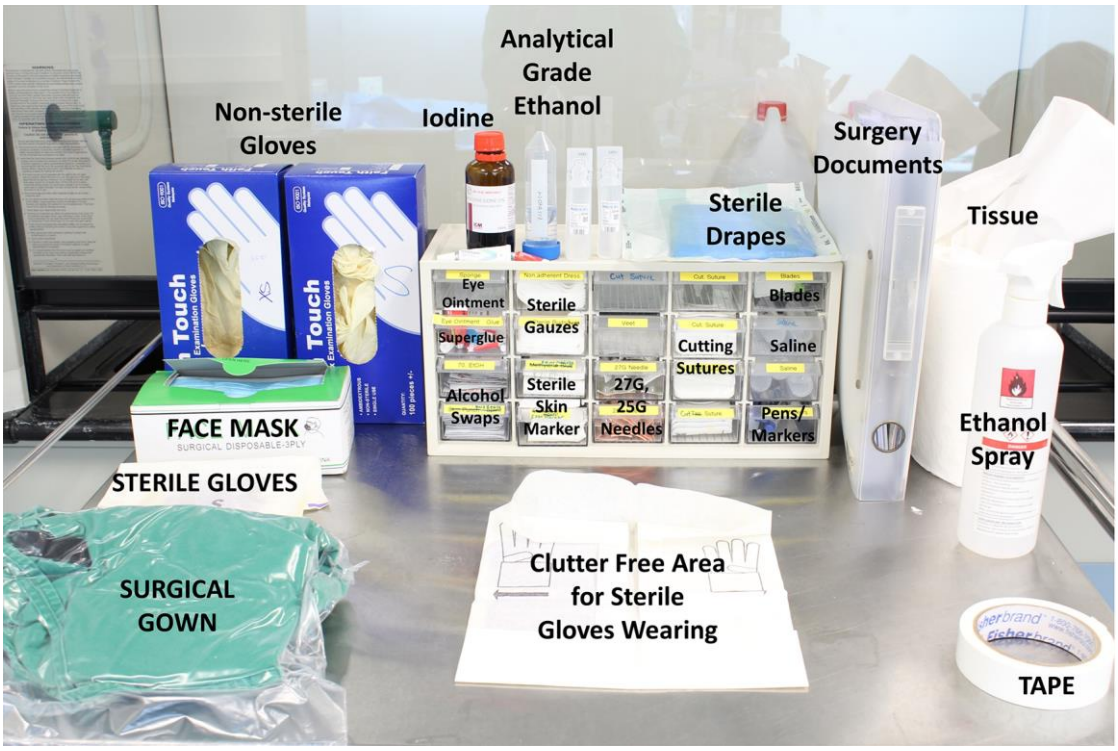

Figure 3.4 Surgery side table.

A sterile template (designed from an autoclave bag) was overlaid on the dorsum and 2 square wound sites measuring 15 mm x 15 mm, located 2.5 cm caudal to the shoulder blades and 3cm apart, were marked out with a sterile skin marker (Figure 3.5A).

To create a superficial wound of approximately 1 mm depth, an iris dissecting forcep (B.Braun, Melsungen, Germany) was used to lift the skin away the underlying fat pad. Thereafter a ligature curved scissor (B.Braun) was used to excise the full-thickness skin along the confines of the wound site (Figure 3.5B, 3.5D). Metzenbaum scissors aided in separating the skin from the underlying fat pad (Figure 3.5C).

To create a deep wound of approximately 3 mm, first create a superficial wound and then using a forcep, gently lift up the underlying fat pad and excise it with a ligature curved scissors along the confines of the square wound. The deep fascia and skeletal muscles can be clearly seen after excision. Note that contralateral wounds on the same rat were excised to the the same depth. Also during excision, isoflurane was increased to 3%.

Surgical procedure: Splinting

Superglue (Liquid; Scotch, 3M, St. Paul, MNA) was applied onto a silicone splint (internal diameter: 15 mm by 1.5 mm, Grace Bio-Labs, Bend, OR) and centred on the wound. (Figure 3.5E, 3.5F). Using a sterile gauze, the splint was gently pressed down (~30 seconds) on the perilesional skin for adherence. The splint was fastened to the edges of the wound with 16 interrupted sutures (Premilene polypropylene monofilament non-absorbable 5/0 cutting suture, B.Braun), in a progression as indicated in Figure 3.5G. As the sutures were inserted through the skin, the isoflurane was increased to 3%, and when it was pulled through and knotted, the isoflurane was reduced to 1%.

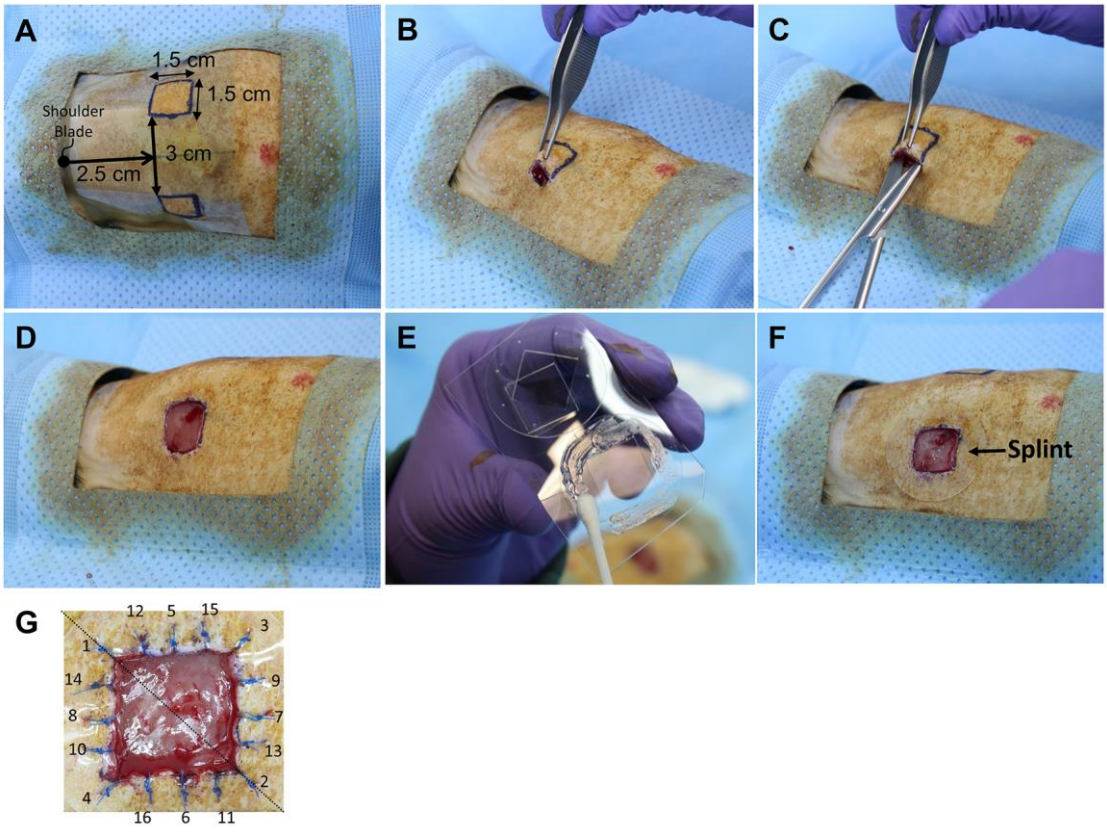

Figure 3.5 Surgical procedures.

This variation in isoflurane levels and high oxygen levels was found to be crucial for the survival of ZDF rats. An initial maintenance on 2% isoflurane and 1.5 litre per minute of oxygen throughout the surgery led to an overdosing of isoflurane in the obese ZDF rats. This is likely attributed to the high absorption of isoflurane in adipose tissue [274]. Such complication was not reported by previous groups using obese ZDF in wound healing studies [20,275], perhaps due to the much shorter surgery period in the absence of splinting.

Post-surgical procedures

Post-Surgical procedures were performed in a laminar flowhood (Figure 3.6). A non-adherent dressing (Guardian, Singapore) was overlaid onto the wound site and held temporarily in place by forceps (Figure 3.7A). Thereafter Opsite was sprayed on the dorsal region and an Opsite Flexifix dressing (Smith & Nephew, London, United Kingdom) was overlaid (Figure 3.7B). Next, a Coban bandage (3M) was placed over the dressing and affixed to the skin with adhesive tapes (Figure 3.7C). Analgesic (meloxicam: 4mg/kg), antibiotics (enrofloxacin 5mg/kg) were given 7-days post-op. 24 hours after surgery, contralateral wounds on the same rat were treated with the same drug i.e. either 0.5 ml CPX+S1P gel or 0.5 ml control gel. A treatment delay of 24 hours was elected to test the translational robustness of CPX+S1P under clinical setting where diabetics are commonly plagued with peripheral neuropathy [367] leading to a loss of cutaneous sensation and a delay in wound treatment. In this experiment, the drug treatments were continued every alternate day at which occasion wounds were photographed (EOS 600D Canon, Tokyo, Japan).

Figure 3.6 Wound dressing setup in a laminar flow hood.

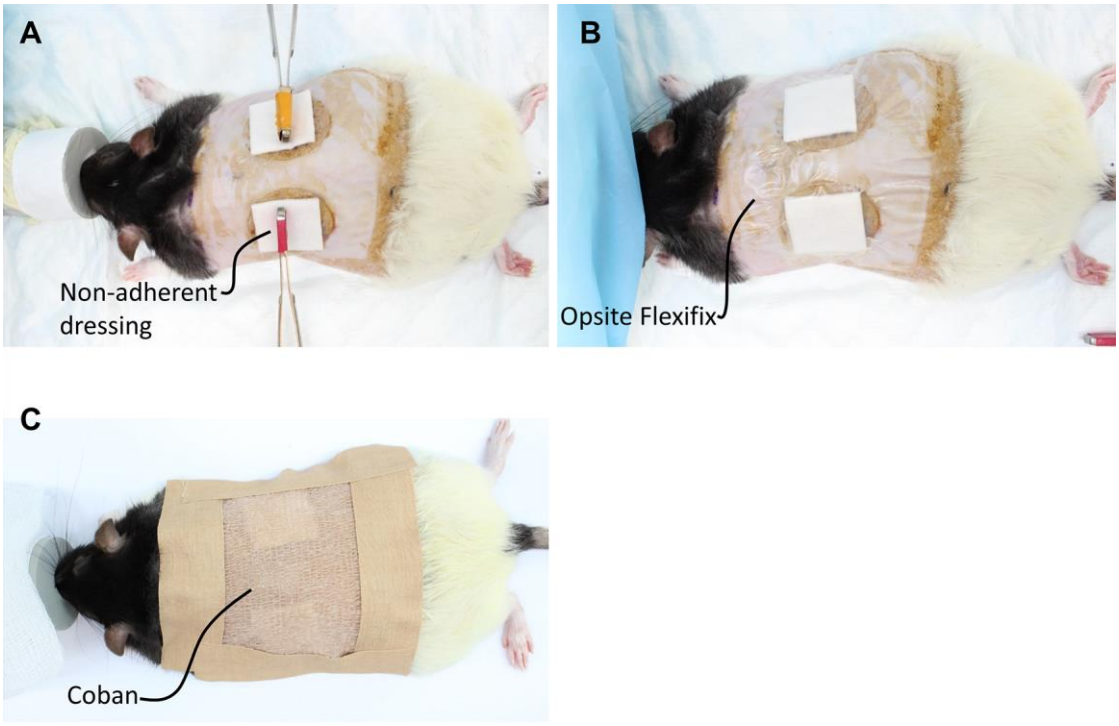

Figure 3.7 Wound dressing procedures.

Wound area measurement

Wound area was measured using ImageJ software calibrated against the internal length of the splint. From the macroscopic images, the margin of advancing epithelium was traced and the area within the margin of advancing epithelium was defined as wound area. Wound size reduction was expressed as $\% \, wound \; area = \frac{wound \; area \; on \; Day \; n}{wound \; area \; on \; Day \; 1} \times 100$. Rats were sacrificed a month post-surgery. As contraction was macroscopically observed to occur in major direction i.e. away from the spine (Figure 3.8), the wounds were bisected along the main direction of contraction. Excised wounds were next fixed in formalin overnight prior to paraffin embedding. All animal experiments were reviewed and approved by the Institutional Animal Care and Use Committee of the Biomedical Research Committee (BRC IACUC, protocol number 140929).

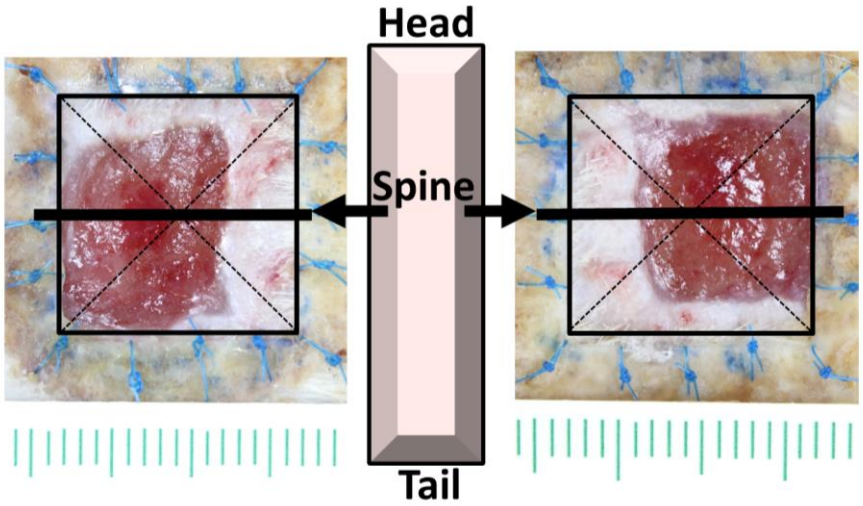

Figure 3.8 Schematics of contralateral wounds on the rat dorsum. Wounds indicated by the square) are bisected along the major direction of contraction i.e. away from the spine (indicated by a single thick solid line).

3.3.5 Histological and immunohistological staining of excised wounds

8 µm paraffin sections from the center of the wound, cut perpendicularly to the wound surface, were stained using standard protocols for hematoxylin and eosin (H&E), Masson's trichrome blue and Picrosirius red. Brightfield images were taken at 20x magnification with an Olympus IX31 microscope (Tokyo, Japan). Antigen retrieval was done at 100°C in Bond™ Epitope Retrieval Solution (Leica, Nußloch, Germany) at pH 9 for 40 minutes. Endogenous peroxidase activity was blocked for 15 minutes in 3% (v/v) hydrogen peroxide and sections were then rinsed 5 times in Bond™ Wash solution (Leica). Sections were blocked in 10% goat serum for 30 minutes prior to incubation with rabbit monoclonal antibodies to alpha-smooth muscle actin (α-SMA) (1:1000 dilution, 2 hours, Abcam), matrix metalloproteinase (MMP)-3 (1:100 dilution, 15 minutes, Abcam); rabbit polyclonal MMP-13 (1:100 dilution, 15minutes, Abcam); mouse monoclonal antibodies to RECA-1 (1:50 dilution for 16hours) and Ki-67 (1:50 dilution for 15 minutes, Dako, Agilent). Bond™ Refine Detection Kit (Leica)– polymer reagent was used to detect the primary antibody and the sections were stained with 3,3'-diaminobenzidine (DAB) as a chromogen and lightly counterstained with Mayer's hematoxylin. Apoptosis was assesed using a terminal deoxynucleotidyl transferase dUTP nick end labeling (TUNEL) assay (Merck Milipore, Danvers, MA, USA). Brightfield images were captured at 20x magnification and merged using the MetaSystem Slide Scanner (Carl Zeiss, Oberkochen, Germany).

3.3.6 Morphometric analysis of immunostained areas

Using ImageJ software immunohistochemical images were first white balanced and deconvoluted into their indiviual components using the Colour devolution plugin [276]. The 3,3'-diaminobenzidine images were converted into an 8-bit image and auto-thresholded to measure percentage area.

3.3.7 Quantification of function vessel density

RECA-1 positive vessels (with lumina containing red blood cells) were counted under a 20x magnification field of view in 6-8 randomly chosen optical fields on 2 adjacent sections (200 µm apart) per wound. The mean cross-sectional area of functional vessels was measured as the area of RECA-1 positive immunofluoresence including the lumen it surrounds. This area was measured using the ROI plugin from ImageJ software.

3.3.8 Evaluation of collagen fiber thickness

Collagen fiber thickness was assessed semiquantitatively by Picrosirius red staining viewed under linear polarized light under which thin collagen fibers appear green to greenish yellow, while thick fibers appear orange to red. To determine the proportion of thin to thick collagen fibers, we resolved the polarized Picrosirius red subtracted image into hue components using the colour threshold plugin in ImageJ. We used the following hue definitions; green to yellow 0-22, and orange to red 22-255. Images from each hue range were

converted to 8-bit hue images and thresholded and the percentage of collagen fibers in each hue per total number of collagen pixels in the image was determined.

3.3.9 MMP *in vitro* activity assay

Human MMP-3 and MMP-13 full length protein (Abcam) were activated using 4-Aminophenylmercuric Acetate (APMA) according to the manufacturer's protocol (MMP activity assay kit ab112147, Abcam). 30 ng of APMA-activated MMP-3 and MMP-13 were mixed with CPX (0 to 100 µM) for 15 min prior to exposure to the MMP red fluorescence resonance energy transfer peptide substrate. As a negative control, APMA-activated MMP-3 was mixed with MMP-3 Inhibitor V (300 ng /100 ul) (Santa Cruz Biotechnology, Santa Cruz, CA) while APMA-activated MMP-13 was mixed with its inhibitor CL82198 hydrochloride (300ng/100ul) (Tocris, Bristol, United Kingdom). Fluorescence signal was captured after one hour using a Tecan microplate reader (Männedorf, Switzerland) with a filter set of Ex/Em = 540/595 nm

3.4 Statistical Analysis

All *in vitro* and *in vivo* work was performed in replicates of 2 to 8 as indicated in the figure legends. Statistical significance was determined by Student's t-test distribution. Differences were considered statistically significant when $p < 0.05$. Data are presented as mean ± standard deviation or mean ± standard error.

Chapter 4

Results

4.1 Hypothesis 1:

CPX+S1P potentiates HIF-1 activity *in vitro*

4.1.1 CPX+S1P potentiates HIF-1α expression

The first Hypothesis in this study was to ascertain whether the combination CPX+S1P potentiates HIF-1 activity in endothelial cells (Methods § 3.1), and this proved to be the case. As HIF-1α stability is a crucial determinant of HIF-1 activity, I identified 5 hours 30 minutes as the optimal time point to detect HIF-1α protein stabilization in HUVECs (hereinafter rounded off to 6 hours for ease of display and reading). During an 8-hour follow-up after 10 μM CPX stimulation, appreciable amounts of HIF-1α protein started to accumulate one hour post-stimulation and attained a maximum at around 6 hours (Figure 4.1A). S1P also induced HIF-1α protein stabilization with similar kinetics (Figure 4.1B).

My lab previously demonstrated that ~10 μM CPX is highly effective in promoting HUVEC sprouting [21]. Accordingly, I identified 10 μM CPX and 0.25 μM S1P as optimal concentrations to increase HIF-1α protein levels *in vitro*. 10μM CPX effectively increases HIF-1α protein levels, with maximum stability beyond 20 μM (Figure 4.2A); however, I chose to use 10 μM for further studies, as higher CPX concentrations can completely cross-inhibit deoxyhypusine hydroxylase in HUVECs, resulting in an inhibition of DNA synthesis and proliferation which are crucial for sprouting [277]. S1P maximally increased HIF-1α protein levels after 6 hours without dose-dependency in the range of 0.125

μM to 1 μM (Figure 4.2B). At 6 hours, the combination of 10 μM CPX + 0.25 μM S1P increased HIF-1α expression levels by 14.0-fold compared to the untreated control, while CPX alone increased it by 10.7-fold and S1P increased it by 1.4-fold (Figure 4.3A). This HIF-1α induction by CPX+S1P exceeded ithe induction power of its individual components (14.0-fold > (10.7+1.4)-fold).

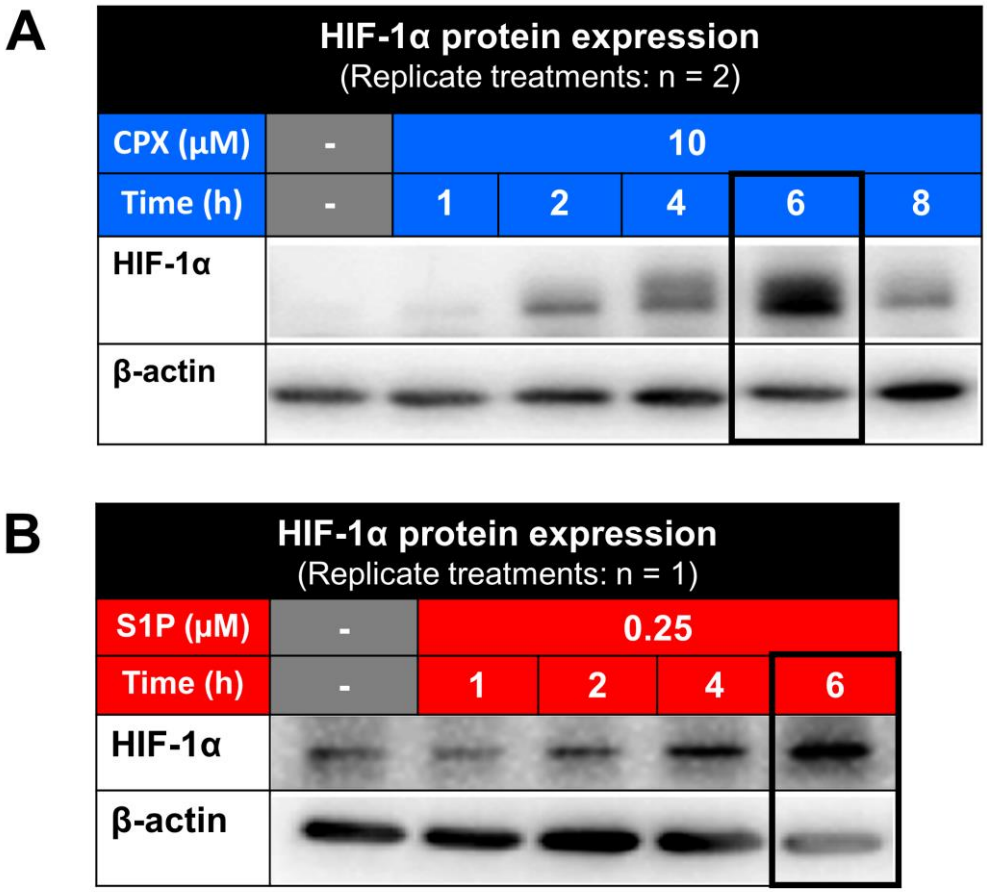

Figure 4.1. Representative western blots of HIF-1α protein and β-actin protein expression in HUVECS after treatment with: **(A)** 10 μM Ciclopirox Olamine (CPX) over time course of 8 hours; **(B)** 0.25 μM Sphingosine-1-Phosphate (S1P) over a time course of 6 hours. No quantitative assessment was made for these data sets, only a qualitative assessment was done.

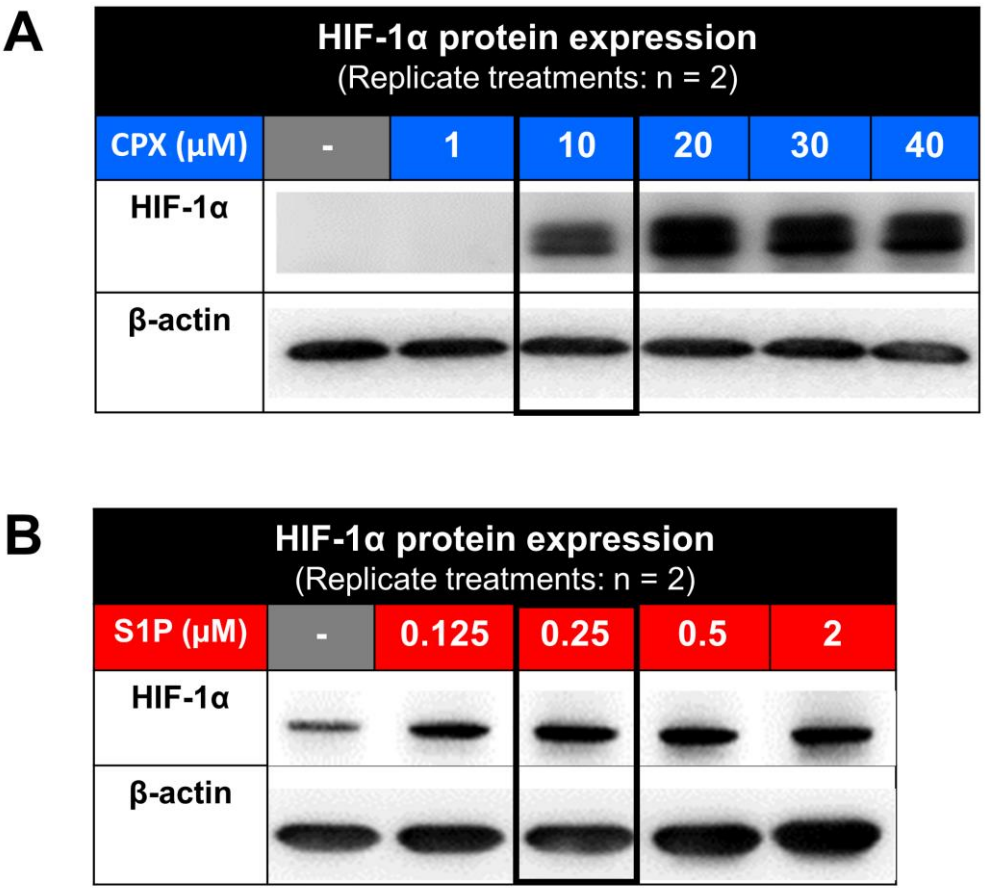

Figure 4.2. Representative western blots of HIF-1α protein and β-actin protein expression in HUVECS after treatment with: **(A)** 1 μM to 40μM CPX after 6hours and **(B)** 0.125 μM to 2 μM S1P after 6 hours. No quantitative assessment was made for these data sets, only a qualitative assessment was done.

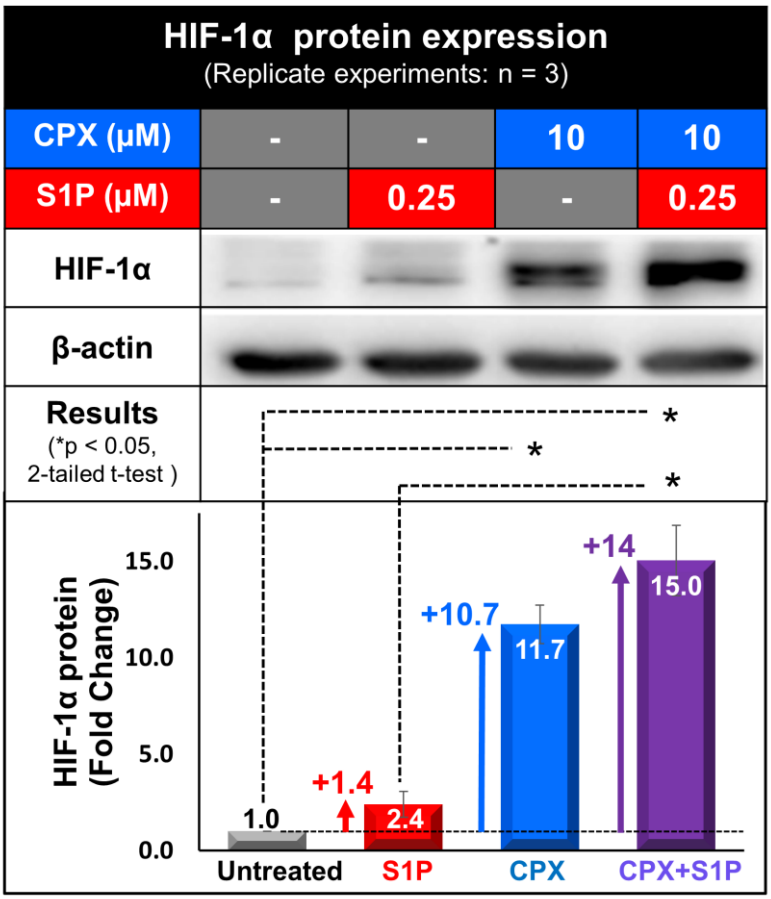

Figure 4.3. Representative western blots of HIF-1α protein and β-actin protein expression after 6 hours in HUVECS treated with individual or combination of 0.25 μM S1P and 10 μM CPX. Quantitative assessment represented in the bar graph is derived from n = 3 replicate experiments. Error bars represent standard error. Each replicate experiment is a singular treatment. CPX+S1P increases HIF-1α protein levels in a manner that exceeds its additive effect. Significance * $p < 0.05$ is derived from Student's two-tailed t-test**.**

4.1.2 CPX+S1P potentiates p42/44 MAPK activity

I determined the activation of p42/44 MAPK by assessing its phosphorylated protein levels (Methods § 3.1). The activation of p42/44 MAPK promotes the transactivation of HIF-1 complex and thus is another positive regulator of HIF-1 activity [243,244]. Compared to the untreated control, 10 μM CPX inhibited phosphorylation of p42/44 MAPK by 0.4-fold while S1P slightly stimulated it by 0.2–fold (Figure 4.4). Interestingly, the addition of 0.25 μM S1P not only reversed CPX's inhibition but also increased the phosphorylation of p42/44 MAPK by 0.8-fold in a manner that exceeds its additive effect of + 0.2-fold.

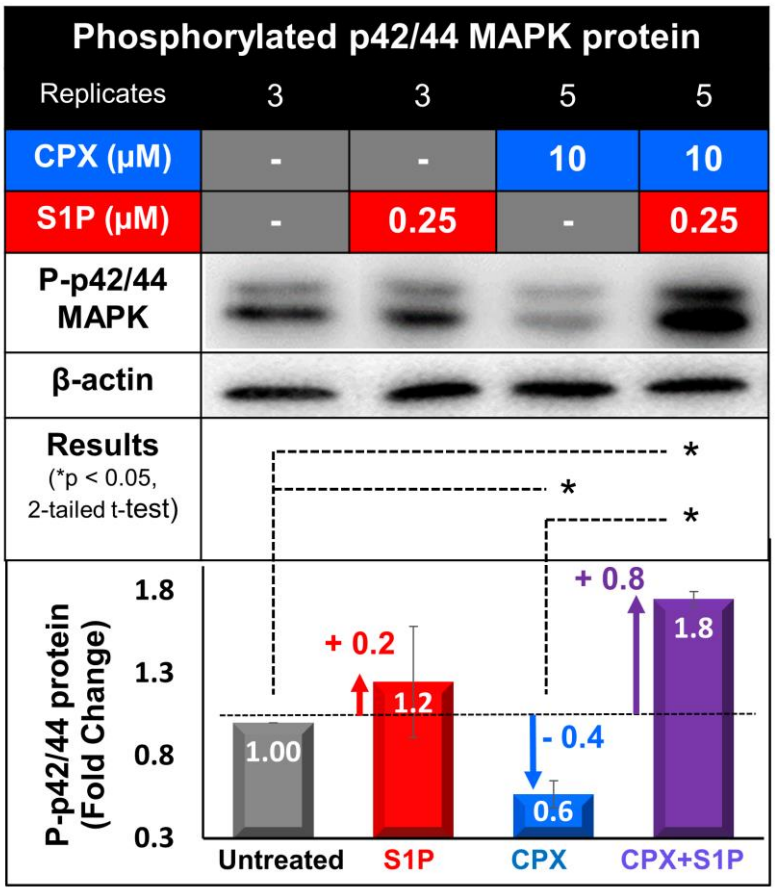

Figure 4.4. Representative western blots of phosphorylated p42/44 MAPK protein and β-actin protein expression after 6 hours in HUVECS treated with individual or combination of 0.25 μM S1P and 10 μM CPX. Quantitative assessment represented in the bar graph is derived from n = 3 or 5 replicate treatments from duplicate experiments. Error bars represent standard error. CPX+S1P increases phosphorylated p42/44 MAPK protein levels in a manner that not only exceeds its additive effect but reverses CPX-induced inhibition. Significance * $p < 0.05$ is derived from Student's two-tailed t-test**.**

4.1.3 CPX+S1P potentiates HIF-1 downstream activity

Having established that CPX+S1P increases two crucial upstream regulators of HIF-1 activity i.e., HIF-1α protein levels and Phosphorylated p42/44MAPK protein levels, I evaluated the protein expression of three HIF-1 downstream angiogenic targets (VEGF, c-MET and eNOS) in the HUVEC monolayer upon treatment with CPX, S1P or its combination (Figure 4.5 to 4.7).

10 µM CPX + 0.25 µM S1P caused an upregulation of all three HIF-1 targets in an additive manner. In the first downstream angiogenic target – VEGF, treatment with CPX alone increased its protein level by 1.1-fold compared to the untreated control while treatment with S1P alone increased it by 0.4-fold. And under their combinatory treatment, VEGF protein levels additively increased by ~ 1.7-fold. In the second downstream angiogenic target – c-MET, treatment with CPX alone induced a 1.6-fold increase in c-MET protein levels compared to the untreated control while treatment with S1P alone induced a 0.7-fold increase. Under their combinatory treatment, c-MET protein levels additively increased by ~2.4-fold. In the third downstream angiogenic target – eNOS, treatment with CPX alone increased eNOS protein levels by 1.0-fold compared to the untreated control while treatment with S1P alone increased it by 0.3-fold. Once again their combinatory treatment additively induced an increase in the eNOS protein levels by 1.0-fold.

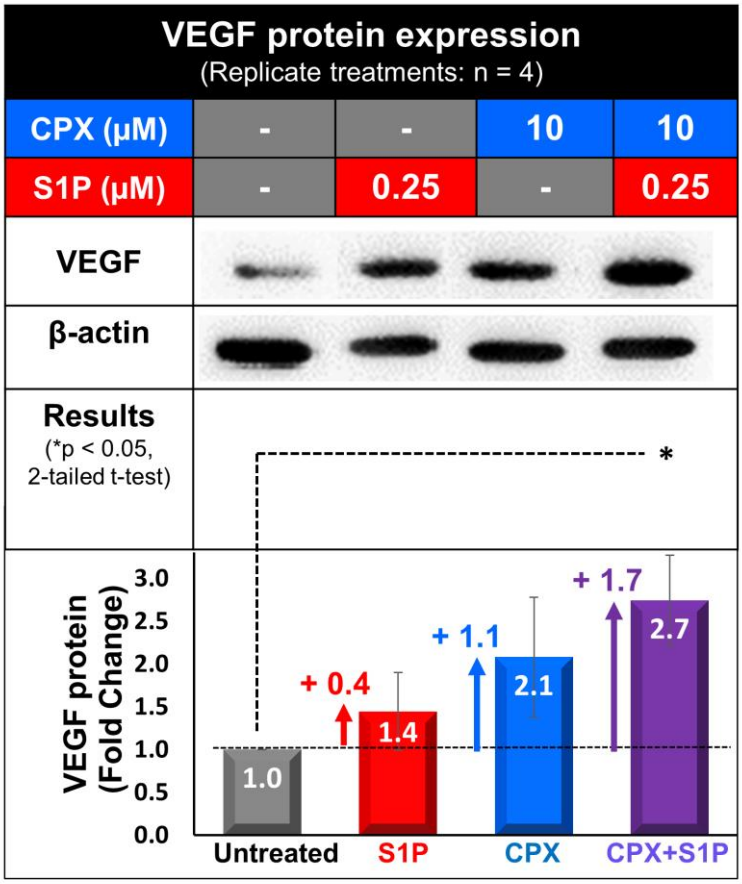

Figure 4.5. Representative western blots of VEGF protein and β-actin protein expression after 6 hours in HUVECS treated with individual or combination of 0.25 μM S1P and 10 μM CPX. Quantitative assessment represented in the bar graph is derived from n = 4 replicate treatments from a single experiment. Error bars represent standard error. CPX+S1P increases VEGF protein level in an additive manner. Significance * $p < 0.05$ is derived from Student's two-tailed t-test**.**

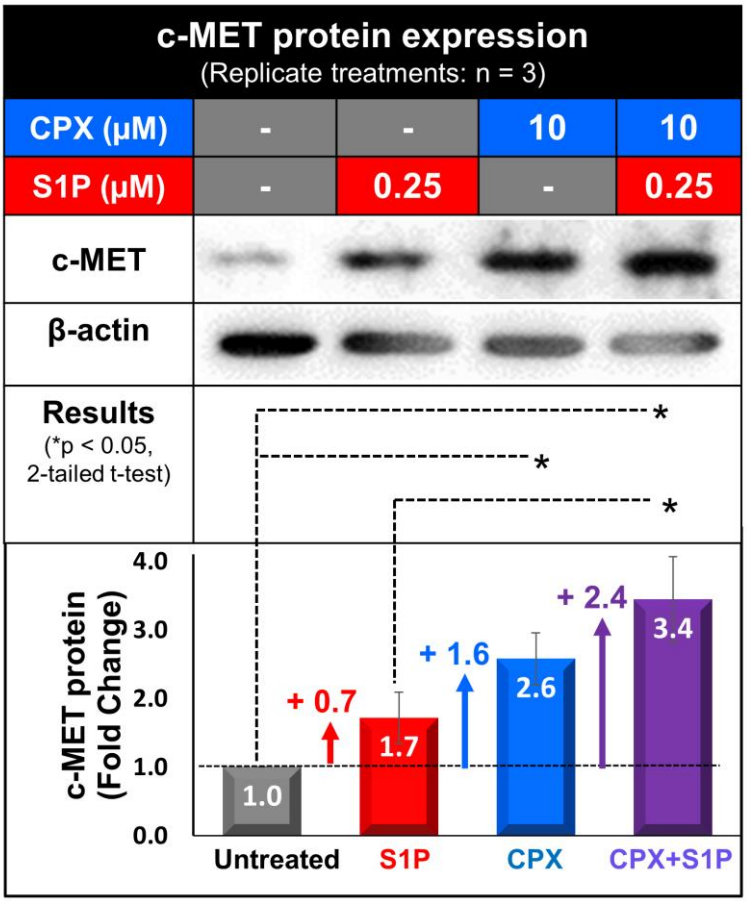

Figure 4.6. Representative western blots of c-MET protein and β-actin protein expression after 6 hours in HUVECS treated with individual or combination of 0.25 μM S1P and 10 μM CPX. Quantitative assessment represented in the bar graph is derived from n = 3 replicate treatments from singular experiment. Error bars represent standard error. CPX+S1P increases c-MET protein level in an additive manner. Significance * $p < 0.05$ is derived from Student's two-tailed t-test**.**

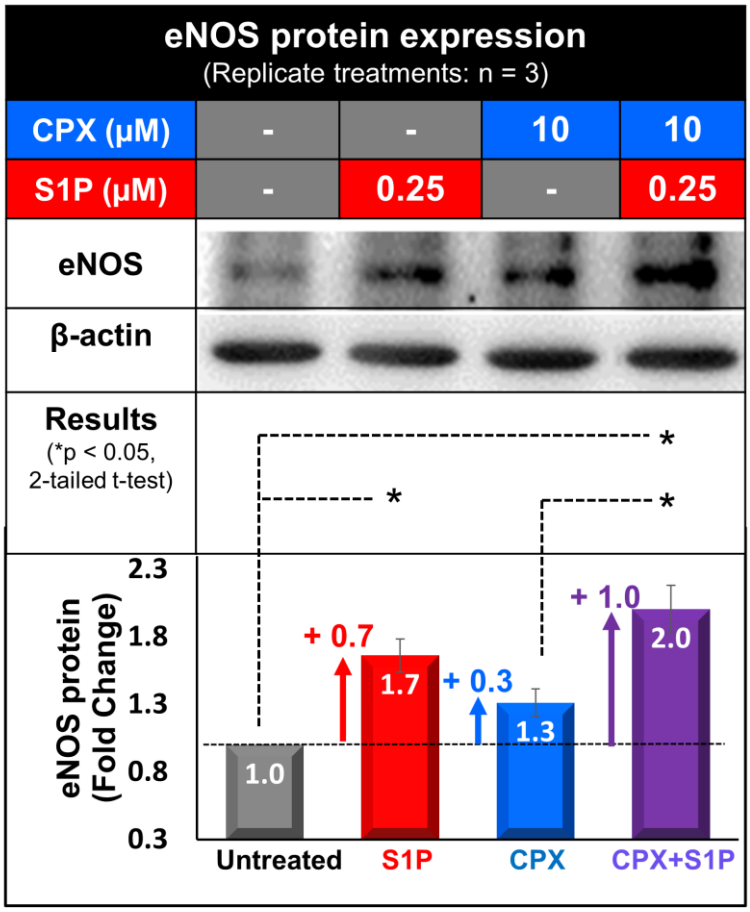

Figure 4.7. Representative western blots of eNOS protein and β-actin protein expression after 6 hours in HUVECS treated with individual or combination of 0.25 μM S1P and 10 μM CPX. Quantitative assessment represented in the bar graph is derived from n = 3 replicate treatments from singular experiment. Error bars represent standard error. CPX+S1P increases eNOS protein level in an additive manner. Significance * $p < 0.05$ is derived from Student's two-tailed t-test**.**

4.2 Hypothesis 2:

CPX+S1P potentiates angiogenesis *in vivo*

The second Hypothesis in this study was to ascertain whether the combination CPX+S1P potentiates functional vessel formation in subcutaneously implanted sponges (Figure 4.8A; Methods § 3.2), and this proved to be the case. Here CPX (0.01 mM to 1 mM) and S1P (0.001 mM to 0.1 mM) were titrated to identify a concentration that would maximally induce endothelial cell (EC) infiltration into the sponge. Surprisingly, the entire range of CPX concentrations proved effective in inducing EC infiltration (Figure 4.8B) without evident dose-dependency in the concentration range chosen. Similarly, the entire range of S1P concentrations tested induced EC infiltration, without evidence for a superior dose (Figure 4.8B). For this *in vivo* study, I chose a concentration of 0.1 mM CPX and 0.01 mM S1P. This combination potentiated EC infiltration in a manner that exceeds their additive effect (Figure 4.9). Compared to the vehicle treatment, CPX alone increases EC infiltration by 1.5-fold, S1P alone by 1.1-fold and its combination increases EC infiltration by 3.6-fold (> 2.6-fold additive effect). Moreover, I noted the formation of long contiguous EC structures under CPX+S1P treatment, suggesting functional vessel formation (Figure 4.9, white arrows). Indeed, FITC-isolectin data revealed non-leaky perfusion of these structures, demonstrating potentiation of functional vessel length under the combined treatment (Figure 4.10).

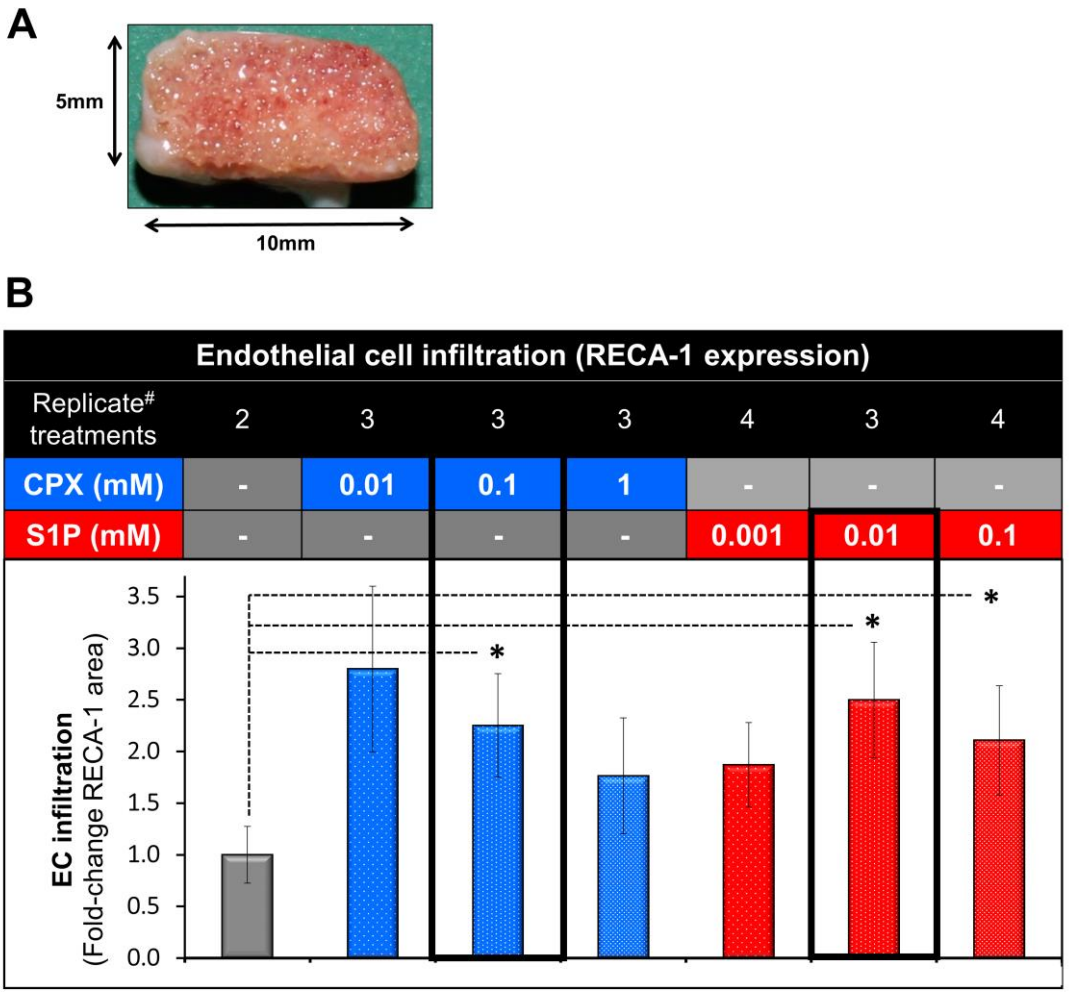

Figure 4.8. (A) Representative image of a PVA sponge explant that was subcutaneously implanted in the dorsum of a Sprague dawley rat for 3 weeks. Macroscopic observation shows granulation tissue infiltration into the centre of the sponge. **(B)** Quantitative assessment of EC infiltration into PVA sponge titrated under CPX: 0.01 mM, 0.1 mM, 1 mM and S1P: 0.001 mM, 0.01 mM and 0.1 mM. Entire titrated range of CPX, S1P induced EC infiltration. Error bars represent standard deviation. Significance * $p < 0.05$ is derived from Student's two-tailed t-test**.** n = replicate treatments in the same animal. #: Reason for n < 4: Sponges explants from sites where rats inflicted additional wounding were excluded from analysis.

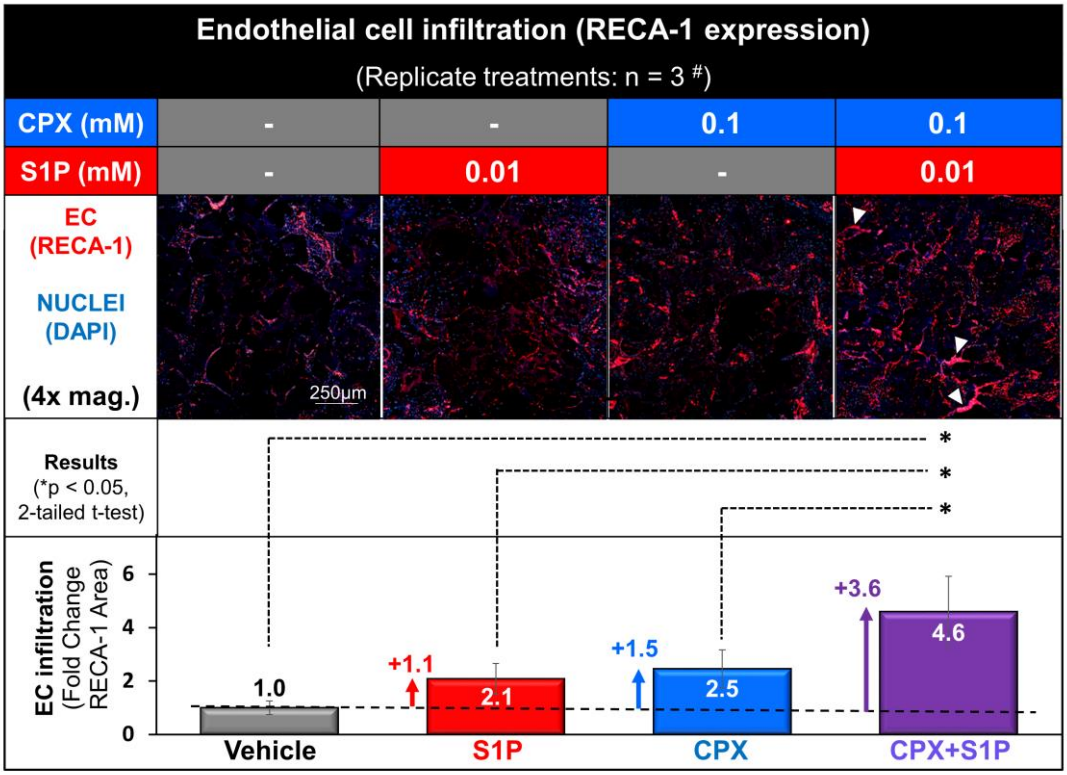

Figure 4.9. EC infiltration into subcutaneously implanted PVA sponges, identified by RECA-1 immunofluoresence (red), was potentiated under the combination of CPX 0.01 mM and S1P 0.01 mM in a manner that exceeds its additive effect. Cell nuclei identified by DAPI (blue). White arrows indicate contiguous structures of endothelial cells. Error bars represent standard deviation. Significance * $p < 0.05$ is derived from Student's two-tailed t-test**.** n = replicate treatments in the same animal. #: Reason for n < 4: Sponges explants from sites where rats inflicted additional wounding were excluded from analysis.

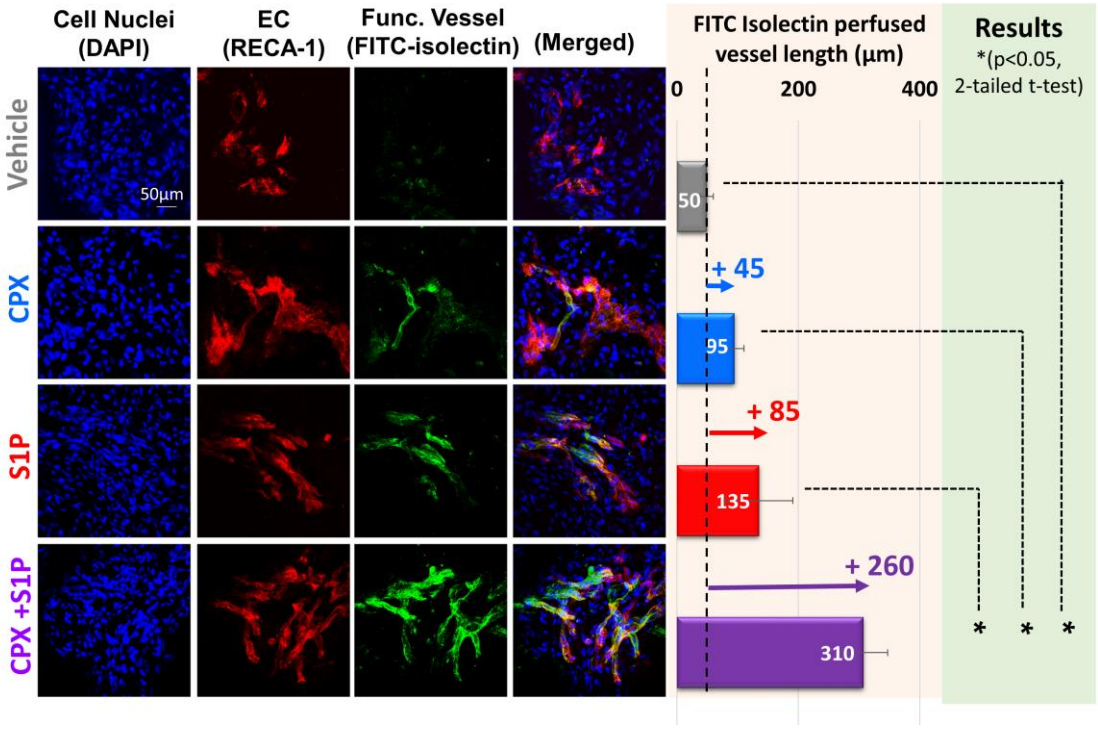

Figure 4.10. Combination of CPX 0.01 mM and S1P 0.01 mM potentiated FITC-isolectin perfused vessel length in a manner that exceeds its additive effect. Images represent 40x magnification of 2D images of vessels projected from 3D confocal stack. Cell nuclei identified by DAPI (blue), EC identified by RECA-1 (red) and functional vessels identified by perfused FITC-isolectin (green). FITC-isolectin vessel length measured using ImageJ plugin – Analyze Skeleton. Vessel length quantified from 5 to 8 random sites in each treatment condition. Error bars represent standard error. Significance * $p < 0.05$ is derived from Student's two-tailed t-test**.**

4.3 Hypothesis 3:

CPX+S1P increases diabetic wound contraction

The third Hypothesis in this study was to ascertain whether the combination CPX+S1P potentiates full-thickness wound contraction in diabetic female ZDF rats. More specifically, I assessed contraction at two wound depths i.e., 1 mm (superficial) and 3 mm (deep) (Methods §3.3.4). CPX+S1P increased contraction in deep but not superficial wounds a month post-wounding.

4.3.1 Severe diabetes successfully induced in female ZDF rats

The experiment began by inducing diabetes in female ZDF rats with a high fat diet. Overt hyperglycemia was seen after 4 weeks of a high fat diet where by non-fasting plasma glucose levels reached 550 mmol/dl (30 mg/L), a threefold increase compared to when maintained on a standard diet (Figure 4.11, Methods § 3.3.4). This hyperglycaemic condition was successfully maintained throughout the course of the experiment. Both nondiabetic and diabetic rats did not display significant differences in weight (Figure 4.11). From 12 weeks of age, the diabetic rats displayed typical hallmark traits of severe diabetes. They exhibited polyuria, urinary tract infection, pressure ulcers and dry skin (Figure 4.12A-C). They also developed fatty liver with hepatocytes containing glycogenated nuclei (glycogen vacuolations of the nuclei) (Figure 4.12D-E). The glomerulus capsular space in the kidney cortex of diabetic rats were also observed to be obliterated with hyaline. A loss of distal tubules were also

observed in the interstitial regions of the kidney cortex and were accompanied by the infiltration of inflammatory cells, a hallmark of glomerulonephritis (Figure 4.12 F-G). These effects were not observed in nondiabetic rats.

Table 6 shows (i) intended number of wounds for the different treatment conditions, (ii) the number of wounds lost (due to serious diabetic complications, isoflurane overdosing, wound infection and splints bitten off by rats) and (iii) the number of wounds remaining 4 weeks post-surgery.

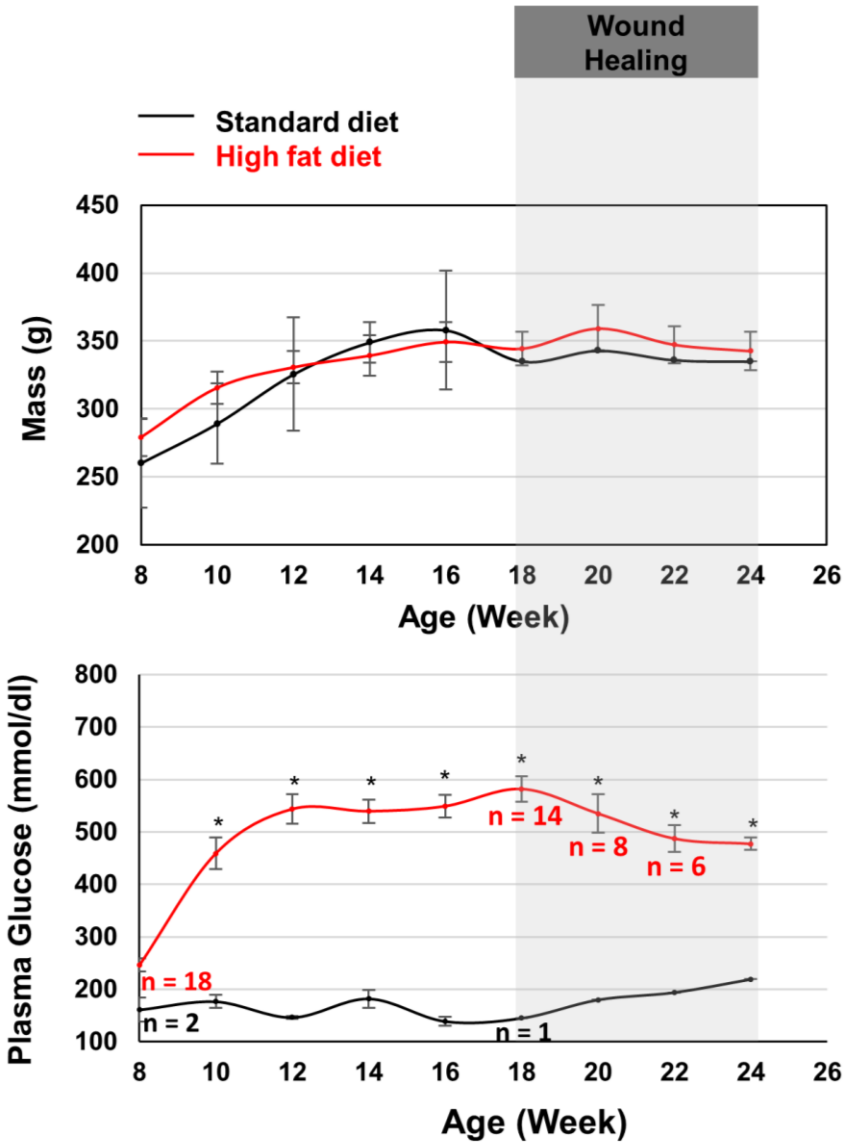

Figure 4.11 Changes in mass (top panel) and non-fasting plasma glucose levels (bottom panel) of female ZDF rats maintained on a standard diet (black line) or a 40% lard high fat diet (red line) from 8-week old for a period of 16 weeks. Increase in plasma glucose levels were observed in ZDF rats maintained on a high fat diet after 2 weeks. Significance * $p < 0.05$ is derived from Student's two-tailed t-test**.** Error bars represent standard error. n = number of rats. For convenience, only changes in n numbers are stated and specified in bottom panel. n values for the top and bottom panels are the same. Wound healing study was conducted when ZDF rats were 18 to 24-week old. The drop in rat numbers at the onset of the wound healing experiment is due to isoflurane overdosing and diabetic complications (Figure 4.12, Table 6).

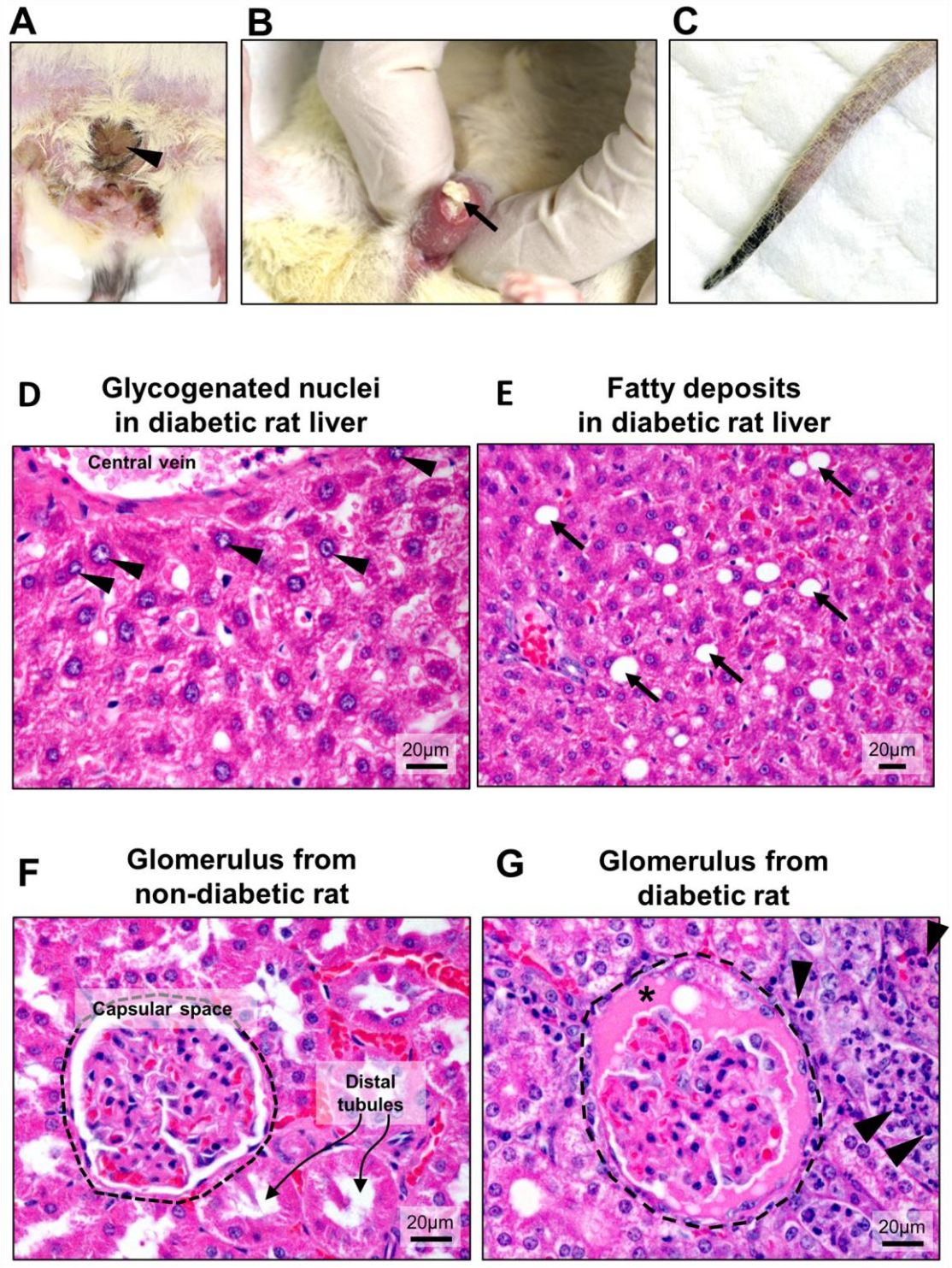

Figure. 4.12 Complications of diabetes in ZDF female rats after 16 weeks of high fat diet. Diabetic rats exhibited **(A)** pressure ulcers in their lower abdomen (arrowhead), **(B)** urinary tract infection with observable pus in their urethra (arrow), **(C)** necrotic tail (rat died prior to surgery). **(D,E)** H&E stained liver cross-section from diabetic female ZDF rat reveals glycogenated hepatocyte nuclei around the central vein (arrowhead) and fatty deposits (arrow). **(F,G)** H&E

stained kidney cortex cross-section from nondiabetic and diabetic rat. Glomerulus is traced with dotted line. *****Hyaline is observed to obliterate capsular space in the glomerulus of diabetic ZDF rats. Inflammatory interstitial infiltration (arrowhead), and loss of distal tubules were were also observed in the diabetic ZDF rat. These effects were not observed in kidney cortex of nondiabetic ZDF rat.

Table 6. Treatment conditions in the 4-week full-thickness skin wound model.

Treatment Conditions			No. of Wounds		
			Original	Lost*	Final
Deep wounds	Diabetic	CPX+S1P	10	6	4
		Vehicle	8	4	4
	Non-Diabetic	Vehicle	2		2
Superficial wounds	Diabetic	CPX+S1P	10	8	2
		Vehicle	8	6	2
	Non-Diabetic	Vehicle	2	2	0

Lost*	Isoflurane Overdosing	Diabetic Complications	Wound Infection	Splints bitten off
	3 Rats (6 Wounds)	2 Rats (4 Wounds)	2 Rats (4 Wounds)	6 Rats (12 Wounds)

4.3.2 Identification of dorsal sites for wound depth variation

I identified dorsal wound sites cranial to the transverse plane as choice sites for excision (Figure 4.13A). These sites possess a fat pad that allows for wound depth variation (Figure 4.13B; Methods § 3.3.4) that is absent in dorsal regions caudal to the transverse plane (Figure 4.13B and 4.13D). I therefore could create a superficial, yet full-thickness wound of ~1 mm depth by excising skin through the *panniculus carnosus* down to the superficial fascial layer (Figure

4.13C; short vertical arrow) or a deep (~3 mm depth) wound reaching down to the deep fascial layer (Figure 4.13C; long vertical arrow).

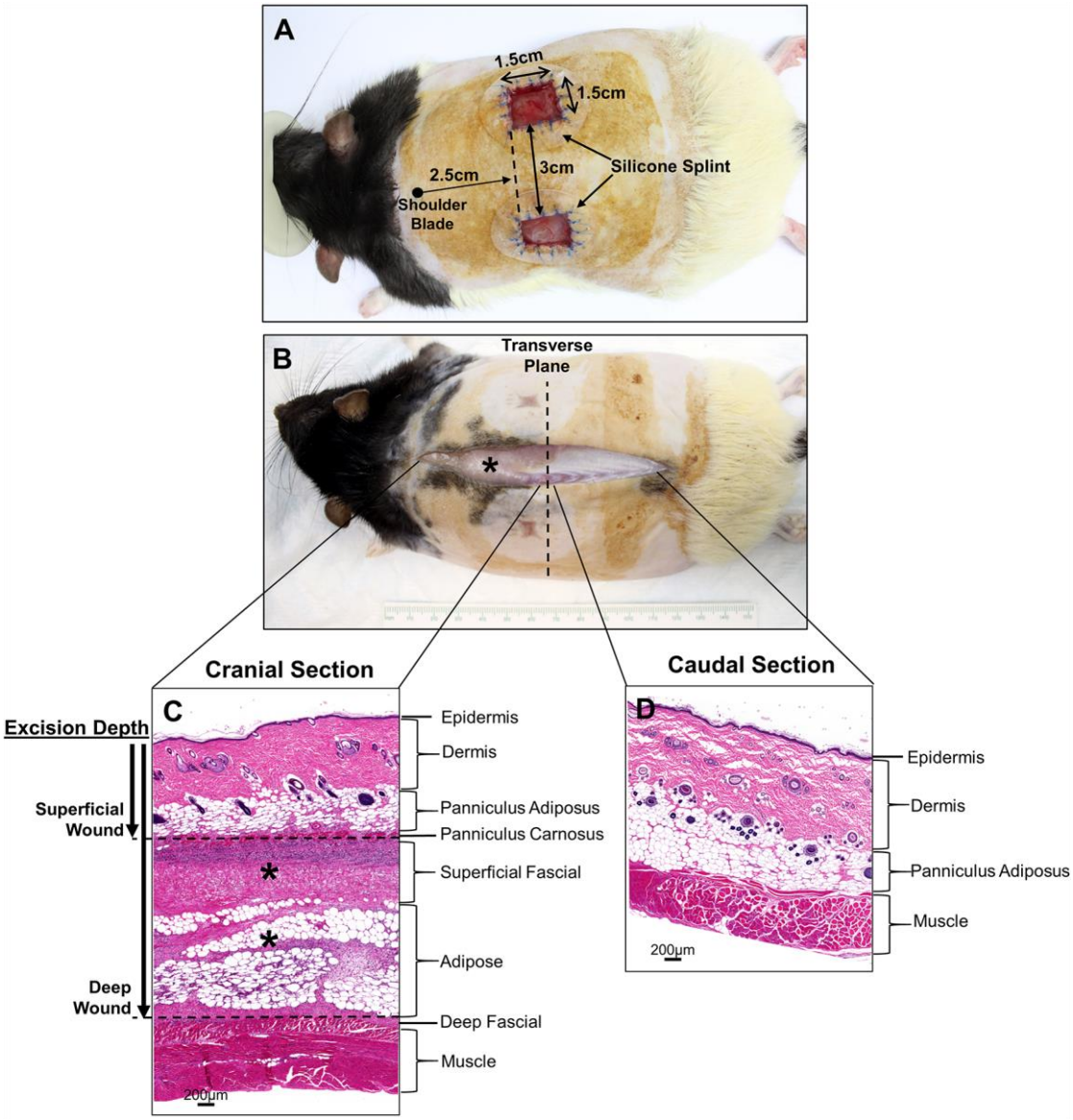

Figure 4.13. Full-thickness wound excisional model. **(A)** Two 1.5 cm by 1.5 cm full thickness skin wound were excised in the dorsal wound sites of female ZDF rats located 2.5 cm from the shoulder blade and 3 cm apart. Silicone splints were superglued to perilesional skin and sutured to the wound edges. **(B)** Full thickness skin incision along the dorsal midline of the ZDF female rat reveals a fat pad (*) located cranially but not caudally to the transverse plane. H&E stained section of skin excised down to the skeletal muscles from regions located cranially **(C),** and caudally **(D)** to the transverse plane. Vertical arrows represent

the two depths of skin excision used in this study. Superficial wounds are excised through the panniculus carnosus down to the superficial fascial. Deep wounds are excised down to the deep fascial layer. Asterisk in **(C)** (*) corresponds to the fat pad seen macroscopically in **(B)**.

4.3.3 Differential effects of CPX+S1P on wound closure at different wound depths

Wound closure was macroscopically analysed through the disappearance of light-reflecting new stroma and the replacement of a non-reflecting fully epithelialized surface (Figure 4.14; Methods § 3.3.4). 0.1 mM CPX + 0.01 mM S1P treatment was found to promote significant diabetic wound closure in deep wounds (Figure 4.14). On day 8, macroscopic images of deep wounds revealed a migration of the mobile perilesional adipose layer into the wound cavity. CPX+S1P treated deep diabetic wounds showed a strikingly redder perilesional adipose layer than control wounds, suggesting an increased vascularization and perfusion. By day 16, CPX+S1P reduced deep diabetic wound-size from 93% to 77% (Figure 4.14) and on day 18 the reduction was found to be significant (* $p < 0.05$). By day 31, CPX+S1P treated deep diabetic wounds were reduced to 27% of the original wound size while the control group was at 42%. Interestingly, CPX+S1P treatment did not significantly increase wound closure in superficial diabetic wounds, although it increased normalization of wound closure towards that of nondiabetic superficial wound healing (Figure 4.15).

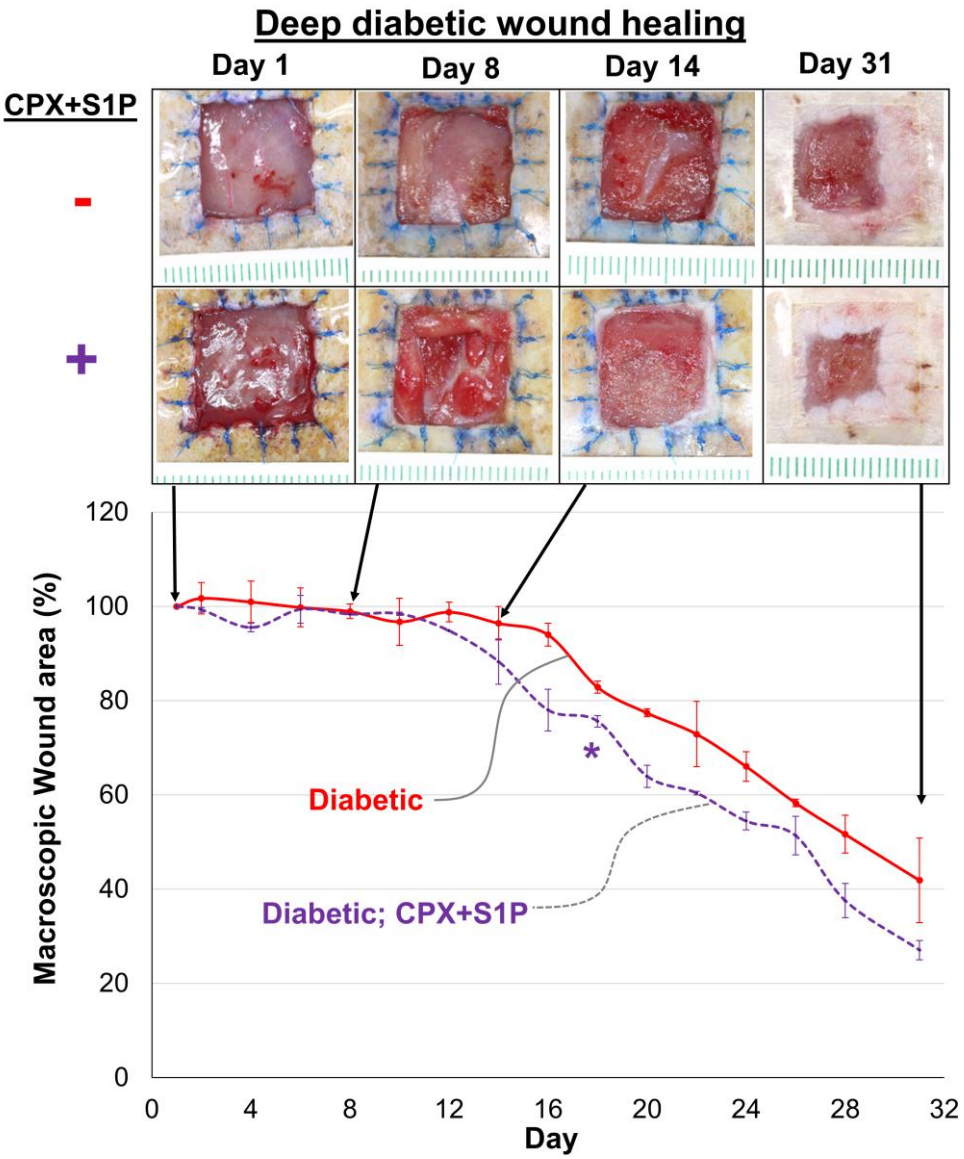

Figure 4.14 Representative macroscopic wound closure images in full-thickness deep diabetic ZDF rat wounds. Wounds were topically treated with or without 0.1 mM CPX + 0.01 mM S1P every other day starting from day 2. A millimetre rule was place beneath each wound when imaged. Graph of macroscopic wound area measured as a percentage of initial wound area reveals a significant increase in CPX+S1P treated deep wound closure on day 18. Wound area was identified as the area within the margin of the leading edge of advancing epithelium and measured using ImageJ software calibrated against the internal length of the splint. Significance * $p < 0.05$ is derived from Student's two-tailed t-test**.** Error bars represent standard error. Day 1 to 7: n = 6 wound replicate treatments. Day 8 onwards: n = 2 wound replicate treatments from the same rat. The drop in n is explained in Table 6.

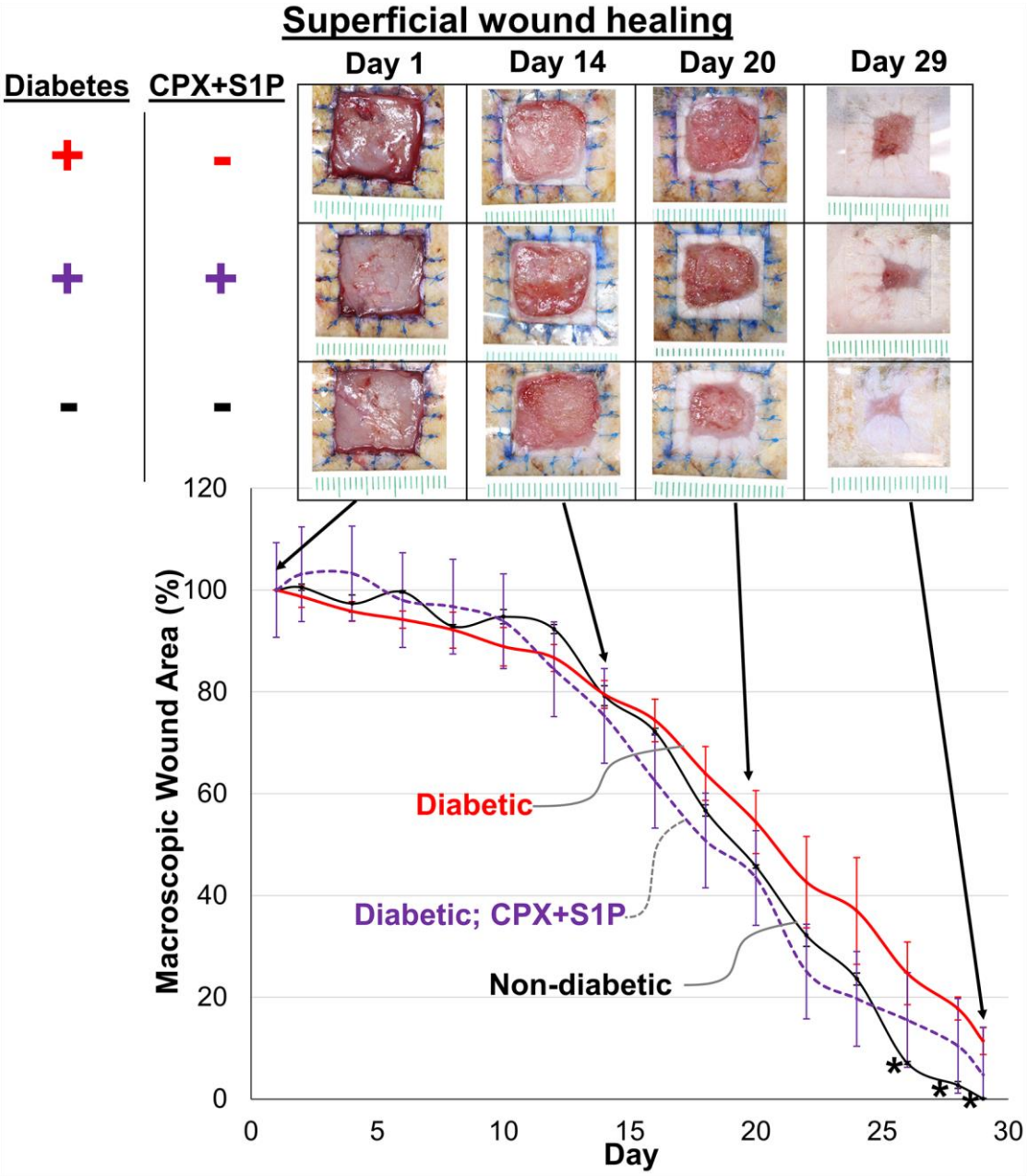

Figure 4.15 Representative macroscopic wound closure images in full-thickness superficial diabetic ZDF rat wounds. Wounds were topically treated with or without 0.1 mM CPX + 0.01 mM S1P every other day starting from day 2. A millimetre rule was place beneath each wound when imaged. Graph of macroscopic wound area measured as a percentage of initial wound area reveals a significant increase in nondiabetic superficial wound closure by day 26. Wound area was identified as the area within the margin of the leading edge of advancing epithelium and measured using ImageJ software calibrated against the internal length of the splint. Significance * $p < 0.05$ (non-diabetic compared against diabetic) is derived from Student's two-tailed t-test**.** Error bars

represent standard error. Day 1 to 7: n = 8 diabetic wound replicate treatments and n = 2 nondiabetic wound replicate treatments from same rat. Day 8 onwards: n = 4 diabetic wound replicate treatments, n = 2 nondiabetic wound replicate treatments from the same rat. The drop in n numbers is explained in Table 6.

4.3.4 Effects of CPX+S1P on wound contraction at different wound depths

To better understand the relationship between wound depth and wound closure, I measured the contribution of contraction and re-epithelialization to wound closure from H&E stained sections (Methods § 3.3.5) and expressed them as a percentage of the original wound length (Figure 4.16).

Re-epithelialization (indicated by the single headed arrow) was measured as the length of keratinocytes extending beyond the end of the unwounded dermis. Wound gap (indicated by the double headed arrow) was measured as the length between the tip of the new epithelial tongue. Contraction was measured with the formula:

$$\%\ Contraction = \frac{Original\ wound\ length - (new\ epithelial\ tongue\ length + wound\ gap)}{Original\ wound\ length} \times 100$$

Even under splinting, superficial diabetic wounds contracted by 51%, and effects of CPX+S1P remained inconspicuous. In contrast, splinted deep diabetic wounds contracted only by 8%, and here CPX+S1P significantly (** $p < 0.01$) rescued contraction from 8% to 39%. At both wound depths, CPX+S1P did not significantly increase re-epithelialization.

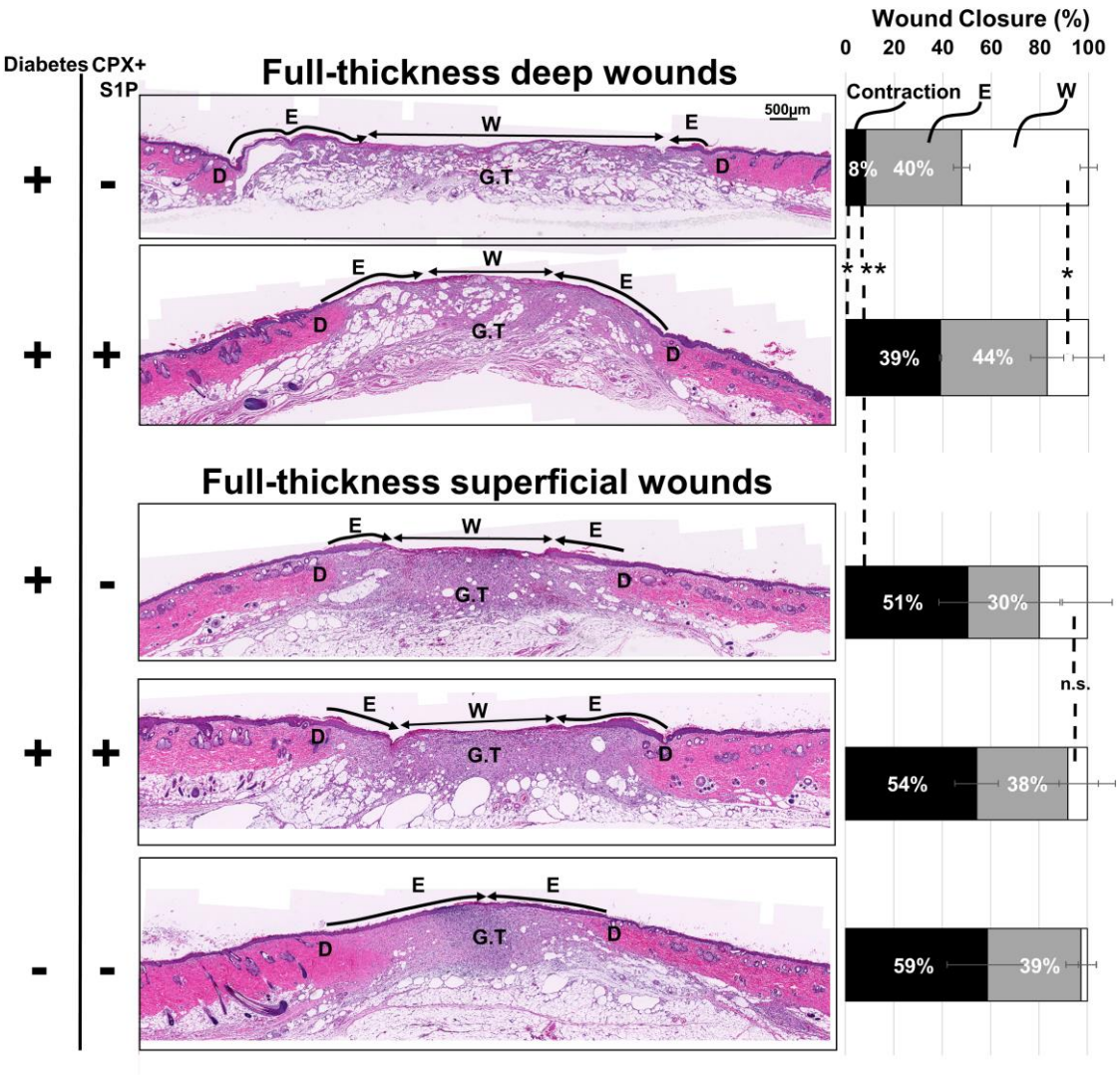

Figure 4.16 Representative haematoxylin and esosin stained full-thickness deep wounds (rows 1 and 2) and full-thickness superficial wounds (rows 3 to 5), a month post-wounding. Graph on the right represents the contribution of wound closure mechanisms: contraction and re-epithelialization. Black area represents contraction, grey area represents re-epithelialization (**E**) and white area the wound gap (**W**). These parameters are assessed from H&E stained tissue sections and expressed as a percentage of the original wound length. Re-epithelialization (indicated by **E** and single headed arrow) is measured as the length of keratinocytes extending beyond the end of the unwounded dermis (indicated by **D**). Wound gap (indicated by the **W** and double headed arrow) is measured as the length between the tip of the new epithelial tongue. Granulation tissue is indicated by **G.T**. Contraction is measured as the

difference between the original wound length and the sum of (wound gap + re-epithelialized length). Contraction was found to be significantly attenuated with an increase in wound depth, while a supplementation of 0.1mM CPX + 0.01mM S1P rescued wound contraction in in deep diabetic wounds. Significance * $p < 0.05$, ** $p < 0.01$ is derived from Student's two-tailed t-test**.** Error bars represent standard deviation. n = 4 superficial diabetic wound replicates and n = 2 deep diabetic & superficial nondiabetic wound replicates from the same rat. Note: The absence of the deep nondiabetic wound control is explained in Table 6.

4.3.5 CPX+S1P enhances granulation tissue in deep diabetic wounds

As wound contraction in humans depends on granulation tissue deposition and compaction, I evaluated the effects of CPX+S1P on collagen deposition in deep diabetic wounds (Methods § 3.3.5). Masson's trichrome blue staining of CPX+S1P-treated deep diabetic wounds suggested a collagen rich granulation matrix (Figure 4.17) while the control diabetic group appeared predominantly in red in the Masson trichrome stain, suggesting a cell-rich and collagen-poor granulation tissue (Figure 4.17). In addition, CPX+S1P treatment appeared to induce more proliferation and less apoptosis in the cellular component of the granulation tissue (Figure 4.18; Methods § 3.3.5).

These data were confirmed semiquantitatively with Picrosirius red staining (Figure 4.19; Methods § 3.3.8). Here sirius red dye binds to collagen, promoting the enhancement of its normal birefringence when the dye molecules are aligned parallel with the long axis of the each collagen molecule. When viewed under polarized light, the color and intensity of birefringence is a result of differences in the pattern of physical aggregation and thickness of collagen

fibres [278]. Thus thin and poorly packed collagen fibres appear green to greenish yellow polarizing colours, while thick and tightly packed fibres exhibit orange to red polarizing colours. CPX+S1P treatment significantly (*$p < 0.01$) increased the proportion of thick and tightly-packed collagen fibres from 42% to 85%, while decreasing thin and poorly packed collagen fibres from 58% to 15% in deep diabetic wounds (Figure 4.19).

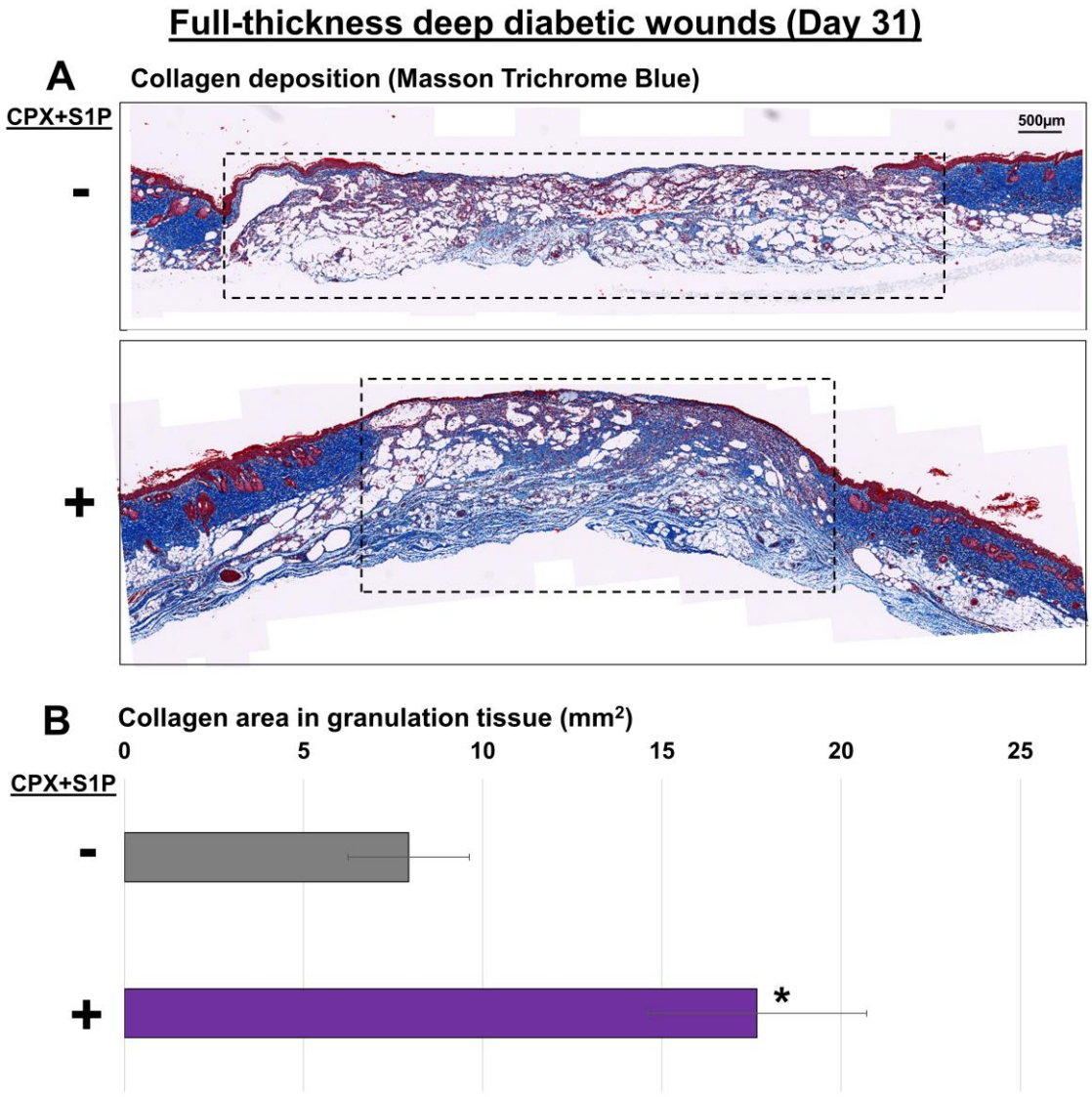

Figure 4.17 A) Representative Masson trichrome blue stained wound sections of full-thickness deep diabetic wounds 31 days post-treatment with or without 0.1 mM CPX + 0.01 mM S1P. Dotted lines indicate granulation tissue region. Qualitatively, CPX+S1P observed to increase collagen (blue stain) within the granulation tissue region. **B)** Quantitative assessment of collagen area derived from polarized picrosirus red stained sections of granulation tissue. The total area of polarized picrosirus red stain from 20x magnification images was thresholded using ImageJ. Significance * $p < 0.05$, is derived from Student's two-tailed t-test**.** Error bars represent standard deviation. n = 2 replicates derived from the same rat.

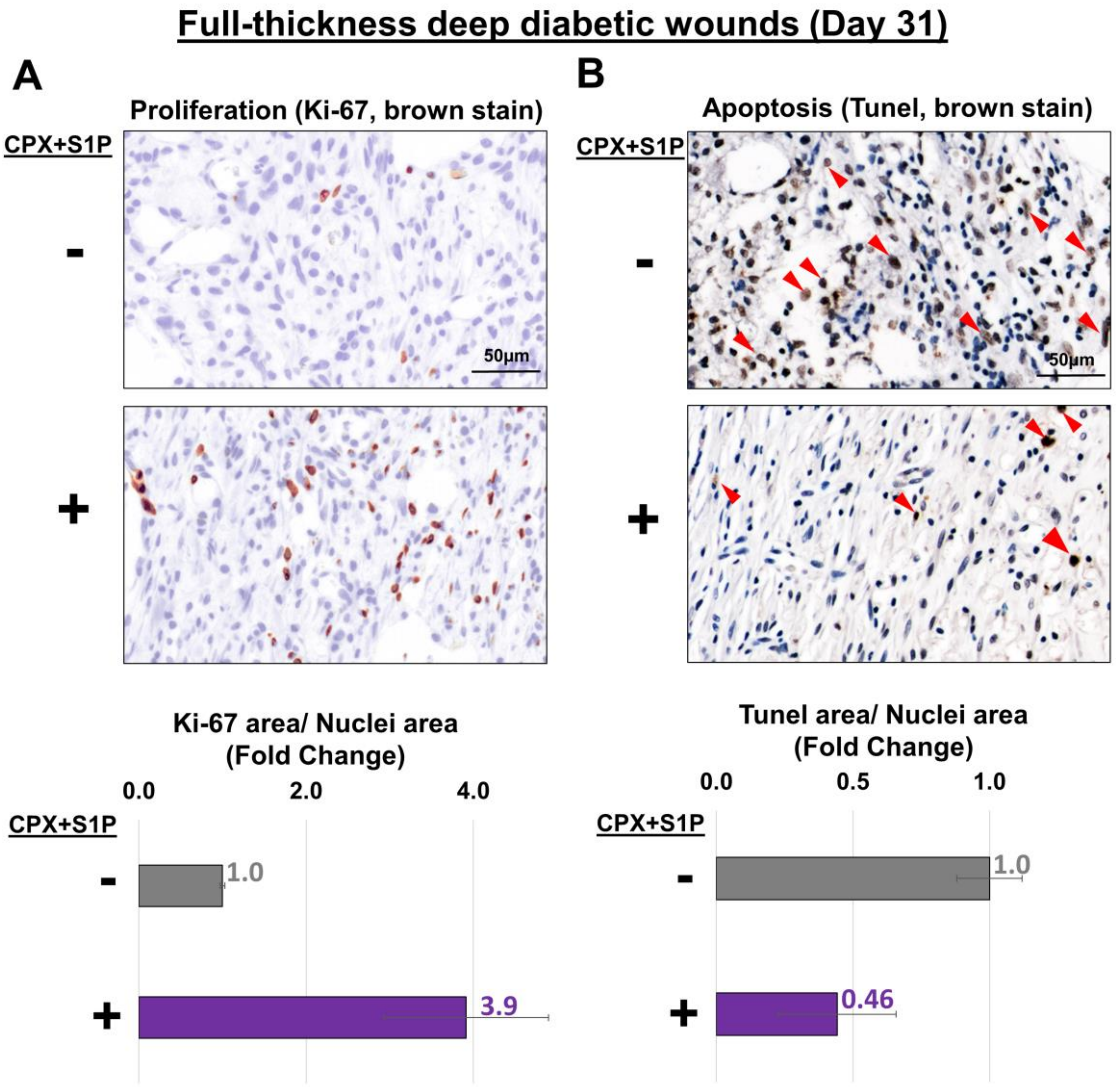

Figure 4.18 Representative images of proliferation and apoptosis in granulation tissue of full-thickness deep diabetic wounds 31 days post-treatment with or without 0.1 mM CPX + 0.01 mM S1P. **(A)** CPX+S1P appeared to increase proliferating cells (Ki-67 brown stain) and **(B)** decrease apoptotic cells (TUNEL brown stain; red arrowhead). Cell nuclei counterstained with hematoxylin. Quantification was done on 4 high powered 20x magnification field in each replicate. Quantification done at 20x magnification field. Increase is not significant as determined by Student's two-tailed t-test * $p < 0.05$**.** Error bars represent standard deviation. n = 2 wound replicates from the same rat.

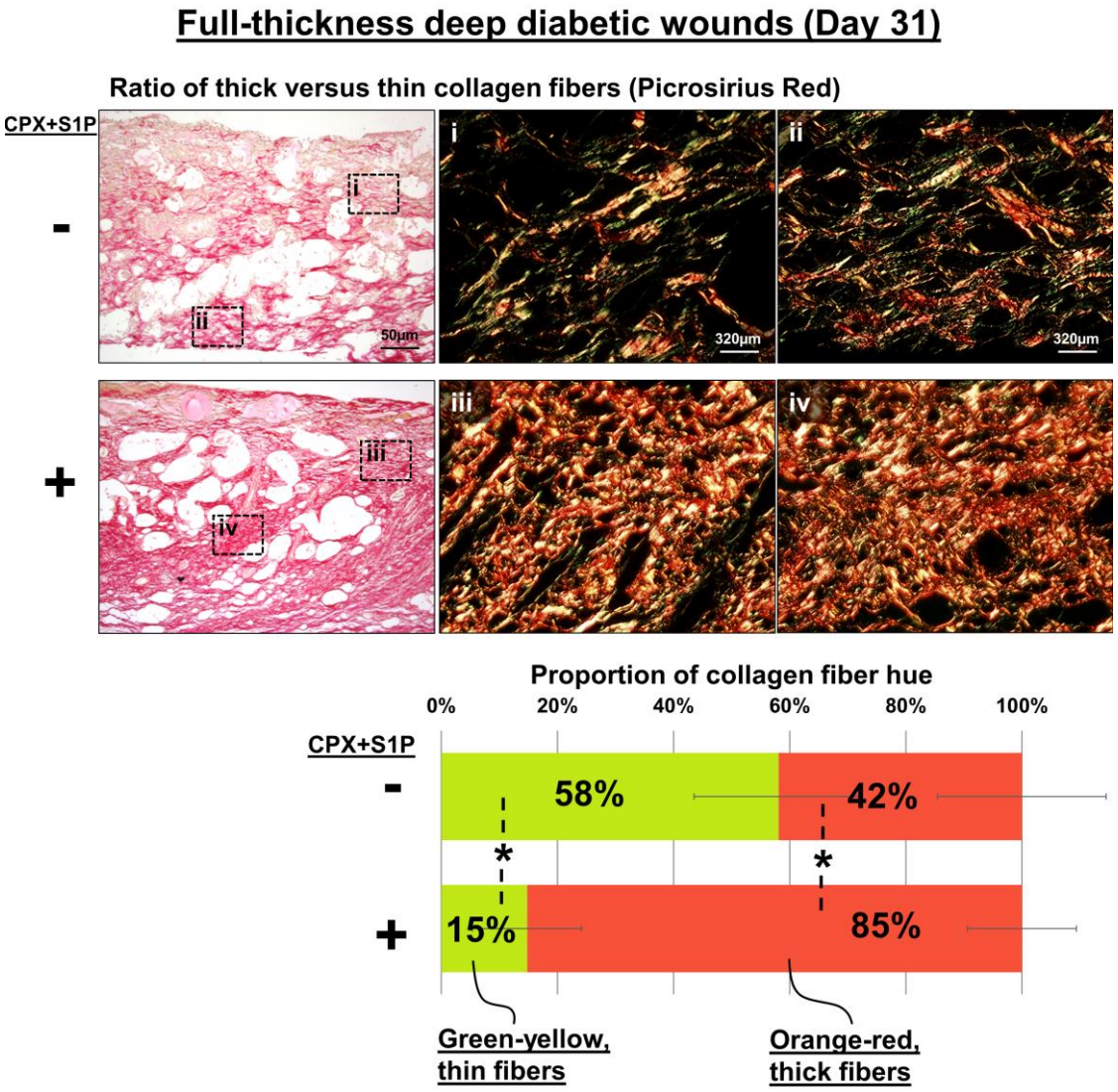

Figure 4.19 Ratio of thick versus thin collagen fibers in full-thickness deep diabetic wounds 31 days post-treatment with or without 0.1 mM CPX + 0.01 mM S1P. Representative images of picrosirius red stained collagen fibers (red). Inset i-iv corresponds to the Picrosirius red images viewed under linearly polarised light at 64x magnification. Here thin and poorly packed collagen fibers exhibit green to yellow polarizing colors, while thick and tightly packed fibers exhibit orange to red polarizing colors. Area of collagen fiber hue measured using ImageJ's colour threshold plugin. Quantification done at 40x magnification field. Significance * $p < 0.05$, is derived from Student's t-test**.** Error bars represent standard error. n = 2 replicates form the same rat. Graph reveals that CPX+S1P treatment significantly increases the proportion of orange to red

collagen fiber hue and decreased the proportion of green to yellow collagen fiber hue.

4.3.6 CPX+S1P promotes large vessel formation

In addition to an increase in collagen deposition and compaction, I observed a concurrent increase in angiogenesis in CPX+S1P treated deep diabetic wounds signified by a 1.8-fold increased in EC infiltration (Figure 4.20A, Methods §3.3.7). However, the total vessel density did not increase but the mean cross-sectional area of functional vessels rose from 300 μm^2 to 860 μm^2. Segregation of vessel-sizes according to their cross-sectional area into small (<200 μm^2), medium (between 200 μm^2 to 1000 μm^2) and large vessels (>1000 μm^2) revealed a significant ($*p < 0.05$) increase in large vessel density under CPX+S1P (Figure 4.20B). Histologically, these large vessels appeared functional, as red blood cells were present in their lumina.

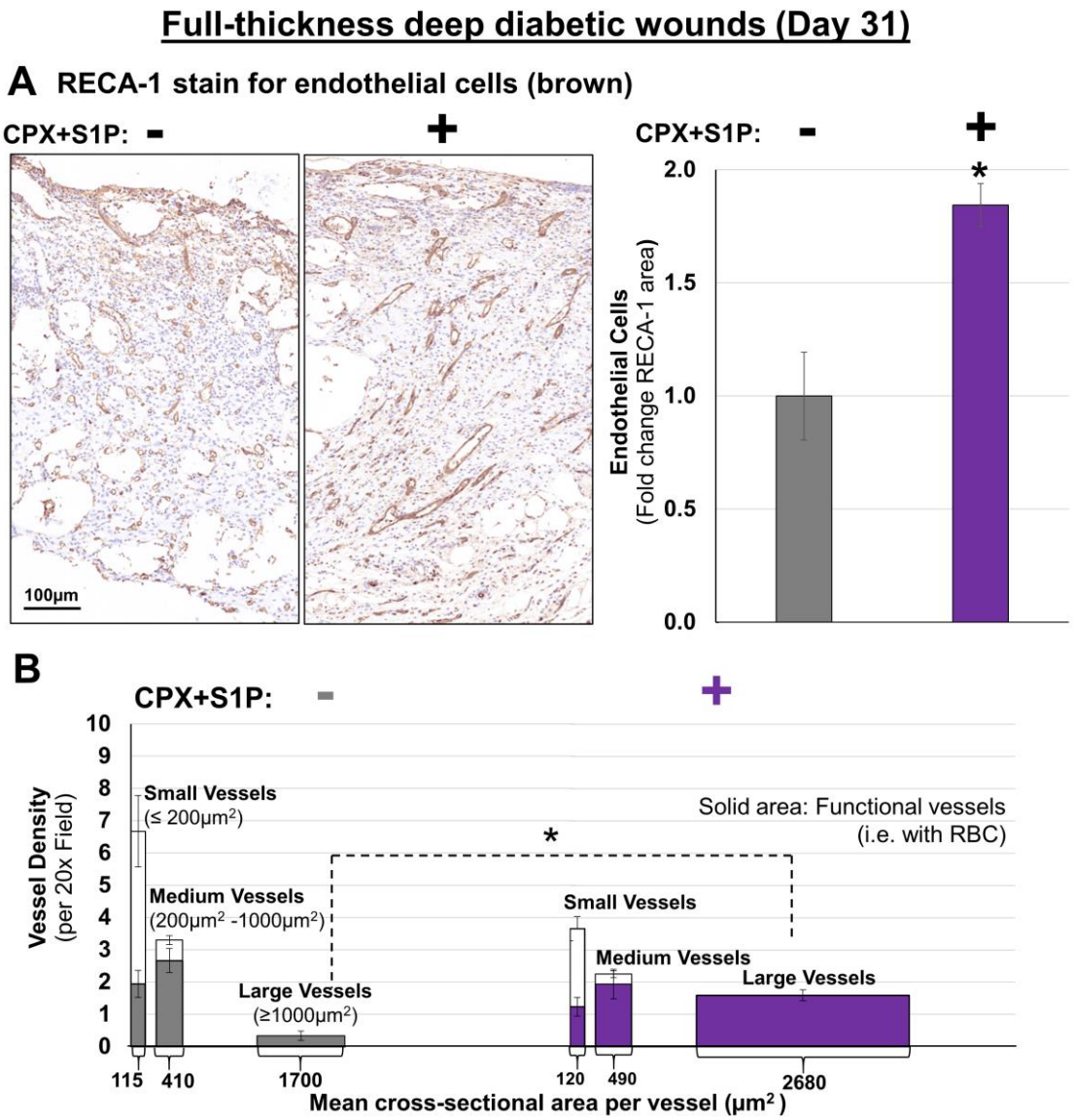

Figure 4.20. Angiogenesis in granulation tissue of full-thickness deep diabetic wounds with or without 0.1mM CPX + 0.01mM S1P treatment 31 days post-wounding. **(A)** Representative Immunohistochemical localization of RECA-1 positive endothelial cells (brown). Nuclei counterstained with haematoxylin (blue). Area quantification was done on 6 20x magnification field in each replicate.Graph of RECA-1 positive area reveals a significant increase in endothelial cell infiltration with CPX+S1P. **(B)** Graph of vessel density of small vessels (cross-sectional area <200 µm^2), medium vessels (cross-sectional area between 200 µm^2 and 1000 µm^2) and large vessels (cross-sectional area >1000 µm^2) induced with or without CPX+S1P treatment. Functional vessels i.e., RECA-1 positive lumina containing red blood cells, are represented by solid

areas. Vessel density quantified from 23 random sites in each treatment condition. Significance * $p < 0.05$, is derived from Student's t-test**.** Error bars represent standard error. n = 2 wound replicate from the same rat.

4.3.7 CPX+S1P reduces α-SMA expression in granulation tissue

An increased presence of myofibroblasts is associated with increased wound contraction. Using α-SMA antibody as marker we found an intense and even distribution of myofibroblasts in the deep diabetic wounds of the control group (Figure 4.21; Methods §3.3.5). At a higher magnification, α-SMA expression was seen to be located specifically at cell to cell junctions forming a cobble-stone like morphology in the upper-half of the granulation tissue (Figure 4.21, inset i); and in the lower-half adopting a typical myofibroblastic morphology (Figure 4.21, inset ii). Interestingly, under CPX+S1P treatment, α-SMA expression was only intense in the upper-half of the granulation matrix with a ~40% decrease in the lower-half of the matrix. α-SMA expression was also observed in spindle-like cells (Figure 4.21, inset iii), but primarily in mature blood vessels in the lower-half of the granulation tissue (Figure 4.21, inset iv).

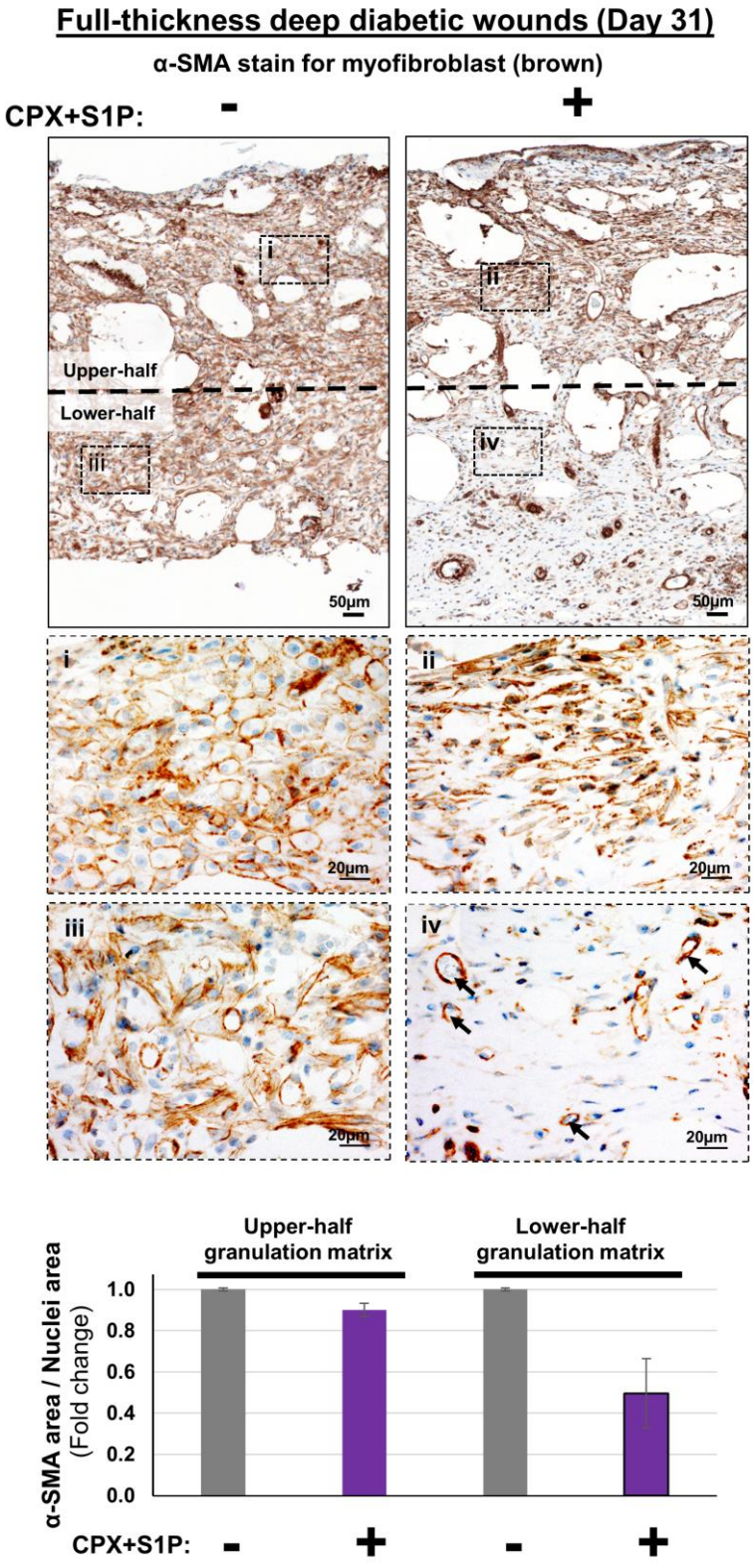

Figure 4.21 Representative Immunohistochemical localization of α-SMA expression (brown) in granulation tissue of deep diabetic full-thickness wounds with or without 0.1mM CPX + 0.01mM S1P treatment 31 days post-wounding. Nuclei counterstained with haematoxylin (blue). Inset i-iv represents a 64x

magnification of the dotted region in images on the top row. Arrows indicate α-SMA postitive blood vessels. Area quantification was done on 4 high powered 20x magnification field in each replicate. Decrease is not significant as determined by Student's two-tailed t-test * $p < 0.05$**.** Error bars represent standard error. n = 2 wound replicates from the same rat.

4.3.8 CPX+S1P reduces MMP-3 and MMP-13 expression

Besides physical rearrangement by myofibroblasts, the compaction of collagen fibers is also regulated by matrix metalloproteinases (MMP). CPX+S1P treatment significantly (* $p < 0.05$) attenuated MMP-13 (collagenase-3) and also attenuated MMP-3 (stromelysin-1) expression by 40% in deep diabetic wounds (Figure 4.22; Methods §3.3.5). At higher magnification, changes in MMP-13 expression pattern were striking (Figure 4.22, inset i-iv). In the control group, MMP-13 expression was diffusely distributed throughout the entire dermal matrix, while exposure to CPX+S1P resulted in a pericellular expression of MMP-13. Using a fluorescence resonance energy transfer (FRET) peptide as a MMP substrate (Methods §3.3.9), I found that CPX alone *in vitro* has the potential to dose-dependently inhibit APMA-activated MMP-3 activity while completely inhibiting APMA-activated MMP-13 at the lowest concentration tested (1 μM; Figure 4.23).

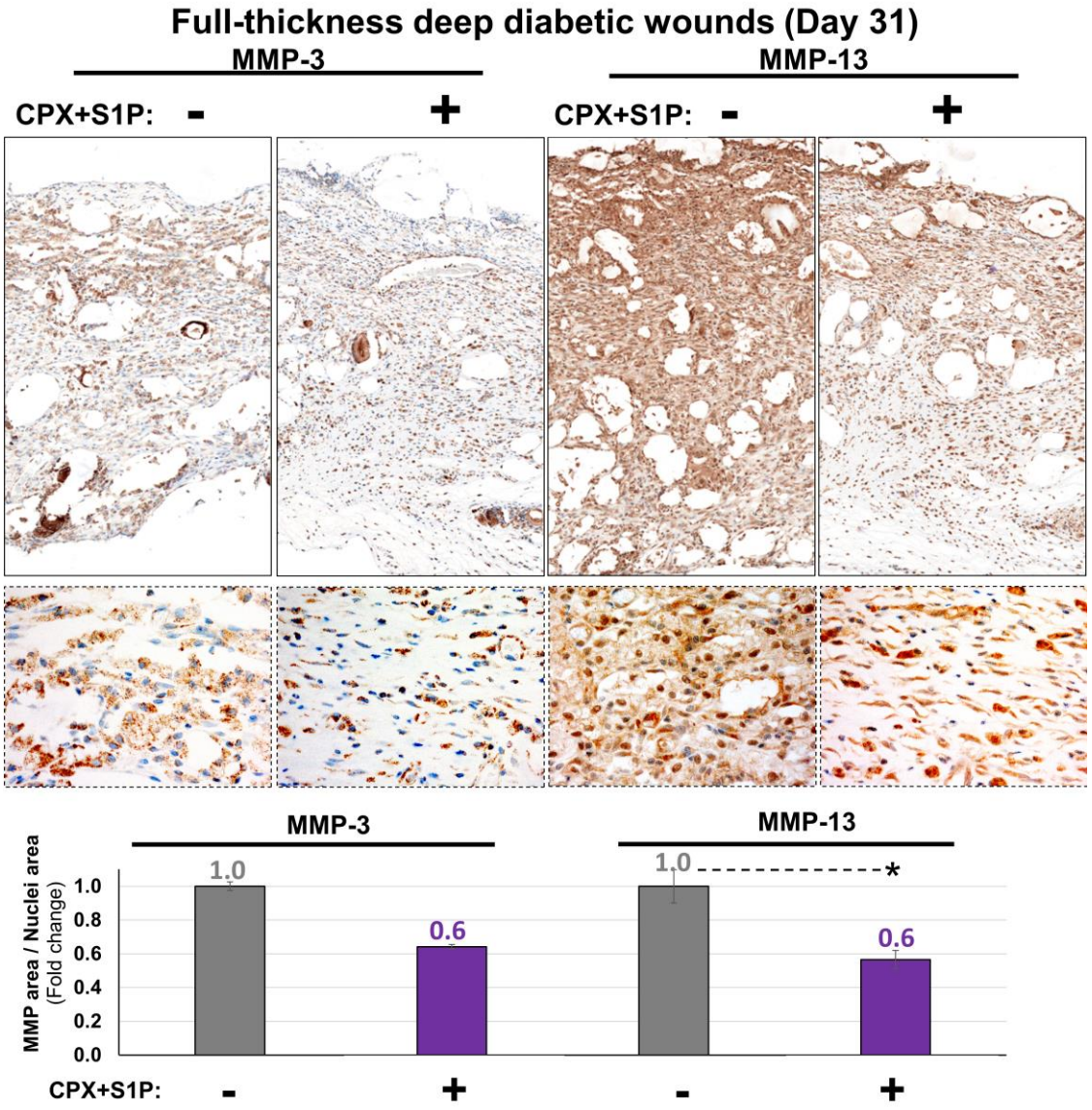

Figure 4.22 Representative Immunohistochemical localization of MMP-3 and MMP-13 expression (brown) in granulation tissue of full-thickness deep diabetic wounds with or without 0.1mM CPX + 0.01mM S1P treatment 31 days post-wounding. Nuclei counterstained with haematoxylin (blue). Inset i-iv shows the magnified images of the selected regions of interest i-iv in the top row. Graph reveals a 40% decrease in MMP-3 and MMP-13 expression in CPX+S1P treated granulation tissue. Area quantification was done at 20x magnification field. Significance * $p < 0.05$ determined by Student's two-tailed t-test**.** Error bars represent standard error. n = 2 wound replicates from the same rat.

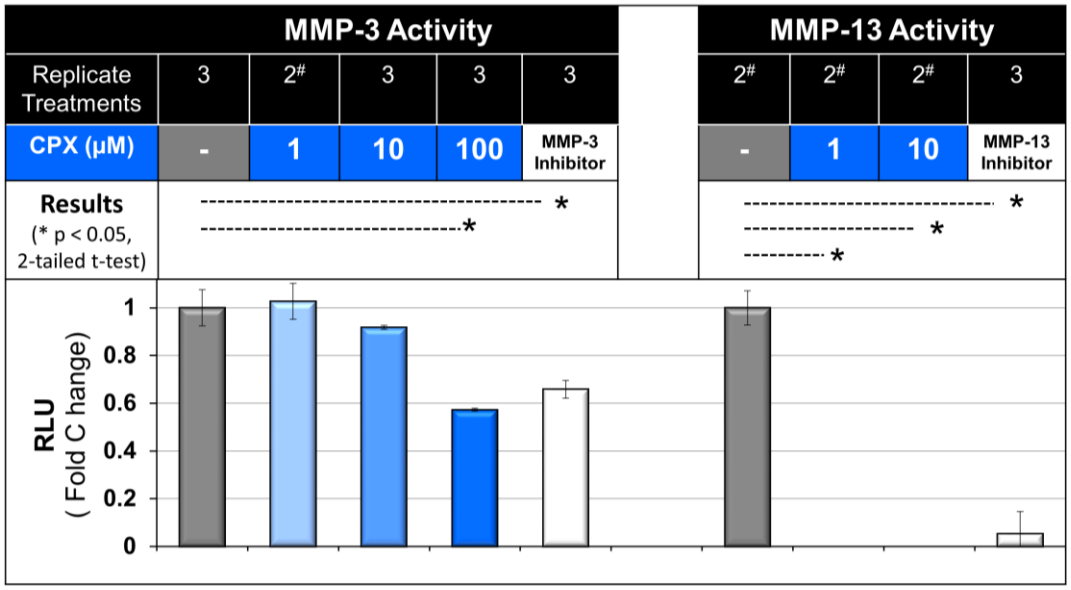

Figure 4.23 *In vitro* MMP-3 and MMP-13 fluorometric assay reveals a dose dependent inhibition of APMA activated MMP-3 activity and a complete inhibition of MMP-13 with a CPX concentration of 1 μM. "+" represents the positive control MMP-3 inhibitor V or MMP-13 inhibitor CL82198 hydrochloride. Significance * $p < 0.05$ determined by Student's two-tailed t-test**.** Error bars represent standard error. n = replicate treatments. **#:** Reason for n < 3: a well was excluded due to the observable presence of air bubbles and/ or dust particles which can affect fluorescence readings.

Chapter 5

Discussion

I have demonstrated here the successful off-label use of anti-fungal drug ciclopirox clamine (CPX) in combination with sphingosine-1-phosphate (S1P) as an attractive proangiogenic drug combination for diabetic wound healing. Both CPX and S1P have been previously shown to be angiogenic on their own as monosubstances [241,279] and their combination was observed by our lab to further increase endothelial cell (EC) sprouting *in vitro* [21]. As an extension to this literature, I assessed if CPX+S1P is able to (i) hyperinduce the angiogenic master regulator HIF-1, (ii) potentiate angiogenesis *in vivo* and (iii) increase diabetic wound contraction.

HIF-1 activation is a crucial angiogenic driver in upregulating the transcription of a variety of angiogenic stimulants [368]. HIF-1 is a heterodimer consisting of a constitutively-expressed HIF-1β subunit and an O_2 – and growth factor-regulated HIF-1α subunit [87] . Of these two subunits, the HIF-1α subunit is the limiting factor in the creation of a functional HIF-1 dimer [88]. HIF-1 activity is promoted by (i) an increase in HIF-1α stabilization [88] and/or (ii) an increase in HIF-1 transcriptional activity [243,244]. Increasing both upstream regulators concurrently results in a greater downstream transcription of angiogenic stimulants compared to increasing one regulator alone [283]. A previous study by Tal et al. (2008) demonstrated that a constitutively stable and a transcriptionally active HIF-1α transgene, when targeted into murine ECs, is able to effectively increase capillary density and blood flow in a hindlimb ischemia model [282, 283]. Nonetheless the long-term safety of human gene therapy remains a concern [226]. Here I demonstrated that the FDA-approved drugs - CPX and S1P potentially amplify both HIF-1 upstream regulators.

I observed in HUVECs that CPX+S1P increase the upstream regulator HIF-1α protein levels in a manner that exceeds its additive effect. It was previously shown that S1P increases HIF-1α translation through the activation of G_i protein pathway [280], while CPX inhibits HIF-1α degradation by Fe^{2+} chelation [159]. Here, Fe^{2+} is a cofactor for the prolyl and asparaginyl hydroxylases that continuously earmark the HIF-1α subunit for proteasomal degradation. As such, it can be speculated that CPX+S1P combination simultaneously leverages on both strategies i.e., increasing HIF-1α synthesis and inhibiting its degradation, to prolong HIF-1α's otherwise short half-life.

CPX+S1P also increases the protein expression of the HIF-1 transcription activator (phosphorylated-p42/44 MAPK) in a manner that exceeds its additive effect. However CPX alone inhibits the expression of phosphorylated-p42/44 MAPK. A similar observation was also reported by Luo et al. (2011) in murine lymphatic EC cultures [281]. Interestingly, supplementation with S1P was able not only to override CPX's suppressive effects and even potentiate it. To date, CPX's inhibitory mechanism and S1P's overriding mechanism remain to be elucidated.

As HIF-1 upstream activity increases, there is a corresponding additive increase in its downstream angiogenic targets: c-MET, VEGF and eNOS [245]. Here c-MET (hepatocyte growth factor receptor) was selected for assessment as it is previously reported to be a marker for the angiogenic phenotype of ECs; being up-regulated only in activated EC during *in vitro* sprouting and down-regulated upon differentiation into capillary-like structures [369]. c-MET also increases EC

proliferation and initiates a downstream cell invasion programme [370,371]. VEGF was assessed as it mediates vascular homeaostasis, EC survival and its absence attenuates EC motility [103,106]. eNOS was also assessed as its absence is known to seriously impair angiogenesis in a murine hindlimb ischemia model; which was not rescuable with the administration of a potent angiogenic recombinant VEGF protein [372], suggesting that eNOS is crucial in mediating a VEGF-induced angiogenesis [373].

Having established that CPX+S1P hyperinduces the angiogenic master regulator HIF-1, I next assessed if it potentiates angiogenesis *in vivo*. Using a well-established subcutaneously implanted PVA sponge model, I demonstrated that combination of CPX+S1P indeed increases EC infiltration and functional vessel length in a manner that exceeds their additive effects. This corroborates with my group's previous *in vitro* observation that CPX+S1P potentiates EC sprout length and infiltration in collagen gel with the formation of true lumina [21]. It is important to highlight here that the results should not be over interpreted given a small sample size from the same rat; and a larger sample size may highlight a possible dorso-ventral gradient of vascular density in rodent dorsum [374] in which a pair-wise analysis of sponges across rats may be required.

As angiogenesis intimately supports skin wound contraction, I next assessed the efficacy of pro-angiogenic CPX+S1P drug treatment in promoting contraction in full-thickness diabetic skin wounds. To do so, I first identified the variables which may affect wound contraction. Kennedy et al. (1979) previously

reported that (i) animal age, (ii) species and (iii) position of wound on the body surface affects wound contraction; while (i) sex of the animal, (ii) time of day of wounding, (iii) wound shape, or (iv) wound size (unless it is so large that it extends over different anatomical regions) do not [375]. Hence in my experiment, I standardized the wound size & located them at fixed distances with reference to the shoulder blade of each rat. Contralateral wounds were also treated with the same drug to avoid any systemic effects. Due to logistical arrangements, I was unable not commence surgery on all the rats at the same age; but all wounds were made on 18- to 20-week old rats.

Treatment with CPX+S1P resulted in a striking increase in large (rather than small or medium) blood vessels in deep diabetic wounds. Previous *in vitro* findings by Nakatsu et al. [111] suggested that the lumina diameter of new sprouts is dependent on the activation of p42/44MAPK pathway in endothelial cells. I thus speculate that potentiation of p42/44 MAPK activity by CPX+S1P may be associated with the *in vivo* observation of large vessel formation.

The observed increased angiogenesis paralleled a stronger accumulation of granulation tissue in deep diabetic wounds. This increase in collagen deposition was unexpected, as the prolyl hydroxylase inhibitor CPX is known to cross-inhibit collagen prolyl hydroxylases, which would predict reduced collagen secretion and deposition [277]. In fact, granulation tissue increase had not been reported in high dose treatment diabetic murine wounds with 50 mM of CPX as the sole drug [130].

In this study, the increase in collagen deposition was also associated with attenuated MMP levels. Diabetic tissue has been shown to overexpress MMPs, in particular MMP-13 and MMP-3 in diabetic ZDF rats [20]. MMP-13 degrades major dermal collagen subtypes I and III while MMP-3 degrades the dermal collagen subtypes III and IV. Using MMP antibodies that recognize total MMP level, CPX+S1P was clearly seen to attenuate both MMP-3 and MMP-13 expression in diabetic wounds. Recent evidence supports a link between S1P and suppression of MMP-3, MMP-13 expression and activity in EC [284] and in human chondrocytes [285] by repressing NF-κB which binds to MMP promoters. *In vitro*, I saw strong inhibition of MMP-3 and MMP-13 activity by CPX alone, which may be partly due to its ability to chelate divalent cations [240] such as Zn^{2+} needed for MMP activity. Interestingly, the localisation of MMP-13 expression resembled that of α-SMA. This may not come as surprise, as MMP-13 was previously found to be expressed abundantly in fibroblastic cells in diabetic rodent wounds [20] and in human myofibroblasts [286].

Cellular contractile forces generated by myofibroblasts are recognized as a contributing factor for granulation tissue compaction [287]. Nonetheless, CPX+S1P treatment did not appear to increase α-SMA expression of myofibroblasts. Instead, I observed a decrease that was spatially confined to the lower half of the granulation tissue. A direct zonal net effect of CPX+S1P on myofibroblast differentiation cannot be excluded at present, but this requires further detailed study. A more straightforward explanation for this observation is a recent discovery that mechanical tension exerted by splinting induces and maintains myofibroblast transdifferentiation [288]. In this study, the splints were

sutured through the dermis and panniculus carnosus but not through the superficial fascia and deep retinacula cutis adipose layer. Therefore, mechanical tension exerted by the splint would likely dominate the upper-half of the granulation tissue.

As the proangiogenic CPX+S1P treatment promoted granulation tissue development, an increase in contraction in deep diabetic wounds followed. However, in superficial wounds, a granulation tissue driven contraction was not discernible despite an increase in angiogenesis (Appendix B). This is not surprising given that contraction in the control group remained extensive at 50 %, even under splinting, masking any pharmacological effect. Such extensive contraction during wound healing is an inherent rodent-specific feature arising from skin laxity, which in humans may be more representative of wound healing in the trunk or perineum [16]. On the contrary, diabetic ulcers exhibit low wound contraction as they are commonly located in the lower- extremity where skin laxity is low [13] and granulation tissue development is slow [289]. Here I managed to emulate this pathology, by exploiting the presence of a dorsal fat pad in the Zucker fatty rat that lies cranial to the transverse plane, to increase the wound depth to ~3 mm. This allowed for the extrusion of the perilesional adipose layer into the deep wound void to retard excessive contraction due to skin laxity [264] whilst providing a large enough wound volume for the gradual development of granulation tissue. Compared to the superficial wounds of ~ 1 mm depth, the deep wounds used in this dissertation is a closer representative of wounds in the human big toe, wherein soft tissue thickness ranges between 4.5 mm to 10.1 mm [377]. Modulating wound depth is thus an elegant solution

for creating a rodent skin model which better emulates human wound healing tissue dynamics, and may pave the path for better assessment and understanding of promoters of diabetic wound healing.

In conclusion, the clinically-used anti-fungal drug CPX and the bioactive lipid S1P represent an attractive drug combination to be repurposed for diabetic wound healing. The ability to amplify HIF-1 activity makes CPX+S1P advantageous in diabetic wounds as they are known to have attenuated HIF-1 activity [153,154]. There might be more to this combination as CPX has also recently been shown to exhibit antibacterial activity [290], which may further add to its utility in treating diabetic wounds which are very susceptible to bacterial biofilm development. Additionally, as high density lipid-S1P plasma levels are known to be suppressed in severe diabetics [179], topical supplementation of S1P has the potential to be even more efficacious for wound treatment in this subset of patients. It is important to note that the results from the deep diabetic wounds were derived from a small sample size of two wounds from the same rat. Recently, Ansell et al. found that wounds derived from the same mouse showed high variability and could be considered as independent biological replicates [376]. Nonetheless, the results should not be over interpreted as a wound sample size beween one to four could hypothetically result in a 30% to 50% difference in wound healing [376]. The reasons for the small sample size in this dissertation has been highlighted in Table 6; where many wounds were lost or excluded from analysis due to isoflurane overdosing, wound infections, diabetic complications and splints bitten off by the rats. The techniques I have acquired to address these issues will be highlighted in the next chapter (§ 6.2.3).

Chapter 6

Conclusion,

Limitations and Future Work

6.1 Conclusion

In this dissertation, I demonstrated the repurposing of two compounds for diabetic wound healing. I combined

(i) Ciclopirox olamine (CPX), a divalent metal chelator FDA-approved as an anti-fungal drug; and

(ii) Sphingosine-1-phosphate (S1P), a lysophospholipid whose analogue is FDA-approved for multiple sclerosis treatment.

The use of this combination was motivated by literature findings that:

(1) Reversing impaired angiogenesis in diabetic wounds promotes granulation tissue accumulation and compaction, accelerating contraction (a wound closure mechanism);

(2) Major inhibitors of angiogenesis can be reversed by divalent metal chelation and S1P supplementation;

(3) CPX and S1P analogues are clinically used, supporting a drug repurposing approach to reduce translational hurdles; and

(4) CPX and S1P previously demonstrated angiogenic synergy *in vitro*.

As an extension of current literature, this dissertation provides the following new insights:

(1) CPX+S1P potentiates a crucial driver of angiogenesis i.e., hypoxia-inducible factor-1 activity in endothelial cells (EC) *in vitro*,

(2) CPX+S1P potentiates EC infiltration and functional vessel length in a subcutaneous sponge implantation rodent model;

(3) CPX+S1P not only increased angiogenesis but also decreased matrix metalloproteinase levels in deep diabetic rodent wounds, resulting in a granulation-tissue driven wound contraction that increases wound closure.

These findings are significant because:

(1) Despite the widely perceived view that a broad band prolyl hydroxylase inhibitor potentially cross-inhibits collagen secretion, I found a surprising increase in collagen deposition in the presence of a low dose of CPX (0.1 mM) as opposed to earlier studies using topical doses up to 50 mM [130].

(2) Current rodent models have not revealed wound sites that allow for wound depth variation. Leveraging on a recent Zucker diabetic fatty rat wound healing model [20], I identified specific wound sites that allow varying of the full thickness skin wound depth from 1 mm (superficial) to 3 mm (deep). This modified model has important clinical translational implications in assessing the efficacy of pharmacological treatments in wound healing. I found that the same pharmacological treatment, though not as effective in promoting granulation tissue in superficial wounds, was effective in deep wounds.

(3) Despite the widely perceived view that splinting retards excessive spontaneous wound contraction in rodents, I found that contraction remained significant at ~50% in splinted diabetic wounds. I present a simple method using wound depth increment (in the presence of splinting) to limit wound contraction to ~8%. This elegant solution overcomes spontaneous

contraction in rodents enabling me to assess granulation-driven wound contraction akin to human tissue.

As the above conclusions are drawn from a small sample size (n = 2 to 8), the next section (§6.2) highlights the limitations in this small study and the further need for larger confirmatory work.

6.2 Limitations and future work

Small studies advantageously allow the Hypothesis to be addressed within a short span of time while avoiding spending too much finances on finding an association when there really is no effect. Nonetheless, a major drawback of small studies is that they can under- or over-estimate the magnitude of an association particularly when experimental limitations are not highlighted. This section thus discusses experimental limitations and suggests future work that may address the limitations.

6.2.1 Preparing a stable S1P solution

The first experimental limitation concerns the preparation of a stable Sphingosine-1-phosphate (S1P) stock solution. As discussed in §3.1.3, this method involves dispersing S1P by sonication in an aqueous buffer solution containing serum albumin [291]. In an aqueous solution, S1P has a low solubility.

Hence serum albumin serves as S1P's carrier by binding reversibly to it [292,293]. Immediately after sonication, the S1P stock solution is clear and devoid of precipitates. However, when kept for more than 12 hours on a shaker at 4^{o}C, precipitates begin to form. The further use of this unstable S1P solution could not induce the hypoxia-inducible factor-1 (HIF-1) activity in HUVECs described in §4.1. This efficacy was only seen when a freshly sonicated S1P stock solution was used. For future clinical applications, it may be pertinent to assess techniques that prolong S1P's solubility; for example by the addition of biocompatible surfactants [294].

6.2.2 Imaging functional vessels

The second set of limitations concerns the procedure of imaging functional vessels in Polyvinyl alcohol (PVA) sponge explants. As discussed in §3.2, FITC-isolectin was first perfused through the rodent tail vein. The PVA sponges were thereafter harvested, bisected, cryosectioned and stained with anti-FITC and RECA-1 antibodies to detect FITC-isolectin and endothelial cells respectively.

The limitations observed in this procedure were:

(1) An assumption was made that 1 ml of FITC-isolectin at 0.5 µg/µl was sufficiently high enough to label most or all of the EC along the perfused vessels in rats. (Note: The volume and concentration were adapted from Kang et al.'s (2011) successful perfusion of FITC-isolectin in mice to detect functional vessels in subcutaneously implanted matrigels [295]. To

compensate for larger-sized rats, I have increased the FITC-isolectin volume by 10 times [from 0.1 ml to 1 ml] as the rat was approximately 10 times heavier than a mouse.)

(2) Up to 20% loss in FITC-isolectin perfusion volume can occur while trying to align needle in the tail vein. Such volume loss may not be considered negligible and needs to be correspondingly compensated in future work.

(3) It can be challenging to obtain intact 1 µm cryosections at similar depths across all sponges as these thin sections tended to tear under steel microtome blades. Future work could consider the use of glass knives tailored for ultramicrotomy. (Note: Ultrathin sections were needed to allow for a cleaner wash off of non-specific antibodies retained by hydrophilic PVA material. For thick sections, high magnification was used to image vessels away from the porous PVA walls.)

Future work can consider the use of X-ray microcomputed tomography (micro-CT) to image functional vasculature. This technique avoids the histological challenges faced. Here rats are first perfused with a contrast agent and micro-CT is then used to visualize the vasculature at the site of interest in intact rats. A three-dimensional reconstruction image of functional vessels is generated. Using a variety of algorithms for advanced quantitative analysis, the vessel volume, diameter and degree of anisotropy can be calculated from the tomographic data [296]. Moreover, micro-CT also allows for measurements of vessel permeability and blood perfusion [297]. This may be particularly relevant

for diabetics who are often plagued with microvascular stasis owing to their low red blood cell (RBC) deformability [298]. As CPX+S1P was observed to increase the large blood vessel density in diabetic wounds (§4.3.6), it may be speculated that CPX+S1P increases blood perfusion. Micro-CT may provide a more conclusive determination. Alternatively, the following non-invasive techniques can be used to measure wound perfusion:

(i) Laser Doppler imaging, which provides a two-dimensional map of microvascular flow over the entire wound surface; and
(ii) transcutaneous oximetry, which reflects the amount of oxygen diffused from the capillaries through the epidermis at perilesional sites.

Both techniques confer the major advantage of real time visualization of wound perfusion without contrast agents, allowing researchers to monitor perfusion development in the same animal over time.

6.2.3 Managing diabetic complications in rats

The third set of limitations concerns the full thickness skin wound model in obese female Zucker Diabetic Fatty (ZDF) rats. Here I observed that:

(1) ZDF rats are hypersensitive to isoflurane.
(2) ZDF diabetic rats develop urinary tract infections.
(3) ZDF diabetic rats develop abdomen pressure sores.

(4) ZDF rats tended to actively bite off parts of the bandage to access the wound.

(5) Sutures attached to the splint surfaced at various time points during the third week post-surgery.

To address these complications, I found the following techniques useful:

(1)To prevent isoflurane overdosing during a 45 minute dorsal wound excision surgery, oxygen levels was doubled to 2 atm and isoflurane levels varied between 1 % and 3 %. (Note: Overdosing was observe to occur after a 45 minutes continuous exposure to 1 atm oxygen and 2% isoflurane).

(2)To reduce urinary tract infection, 5 ml of saline was injected daily subcutaneously.

(3)To reduce pressure sores, rats were encouraged to move freely by taping wound dressings only to its back and not entirely across the dorsum and upper abdomen.

(4)To prevent the bandage from being completely bitten off, the bandage was double folded to increase its thickness and replaced daily.

(5)To reattach the splint to the skin after sutures have surfaced, superglue was applied daily to the splint. Resuturing was avoided as it may induce additional trauma to the wound. Nonetheless, future work would need to standardize the time point to remove all sutures across the rats as the glue and sutures may exert different tensions on the perileisional skin affecting wound closure.

6.2.4 Measuring wound contraction

The fourth set of limitations concerns the method of measuring wound contraction histologically (§4.3.4):

(1) Histological contraction measurements may not be representative of overall wound contraction. In rats, mid-dorsal wound contraction is not uniform. There is a tendency for the lateral edges of the wound to move closer together than the anterior and posterior edges [15]. Thus contraction measurements in this study may be more representative of central wound contraction wherein histological measurements were taken. This may not be directly comparable to macroscopic measurements done in other studies.

(2) wounds with a high fat content tend to tear easily when sectioning. Hence it can be challenging to derive intact sections from similar depth intervals across all rats.

Future work to assess overall wound contraction can be done through macroscopic measurements of tattooed perilesional skin. In this approach India ink is use to tattoo grids around the dermal edges of the wound defect to locate the original defect perimeter without ambiguity [15]. Thereafter, planimetry or computerized morphometric image analysis is used to measure the defect area over time [15]. However, this approach may be challenging for splinted wound models as tattooed marks are concealed by glued splints.

6.2.5 Limited efficacy in re-epithelialization

The fifth limitation concerns the lack of efficacy by CPX+S1P in promoting re-epithelialization (§4.3.4). As discussed in §2.1, the wound closure mechanism involves both contraction and re-epithelialization. Both mechanisms are impaired in chronic wounds [13,28]. To futher accelerate diabetic wound closure, future work may consider combining CPX+S1P with re-epithelialization activating treatments. An example of such treatments involves downregulating overexpressed desmosomes and hemidesmosomes in the epidermis [303,304].

6.2.6 Non-clinical representation of wound environment

The sixth limitation concerns the use of a sterile and non-ischemic diabetic wound model. This may not be representative of the clinical challenges such as the persistent infections in diabetic wounds plagued with ischemia [299]. Here traditional route of systemic antibiotic delivery is ineffective with a poor wound perfusion. Such prolong infections can significantly impede wound healing rates by 40% [300]. To better represent these clinical challenges, future work can modify the diabetic ZDF wound model to exhibit:

(1) ischemia, by surgical incisions to generate a bipedicle dorsal skin flap [301], and
(2) infection, by introducing well-known virulence bacteria such as *S. aureus*, β-hemolytic streptococci, *Enterobacteriaceae* and anaerobes into the wound [302].

Evaluating the efficacy of CPX+S1P to promote diabetic wound healing under these additional casual factors allows for a more conclusive assessment of its translational robustness.

6.3 Concluding Remark

This dissertation provides a proof of concept that the CPX+S1P is an attractive proangiogenic drug treatment to be repurposed to promote diabetic skin wound healing.

Appendices

Appendix A

Biological dressings: Cell-free and Cell-containing matrices

Immediate wound coverage has been a major tool in diabetic wound management. Since the early 1500s, skin grafts have been used to restore wound defects [378]. However, concerns over the availability of sufficient healthy skin, the health risks associated with the procedure and donor-site morbidity have been a cause for concern. These disadvantages have led to the development of 3-dimensional tissue-engineered biodegradable skin scaffolds. These scaffolds are laid over the wound site and are gradually infiltrated by cells and incorporated into the wound bed. They can be classified into two categories: (i) cell-free matrices or (ii) cell-containing matrices.

Cell-free matrices

Examples of cell-free matrices used clinically on diabetic foot ulcers are:

1) Promogran (Johnson & Johnson, New Brunswick, NJ), a combination of 55% collagen and 45% oxidized regenerated cellulose matrix [379];
2) Fibracol (Medline Industries Inc., Mundelein, Illinois), a combination of 90% collagen and 10% calcium alginate [380];
3) Formulated Collagen gel (Cardium Therapeutics Inc., San Diego, CA), a 2.6% bovine collagen in a specialized buffer [381];
4) Oasis® (Healthpoint Ltd, Fort Worth, TX), collagen matrix derived from submucosa of porcine small intestine [382];
5) Graftjacket (Kinetic Concepts Inc, San Antonio, TX), a decellularized human dermal matrix [383];

6) Integra® (Integra LifeSciences, Plainsboro, NJ), bovine tendon collagen and glycosaminoglycan matrix [384].

These collagen containing matrices serve to absorb and trap the wound exudates which contain high levels of MMP; thereby reducing matrix degradation [385]. The presence of polysaccharides in some of these matrices is said to bind iron and zinc which are catalysts for ROS generation and MMP activity respectively, resulting in a reduction of MMP (MMP-2, MMP-9) and ROS levels [386]. Polysaccharides also bind and stabilize growth factors, allowing them to be re-delivered in their active form when the biodegradable matrices are re-absorb [387]. Nonetheless, the efficacy of these cell-free matrices in decreasing the mean time of healing was only as effective as that of standard treatment with a moisten gauze [205]. It remains unknown if these matrices address the impaired HIF-1 activity in diabetic wounds to promote the release of downstream angiogenic stimulants. It is believed that a combinatory treatment of growth factor supplementation and cell-free matrice is a more efficacious approach in wound healing than an individual treatment with cell-free matrice [225].

Cell-containing matrices

Cell-containing matrices propose to provide an additional advantage to cell-free matrices by including growth factor releasing allogenic or autologous cells such as keratinocytes or fibroblasts. Allogenic cells can be cultured more rapidly than adult cells. This permits immediate graft availability with the possibility for bulk

manufacturing [230]. Examples of cell-containing matrices used clinically on diabetic foot are:

1) Dermagraft (Advanced Biohealing Westport, CT, USA), human neonatal foreskin fibroblast embedded in a three-dimensional polyglactin scaffold [388];
2) Apligraf® (Organogenesis Inc., Canton, MA), a bi-layer skin product with the dermal layer consisting of neonatal foreskin fibroblast embedded in a bovine collagen matrix covered by an epidermal layer with human keratinocytes [389];
3) OrCel® (Ortec International Inc., New York, NY, USA), a bi-layer skin product with the dermal layer consisiting of a porous collagen sponge containing cocultured allogeneic keratinocytes and fibroblasts harvested from human neonatal foreskin [390, 391];
4) EpiDex® (Euroderm GmbH, Germany, Leipzig), autologous fully differentiated, stratified keratinocytes derived from the patient's outer root hair sheath [392].

Although these cell-containing matrices are capable of secreting and releasing multiple angiogenic growth factors such as PDGF-BB into the wound bed [393], the success and survival of this bioengineered skin depends on a well-vascularised wound bed. Its clinically effectiveness was reportedly seen only in non-ischemic and non-infected, chronic plantar diabetic foot ulcer [205, 394]. Moreover the time taken for matrices such as Integra to be re-vascularised is clinically long (~10 days to 15 days) [393]. As the viability of these cells

decrease, the efficacy of the matrice also decreases [395]. The introduction of allogenic cells come with several additional disadvantages such as a short shelf-life of 5-days, an increase risk of disease transmittance and a poor-cost to benefit ratio [396]. Fibroblast-seeded products such as DermaMatrix cost ~30-60 USD per square centimeter and are much more costly than cell-free matrices [396]. The addition of the keratinocyte layer such as in Apligraf doubles the cost [396]. Moreover, with a short life span of allogenic cells, these matrices are temporary and will be replaced one to two months later with a split thickness skin autograft [393].

Modalities: NPWT, USH, HBO

Besides biological dressings, three modalities: 1) negative pressure wound therapy (NPWT), 2) ultrasound healing therapy (USH) and 3) hyperbaric oxygen therapy (HBO), have emerged with a proposed efficacy that increases HIF-1 activity and reduces MMP levels in diabetic wounds.

Negative pressure wound therapy (NPWT)

NPWT is approved by FDA since 1995 (Vacuum Assisted Closure, Kinetic Concepts Inc., San Antonio, TX) [397]. This technology involves creating a tightly sealed dressing around the wound and thereafter a suction pump is applied to create a continuous or intermitted negative pressure across the wound. This process drains the bacteria laden and high MMP wound exudates [398]. With negative pressures of ~125mmHg, tissue deformation occurs at the wound edges occluding capillary vessels [399, 400]. A ~0.5 cm ischemic zone is induced at the wound edges while perfusion ~2.5cm away from the wound

edge is increased [399, 400]. This transient ischemia at the wound edge is believe to trigger a release of HIF-1 downstream pro-angiogenic such as VEGF, bFGF, TGF-β, PDGF-B, which results in an increase in microvessel density, lumen size, and granulation tissue formation [399, 401 - 403]. Although NPWT is widely regarded as safe and effective, its efficacy is only seen in wound beds that are well-vascularised [404, 405], with limited benefit in ischemic wounds [399, 406, 407]. Moreover NPWT may further induce necrosis at wound edges of ischemic wounds [405]. As NPWT has to be given for at least 22 hours per day for an optimal outcome, the patient's quality of life may be comprised [399, 408]. Patients may also experience an initial pain with negative pressure suction [399, 408]. Depending on the pressure magnitude and cyclical application, its angiogenic efficacy remains debatable with several studies observing no benefits in increasing HIF-1 activity and pro-angiogenic growth factor levels (reviewed in Glass et al., 2014) [401]. It remains unknown if NPWT aids in decreasing ROS and AGE levels, and if it increases S1P levels in the diabetic wound. Clinical studies comparing NPWT to standard care (advance moist wound therapy, saline gauze) showed no conclusive improvements in the mean time of diabetic ulcer healing [401].

Ultrasound Healing therapy (USH)

USH (MIST Therapy, Celleration, Inc., Eden Prairie, MN) is approved by FDA since 2005 to deliver noncontact low-energy ultrasound to the wound bed through a continuous saline mist [409]. Ultrasound is defined as a mechanical vibration transmitted at a frequency above the upper limit of human hearing (>20 kilohertz). USH induces mechanical deformation of the cell membrane

stimulating mechanical transduction signals in fibroblasts to increase secretion pro-angiogenic growth factors such as TGF-β1 and VEGF production [410, 411]. USH also increases p42/44 MAPK signalling [411], which may contribute to an increased vessel size observed in USH treated diabetic murine wounds [111, 412]. Nonetheless, it remains unknown if USH decreases ROS, AGE and MMP levels and if it increases S1P levels in the diabetic wound. A recent review by Game et al. (2012) reported few randomised controlled trials to support the use of USH in promoting diabetic wound healing [413].

Hyperbaric oxygen therapy (HBO)

HBO therapy is an expensive therapy which requires the patient to breathe an intermittent administration of 100% oxygen under elevated atmospheric pressures, for a few hours over 30-40 sessions [414]. HBO clinical trials for diabetic foot ulcers healing was first reported in 1987 by Baroni and colleagues. During treatment, the arterial oxygen tension often exceeds 2000 mmHg and levels of 200 to 400 mmHg occur in tissues [414]. Oxygen inhaled under elevated pressure dissolves in plasma, in the absence of haemoglobin. Its diffusion from functional capillaries depends on oxygen partial pressure instead of haemoglobin levels. As such, oxygen diffusion into the wound increase with an increase in atmospheric pressure. HBO elevates wound oxygen tension levels, promoting fibroblast replication and collagen deposition [415]. Nonetheless, its efficacy in increasing angiogenesis in diabetic wounds remains unclear. Conflicting data surrounds HBO's ability to increase HIF-1 activity and its downstream angiogenic stimulants [416, 417]. Studies supporting an increase in HIF-1 activity propose that HBO first increases ROS level, which in

turn increases antioxidants production such as thioredoxin and thioredoxin reductase, which is a non-hypoxia activator of HIF-1 [416, 418]. A recent clinical trial found HBO ineffective in decreasing diabetic foot ulcer size or time to healing [419].

Appendix B

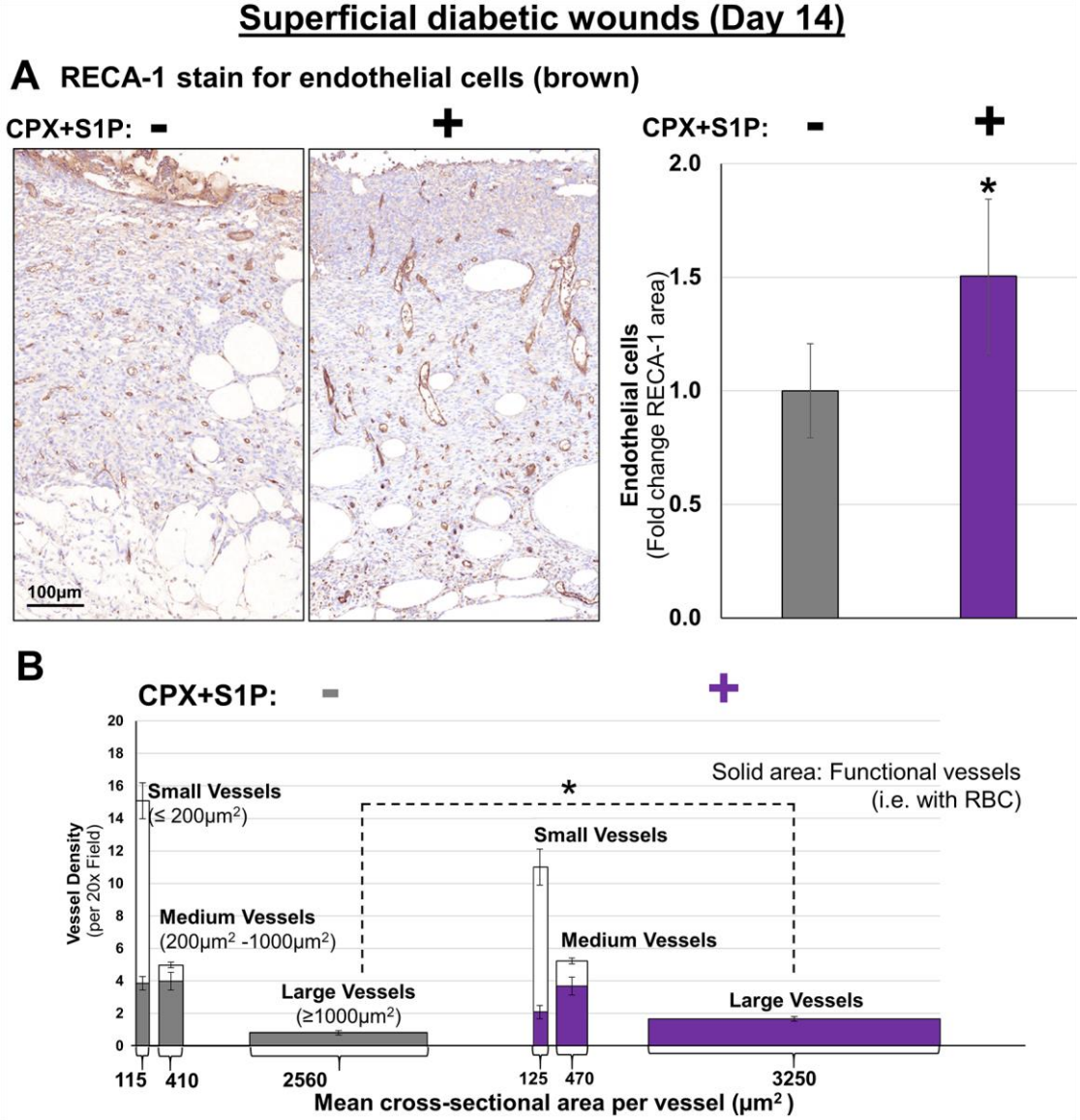

Figure B1. Angiogenesis in granulation tissue of superficial diabetic wounds with or without 0.1mM CPX + 0.01mM S1P treatment 14 days post-wounding. **(A)** Representative Immunohistochemical localization of RECA-1 positive endothelial cells (EC) (brown). Nuclei counterstained with haematoxylin (blue). Graph of RECA-1 positive area reveals a significant increase in EC infiltration with CPX+S1P. Area quantification was done on 12 20x magnification field in each replicate **(B)** Graph of vessel density of small vessels (cross-sectional area <200 µm^2), medium vessels (cross-sectional area between 200 µm^2 and 1000 µm^2) and large vessels (cross-sectional area >1000 µm^2) induced with or without CPX+S1P treatment. Functional vessels i.e., RECA-1 positive lumina containing red blood cells, are represented by solid areas. Vessel density quantified from 24 random sites in each treatment condition. Significance * $p <$

0.05, is derived from Student's t-test**.** Error bars represent standard error. n = 4 wound replicates.

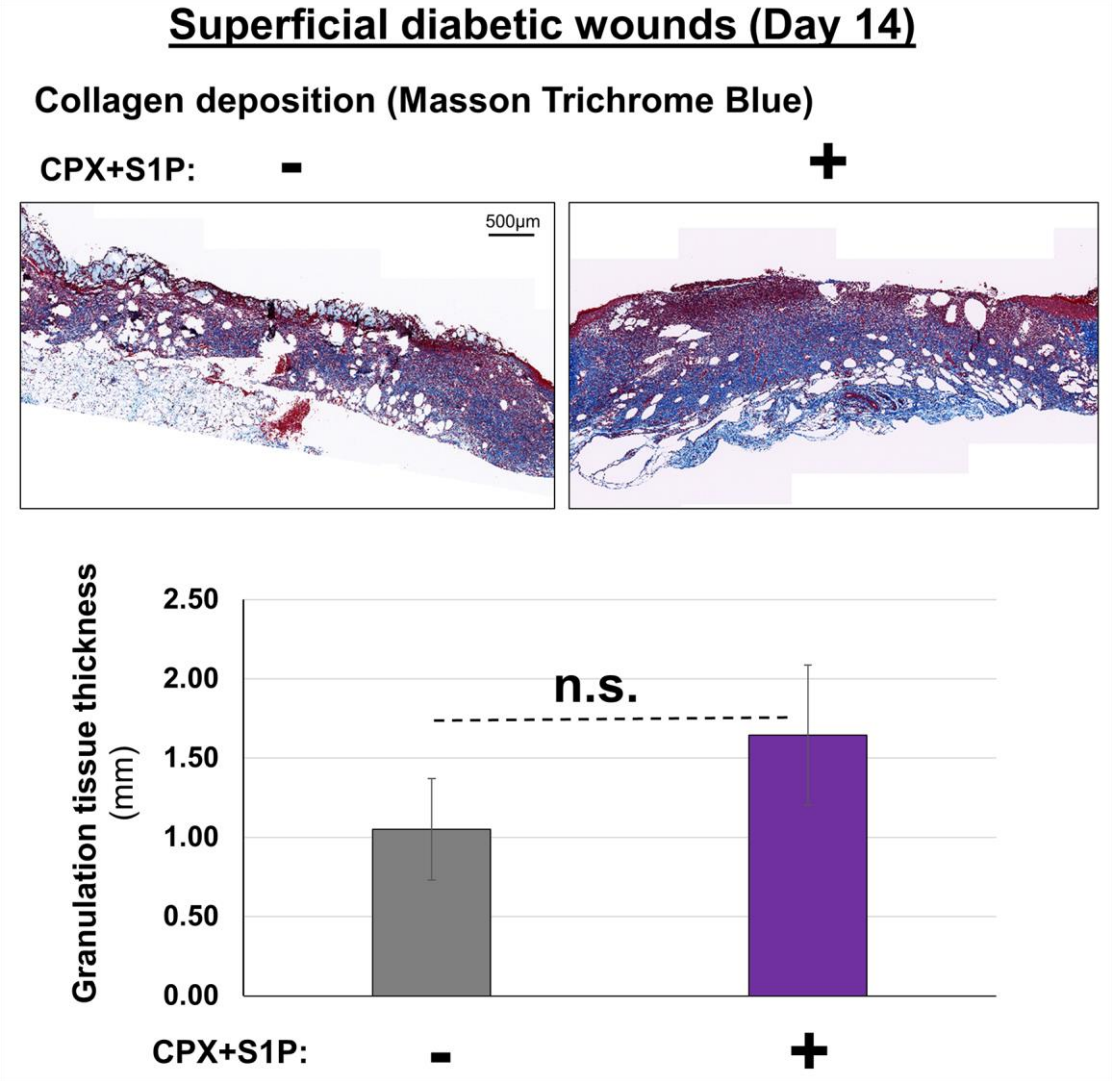

Figure B2. Representative Masson's trichrome blue stained granulation tissue of superficial diabetic wounds 14 days post-treatment with or without 0.1 mM CPX + 0.01 mM S1P. Collagen area (blue stain) thresholded using ImageJ. Graph reveals no significant increases in granulation tissue thickness Quantification done at 20x magnification field. Significance * $p < 0.05$, is derived from Student's two-tailed t-test**.** Error bars represent standard error. n = 4 wound replicates.

References

1. Arnold M. Hypoglycemia and Hyperglycemia. In: Ross T, Boucher J, O'Connell B, editor. *American Dietetic Association Guide to Diabetes Medical Nutrition Therapy and Education*. American Dietetic Association; 2005. p. 128.

2. Kota SK, Meher LK, Jammula S, Kota SK, Krishna SVS, Modi KD, et al. Aberrant angiogenesis: The gateway to diabetic complications. *Indian J Endocr Metab* 2012;16(6):918-930.

3. Frank IH, Silver A. Diabetic foot lesions. Preliminary report on a method of healing. *J Am Podiatry Assoc* 1962;52:596-598.

4. Balassa J. Treatment of a stasis ulcer in a diabetic with local application of insulin. *Med J Aust* 1967;2(13):604-605.

5. Rosenberg CS. Wound healing in the patient with diabetes mellitus. *Nurs Clin North Am* 1990;25(1):247-261.

6. Intine RV, Olsen AS, Sarras MP. A zebrafish model of diabetes mellitus and metabolic memory. *J Vis Exp* 2013;(72):e50232.

7. Ceriello A, Ihnat MA, Thorpe JE. Clinical review 2: The "metabolic memory": is more than just tight glucose control necessary to prevent diabetic complications? *J Clin Endocrinol Metab* 2009;94(2):410-415.

8. Wu S, Driver V, Wrobel J, Armstrong D. Foot ulcers in the diabetic patient, prevention and treatment. *Vasc Health Risk Manag* 2007;3(1):65-76.

9. Apelqvist J, Bakker K, van Houtum WH, Nabuurs-Franssen MH, Schaper NC. International consensus and practical guidelines on the management and the prevention of the diabetic foot. International Working Group on the Diabetic Foot. *Diabetes Metab Res Rev* 2000;16 Suppl 1:S84-S92.

10. Cook JJ, Simonson DC. Epidemiology and Health Care Cost of Diabetic Foot Problems. In: Veves A, Giurini, J, LoGerfo F, editor. *The Diabetic Foot Medical and Surgical Management*. 3 ed. New York: Humana Press; 2012. p. 17-32.

11. International Working Group on the Diabetic Foot [Internet]. [updated 2015; cited Jan 2016]. Available from: http://iwgdf.org/

12. Sussman C, Bates-Jensen BM. Introduction to wound diagnosis. In: Sussman, C; Bates-Jensen, BM, editor. *Wound Care*. Baltimore, MD, USA: Lippincott Williams & Wilkins; 2007. p. 22.

13. Levinson H. A Paradigm of Fibroblast Activation and Dermal Wound Contraction to Guide the Development of Therapies for Chronic Wounds and Pathologic Scars. *Adv Wound Care* 2013;2(4):149-159.

14. Catty RHC. Healing and contraction of experimental full-thickness wounds in human. *Br J Surg* 1965;52(7):542-548.

15. Yannas IV. The Defect Closure Rule. In: Yannas, IV, editor. *Tissue and Organ Regeneration in Adults*. New York: Springer; 2001. p. 70-87.

16. Berry DP, Harding KG, Stanton MR, Jasani B, Ehrlich HP. Human wound contraction: collagen organization, fibroblasts, and myofibroblasts. *Plast Reconstr Surg* 1998;102(1):124-131.

17. Ehrlich HP, Hunt TK. Collagen Organization Critical Role in Wound Contraction. *Adv Wound Care* 2012;1(1):3-9.

18. Arnold F, West D. Angiogenesis in wound healing. *Pharmacol Ther.* 1991;52(3):407-422.

19. DiPietro L. Angiogenesis and scar formation in healing wounds. *Curr Opin Rheumatol.* 2013;25(1):87-91.

20. Slavkovsky R, Kohlerova R, Tkacova V, Jiroutova A, Tahmazoglu B, Velebny V, et al. Zucker diabetic fatty rat: a new model of impaired cutaneous wound repair with type II diabetes mellitus and obesity. *Wound Repair Regen* 2011;19(4):515-525.

21. Lim SH, Kim C, Aref AR, Kamm RD, Raghunath M. Complementary effects of ciclopirox olamine, a prolyl hydroxylase inhibitor and sphingosine 1-phosphate on fibroblasts and endothelial cells in driving capillary sprouting. *Integr Biol* 2013;5(12):1474-1484.

22. Sontheimer RD. Skin is not the largest organ. J Invest Dermatol 2014;134(2):581-582.

23. Baranoski S. Integumentory Anatomy: Skin-The largest organ. In: McCulloch JM, Kloth LC, editor. *Wound Healing*. 4 ed. Philadelphia: F.A. Davis; 2010. p. 1-4.

24. Olczyk P, Mencner Ł, Komosinska-Vassev K. The role of the extracellular matrix components in cutaneous wound healing. *BioMed Res. Int.* 2014;2014:747584.

25. Hunt D. Diabetes: foot ulcers and amputations. *BMJ Clin Evid* 2011:0602.

26. Winter G. Formation of the scab and role of epithelialization in the skin of young domestic pigs. *Nature* 1962;193:293-294.

27. Stenn K, Depalma L. Re-epithelialization. In: Clarke RAF; Hensen PM, editor. *The molecular and cellular biology of wound repair*.New York: Plenum; 1988. p. 321-35.

28. Pastar I, Stojadinovic O, Yin NC, Ramirez H, Nusbaum AG, Sawaya A, et al. Epithelialization in Wound Healing: A Comprehensive Review. *Adv Wound Care* 2014;3(7):445-464.

29. Grillo H, Potsaid M. Studies in wound healing. IV. Retardation of contraction by local X-irradiation, and observations relating to the origin of fibroblasts in repair. *Ann Surg* 1961;154:741-750.

30. Peacock Jr E. Wound healing and wound care. In: Schwartz SI, Shires GT, Spencer FC, Storer EH, editor. *Principles of Surgery*. New York: McGraw-Hill; 1984.

31. Winkle V. Wound contraction. *Surg. Gyn. Obstet.* 1967;125:131.

32. Ramirez AT, Soroff HS, Schwartz MS, Mooty J, Pearson E, Raben MS, et al. Experimental wound healing in man. *Surg Gynecol Obstet* 1969;128(2):283-293.

33. Bullard KM, Lund L, Mudgett JS, Mellin TN, Hunt TK, Murphy B, et al. Impaired wound contraction in stromelysin-1-deficient mice. *Ann Surg* 1999;230(2):260-265.

34. Tomasek JJ, Gabbiani G, Hinz B, Chaponnier C, Brown RA. Myofibroblasts and mechano-regulation of connective tissue remodelling. Nat Rev Mol Cell Biol 2002;3(5):349-363.

35. Hinz B, Phan SH, Thannickal VJ, Galli A, Bochaton-Piallat ML, Gabbiani G, et al. The myofibroblast: one function, multiple origins. Am J Pathol 2007;170(6):1807-1816.

36. Eming SA, Brachvogel B, Odorisio T, Koch M. Regulation of angiogenesis: wound healing as a model. Prog Histochem Cytochem 2007;42(3):115-170.

37. Cohen M, Giladi M, Mayo A, Shafir R. The granulometer—a pocket scale for the assessment of wound healing. Ann Plast Surg 1998;40:641-645.

38. Vermeulen H, Ubbink D, Schreuder S, Lubbers M. Inter and intra-observer (dis)agreement among nurses and doctors to classify colour and exudation of open surgical wounds according to the Red-Yellow-Black scheme. J Clin Nurs 2007;16:1270-1277.

39. Bates-Jensen B, Vredevoe D, Brecht M. Validity and reliability of the pressure sore status tool. Decubitus 1992;5:20-28.

40. Sanada H, Moriguchi T, Miyachi Y, Ohura T, Nakajo T, Tokunaga K, et al. Reliability and validity of DESIGN, a tool that classifies pressure ulcer severity and monitors healing. J Wound Care 2004;13:13-18.

41. Sen CK. Wound healing essentials: let there be oxygen. Wound Repair Regen 2009;17(1):1-18.

42. Spyrou GE, Watt DA, Naylor IL. The origin and mode of fibroblast migration and proliferation in granulation tissue. Br J Plast Surg 1998;51(6):455-461.

43. Chang Y, Li H, Guo Z. Mesenchymal stem cell-like properties in fibroblasts. Cell Physiol Biochem 2014;34(3):703-714.

44. Stocum D. Regenerative Biology. In: Stocum, DL, editor. Regenerative Biology and Medicine. 2 ed. China: Academic Press; 2012. p. 28.

45. Ross R, Everett NB, Tyler R. Wound healing and collagen formation. VI. The origin of the wound fibroblast studied in parabiosis. J Cell Biol 1970;44(3):645-654.

46. Hadfield G. The tissue of origin of the fibroblasts of granulation tissue. Br J Surg 1963;50(226):870-881.

47. Sartore S, Chiavegato A, Faggin E, Franch R, Puato M, Ausoni S, et al. Contribution of adventitial fibroblasts to neointima formation and vascular remodeling: from innocent bystander to active participant. Circ Res 2001;89(12):1111-1121.

48. Sundberg C, Ivarsson M, Gerdin B, Rubin K. Pericytes as collagen-producing cells in excessive dermal scarring. Lab Invest 1996;74(2):452-466.

49. Sen CK, Roy S. Redox signals in wound healing. Biochim Biophys Acta 2008;1780(11):1348-1361.

50. Jiang F, Liu GS, Dusting GJ, Chan EC. NADPH oxidase-dependent redox signaling in TGF-β-mediated fibrotic responses. Redox biology 2014;2:267-272.

51. Hunt T. Oxygen and skin wound healing. In: Rovee, DT; Maibach, HI, editor. The Epidermis in Wound Healing. Boca Raton, Florida: CRC Press; 2003. p. 189.

52. Jonsson K, Jensen JA, Goodson WH, Scheuenstuhl H, West J, Hopf HW, et al. Tissue oxygenation, anemia, and perfusion in relation to wound healing in surgical patients. Ann Surg 1991;214(5):605-613.

53. Caselli A, Latini V, Lapenna A, Di Carlo S, Pirozzi F, Benvenuto A, et al. Transcutaneous oxygen tension monitoring after successful revascularization in diabetic patients with ischaemic foot ulcers. Diabet Med 2005;22(4):460-465.

54. Yang P, Pei Q, Yu T, Chang Q, Wang D, Gao M, et al. Compromised Wound Healing in Ischemic Type 2 Diabetic Rats. PloS one 2016;11(3):e0152068.

55. Gabbiani G. The myofibroblast in wound healing and fibrocontractive diseases. J Pathol 2003;200(4):500-503.

56. Betz P, Nerlich A, Wilske J, Tübel J, Penning R, Eisenmenger W, et al. Time-dependent appearance of myofibroblasts in granulation tissue of human skin wounds. Int J Legal Med 1992;105(2):99-103.

57. Gabbiani G, Ryan GB, Majne G. Presence of modified fibroblasts in granulation tissue and their possible role in wound contraction. Experientia 1971;27(5):549-550.

58. Hinz B, Phan SH, Thannickal VJ, Prunotto M, Desmoulière A, Varga J, et al. Recent developments in myofibroblast biology: paradigms for connective tissue remodeling. Am J Pathol 2012;180(4):1340-1355.

59. Muehlich S, Schneider N, Hinkmann F, Garlichs CD, Goppelt-Struebe M. Induction of connective tissue growth factor (CTGF) in human endothelial cells by lysophosphatidic acid, sphingosine-1-phosphate, and platelets. Atherosclerosis 2004;175(2):261-268.

60. Grotendorst GR. Connective tissue growth factor: a mediator of TGF-beta action on fibroblasts. Cytokine Growth Factor Rev 1997;8(3):171-179.

61. Kothapalli D, Frazier KS, Welply A, Segarini PR, Grotendorst GR. Transforming growth factor beta induces anchorage-independent growth of NRK fibroblasts via a connective tissue growth factor-dependent signaling pathway. Cell Growth Differ 1997;8(1):61-68.

62. Frazier K, Williams S, Kothapalli D, Klapper H, Grotendorst GR. Stimulation of fibroblast cell growth, matrix production, and granulation tissue formation by connective tissue growth factor. J Invest Dermatol 1996;107(3):404-411.

63. Duncan MR, Frazier KS, Abramson S, Williams S, Klapper H, Huang X, et al. Connective tissue growth factor mediates transforming growth factor beta-induced collagen synthesis: down-regulation by cAMP. FASEB journal : official

publication of the Federation of American Societies for Experimental Biology 1999;13(13):1774-1786.

64. Grotendorst GR, Rahmanie H, Duncan MR. Combinatorial signaling pathways determine fibroblast proliferation and myofibroblast differentiation. FASEB journal : official publication of the Federation of American Societies for Experimental Biology 2004;18(3):469-479.

65. Petrov VV, Fagard RH, Lijnen PJ. Stimulation of collagen production by transforming growth factor-beta1 during differentiation of cardiac fibroblasts to myofibroblasts. Hypertension 2002;39(2):258-263.

66. Tomasek JJ, Haaksma CJ, Schwartz RJ, Howard EW. Whole animal knockout of smooth muscle alpha-actin does not alter excisional wound healing or the fibroblast-to-myofibroblast transition. Wound Repair Regen 2013;21(1):166-176.

67. Castella LF, Buscemi L, Godbout C, Meister JJ, Hinz B. A new lock-step mechanism of matrix remodelling based on subcellular contractile events. J Cell Sci 2010;123(Pt 10):1751-1760.

68. Modarressi A, Pietramaggiori G, Godbout C, Vigato E, Pittet B, Hinz B, et al. Hypoxia impairs skin myofibroblast differentiation and function. J Invest Dermatol 2010;130(12):2818-2827.

69. Paul Ehrlich H, Sun B, Kainth KS, Kromah F. Elucidating the mechanism of wound contraction: rapid versus sustained myosin ATPase activity in attached-delayed-released compared with free-floating fibroblast-populated collagen lattices. Wound Repair Regen 2006;14(5):625-632.

70. Ehrlich H. Fibroblast populated collagen lattice. In: DiPietro, L.A.; Burns A.L., editor. Wound Healing. New Jersey: Springer Science & Business Media; 2003. p. 467.

71. Yannas I. The relation between wound contraction, scar formation and regeneration. Scar J 2008;(1):1-15.

72. Tonnesen MG, Feng X, Clark RAF. Angiogenesis in Wound Healing. Journal of Investigative Dermatology Symposium Proceedings 2000;5(1):40-46.

73. Bazzoni G, Dejana E. Endothelial cell-to-cell junctions: molecular organization and role in vascular homeostasis. Physiol Rev 2004;84(3):869-901.

74. Garcia-Medina J, Del-Rio-Vellosillo M, Gracia-Medina M, et al. Diabetic Retinopathy and Oxidative Stress. In: Preedy, VR, editor. Diabetes. USA: Academic Press; 2014. p. 38.

75. Davis GE, Senger DR. Endothelial extracellular matrix: biosynthesis, remodeling, and functions during vascular morphogenesis and neovessel stabilization. Circ Res 2005;97(11):1093-1107.

76. Eichmann A, Pardanaud L. Emergence of Endothelial Cells During Vascular Development. In: Feige, Jean-Jacques; Pagès, Gilles; Soncin, Fabrice, editor. Molecular Mechanisms of Angiogenesis. France: Springer; 2014. p. 4.

77. Adair T, Montani JP. Chapter 1. Overview of Angiogenesis. In: Adair, T.H., editor. Angiogenesis. San Rafael (CA): Morgan & Claypool Publishers; 2010. p. 71.

78. Ausprunk DH, Folkman J. Migration and proliferation of endothelial cells in preformed and newly formed blood vessels during tumor angiogenesis. Microvasc Res 1977;14(1):53-65.

79. Burri PH, Tarek MR. A novel mechanism of capillary growth in the rat pulmonary microcirculation. Anat Rec 1990;228:35-45.

80. Burri PH, Hlushchuk R, Djonov V. Intussusceptive Angiogenesis: Its Emergence, Its Characteristics, and Its Significance. Dev Dyn 2004;231:474-488.

81. Djonov V, Baum O, Burri PH. Vascular remodeling by intussusceptive angiogenesis. Cell Tissue Res 2003;314(1):107-117.

82. Adams RH, Alitalo K. Molecular regulation of angiogenesis and lymphangiogenesis. Nat Rev Mol Cell Biol 2007;8(6):464-478.

83. Potente M, Gerhardt H, Carmeliet P. Basic and Therapeutic Aspects of Angiogenesis. Cell 2011;146(6):873-887.

84. Haroon Z, Raleigh J, Greenberg C, Dewhirst M. Early wound healing exhibits cytokine surge without evidence of hypoxia. Ann Surg. 2000;231(1):137-147.

85. Remensnyder JP, Majno G. Oxygen gradients in healing wounds. Am J Pathol 1968;52(2):301-323.

86. Semenza GL, Wang GL. A nuclear factor induced by hypoxia via de novo protein synthesis binds to the human erythropoietin gene enhancer at a site required for transcriptional activation. Mol Cell Biol. 1992;12(12):5447-5454.

87. Cassavaugh J, Lounsbury K. Hypoxia-mediated biological control. J Cell Biochem. 2011;112(3):735-744.

88. Ke Q, Costa M. Hypoxia-Inducible Factor-1 (HIF-1). Mol Pharmacol 2006;70(5):1469-1480.

89. Pugh C, Rourke J, Nagao M, Gleadle J, Ratcliffe P. Activation of Hypoxia-inducible Factor-1; Definition of Regulatory Domains within the α Subunit. J Biol Chem 1997;272:11205-11214.

90. Wang GL, Jiang BH, Rue EA, Semenza GL. Hypoxia-inducible factor 1 is a basic-helix-loop-helix-PAS heterodimer regulated by cellular O2 tension. Proc Natl Acad Sci U S A 1995;92(12):5510-5514.

91. Iyer NV, Leung SW, Semenza GL. The human hypoxia-inducible factor 1alpha gene: HIF1A structure and evolutionary conservation. Genomics 1998;52(2):159-165.

92. Lando D, Peet DJ, Gorman JJ, Whelan DA, Whitelaw ML, Bruick RK, et al. FIH-1 is an asparaginyl hydroxylase enzyme that regulates the transcriptional activity of hypoxia-inducible factor. Genes Dev 2002;16:1466-1471.

93. Epstein AC, Gleadle JM, McNeill LA, Hewitson KS, O'Rourke J, Mole DR, et al. C. elegans EGL-9 and mammalian homologs define a family of dioxygenases that regulate HIF by prolyl hydroxylation. Cell 2001;107(1):43-54.

94. Fraisl P, Aragonés J, Carmeliet P. Inhibition of oxygen sensors as a therapeutic strategy for ischaemic and inflammatory disease. Nat Rev Drug Discov 2009;8(2):139-152.

95. Ehrismann D, Flashman E, Genn D, Mathioudakis N, Hewitson K, Ratcliffe P, et al. Studies on the activity of the hypoxia-inducible-factor hydroxylases using an oxygen consumption assay. Biochem J. 2007;401(1):227-234.

96. Kaelin WG, Ratcliffe PJ. Oxygen sensing by metazoans: the central role of the HIF hydroxylase pathway. Mol Cell 2008;30(4):393-402.

97. Kallio PJ, Wilson WJ, O'Brien S, Makino Y, Poellinger L. Regulation of the hypoxia-inducible transcription factor 1alpha by the ubiquitin-proteasome pathway. J Biol Chem 1999;274(10):6519-6525.

98. Semenza GL. Targeting HIF-1 for cancer therapy. Nat Rev Cancer 2003;3(10):721-732.

99. Ruas JL, Poellinger L, Pereira T. Role of CBP in regulating HIF-1-mediated activation of transcription. J Cell Sci 2005;118(Pt 2):301-311.

100. Manalo DJ, Rowan A, Lavoie T, Natarajan L, Kelly BD, Ye SQ, et al. Transcriptional regulation of vascular endothelial cell responses to hypoxia by HIF-1. Blood 2005;105(2):659-669.

101. Calvani M, Rapisarda A, Uranchimeg B, Shoemaker R, Melillo G. Hypoxic induction of an HIF-1alpha-dependent bFGF autocrine loop drives angiogenesis in human endothelial cells. Blood. 2006;107(7):2705-2712.

102. Senger DR, Galli SJ, Dvorak AM, Perruzzi CA, Harvey VS, Dvorak HF, et al. Tumor cells secrete a vascular permeability factor that promotes accumulation of ascites fluid. Science 1983;219(4587):983-985.

103. Brown LF, Yeo KT, Berse B, Yeo TK, Senger DR, Dvorak HF, et al. Expression of vascular permeability factor (vascular endothelial growth factor) by epidermal keratinocytes during wound healing. J Exp Med 1992;176(5):1375-1379.

104. Carmeliet P, Ferreira V, Breier G, Pollefeyt S, Kieckens L, Gertsenstein M, et al. Abnormal blood vessel development and lethality in embryos lacking a single VEGF allele. Nature 1996;380(6573):435-439.

105. Adair TH, Montani JP. Overview of Angiogenesis. In: Adair TH, editor. Angiogenesis. San Rafael (CA): Morgan & Claypool Publishers; 2010. p. 71.

106. Wang S, Li X, Parra M, Verdin E, Bassel-Duby R, Olson EN, et al. Control of endothelial cell proliferation and migration by VEGF signaling to histone deacetylase 7. Proc Natl Acad Sci U S A 2008;105(22):7738-7743.

107. Detmar M, Brown LF, Berse B, Jackman RW, Elicker BM, Dvorak HF, et al. Hypoxia regulates the expression of vascular permeability factor/vascular endothelial growth factor (VPF/VEGF) and its receptors in human skin. J Invest Dermatol 1997;108(3):263-268.

108. Murphy G, Willenbrock F, Crabbe T, O'Shea M, Ward R, Atkinson S, et al. Regulation of matrix metalloproteinase activity. Ann N Y Acad Sci 1994;732:31-41.

109. Siekmann AF, Lawson ND. Notch signalling limits angiogenic cell behaviour in developing zebrafish arteries. Nature 2007;445(7129):781-784.

110. Tang N, Wang L, Esko J, Giordano F, Huang Y, Gerber H, et al. Loss of HIF-1alpha in endothelial cells disrupts a hypoxia-driven VEGF autocrine loop necessary for tumorigenesis. Cancer Cell. 2004;6(5):485-495.

111. Nakatsu MN, Sainson RCA, Pérez-del-Pulgar S, Aoto JN, Aitkenhead M, Taylor KL, et al. VEGF(121) and VEGF(165) regulate blood vessel diameter through vascular endothelial growth factor receptor 2 in an in vitro angiogenesis model. Lab Invest 2003;83(12):1873-1885.

112. Nagy J, Benjamin L, Zeng H, Dvorak A, Dvorak H. Vascular permeability, vascular hyperpermeability and angiogenesis. Angiogenesis. 2008;11(2):109-119.

113. Dvorak H, Sioussat T, Brown L, Berse B, Nagy J, Sotrel A, et al. Distribution of Vascular Permeability Factor (Vascular. Endothelial Growth Factor) in Tumors: Concentration in Tumor Blood Vessels. J Exp Med 1991;174:1275-1278.

114. Yamakawa M, Liu LX, Date T, Belanger AJ, Vincent KA, Akita GY, et al. Hypoxia-inducible factor-1 mediates activation of cultured vascular endothelial cells by inducing multiple angiogenic factors. Circ Res 2003;93(7):664-673.

115. Hirschi KK, Rohovsky SA, Beck LH, Smith SR, D'Amore PA. Endothelial cells modulate the proliferation of mural cell precursors via platelet-derived growth factor-BB and heterotypic cell contact. Circ Res 1999;84(3):298-305.

116. Yatomi Y, Igarashi Y, Yang L, Hisano N, Qi R, Asazuma N, et al. Sphingosine 1-phosphate, a bioactive sphingolipid abundantly stored in platelets, is a normal constituent of human plasma and serum. J Biochem 1997;121(5):969-973.

117. Lucke S, Levkau B. Endothelial functions of sphingosine-1-phosphate. Cell Physiol Biochem 2010;26(1):87-96.

118. Sivan-Loukianova E, Awad OA, Stepanovic V, Bickenbach J, Schatteman GC. CD34+ blood cells accelerate vascularization and healing of diabetic mouse skin wounds. J Vasc Res 2003;40(4):368-377.

119. Tchaikovski V, Waltenberger J. Angiogenesis and arteriogenesis in diabetes mellitus. In: Deindl, Elisabeth; Kupatt, Christian, editor. Therapeutic Neovascularization – Quo vadis? Netherlands: Springer Science & Business Media; 2007. p. 51-54.

120. Brownlee M. Biochemistry and molecular cell biology of diabetic complications. Nature 2001;414(6865):813-820.

121. Brownlee M. The pathobiology of diabetic complications: a unifying mechanism. Diabetes 2005;54(6):1615-1625.

122. Kaiser N, Sasson S, Feener EP, Boukobza-Vardi N, Higashi S, Moller DE, et al. Differential regulation of glucose transport and transporters by glucose in vascular endothelial and smooth muscle cells. Diabetes 1993;42(1):80-89.

123. Heli H, Mirtorabi S, Karimian K. Advances in iron chelation: an update. Expert opinion on therapeutic patents 2011;21(6):819-856.

124. van den Oever IAM, Raterman HG, Nurmohamed MT, Simsek S. Endothelial dysfunction, inflammation, and apoptosis in diabetes mellitus. Mediators Inflamm 2010;2010:792393.

125. Marcus S, Dharmalingam M. Iron, Oxidative Stress and Diabetes,. In: Preedy, Victor R, editor. Diabetes. USA: Academic Press; 2014. p. 280.

126. Lipinski B, Pretorius E. Novel pathway of iron-induced blood coagulation: implications for diabetes mellitus and its complications. Pol Arch Med Wewn 2012;122(3):115-122.

127. Thangarajah H, Yao D, Chang EI, Shi Y, Jazayeri L, Vial IN, et al. The molecular basis for impaired hypoxia-induced VEGF expression in diabetic tissues. Proc Natl Acad Sci U S A 2009;106(32):13505-13510.

128. Thangarajah H, Vial IN, Grogan RH, Yao D, Shi Y, Januszyk M, et al. HIF-1alpha dysfunction in diabetes. Cell Cycle 2010;9(1):75-79.

129. Nakashima T, Sato E, Niwano Y, Kohno M, Muraoka W, Oda T, et al. Inhibitory or scavenging action of ketoconazole and ciclopiroxolamine against reactive oxygen species released by primed inflammatory cells. Br J Dermatol 2007;156(4):720-727.

130. Ko SH, Nauta A, Morrison SD, Zhou H, Zimmermann A, Gurtner GC, et al. Antimycotic ciclopirox olamine in the diabetic environment promotes angiogenesis and enhances wound healing. PloS one 2011;6(11):e27844.

131. Araszkiewicz A, Naskret D, Niedzwiecki P, Samborski P, Wierusz-Wysocka B, Zozulinska-Ziolkiewicz D, et al. Increased accumulation of skin advanced glycation end products is associated with microvascular complications in type 1 diabetes. Diabetes Technol Ther 2011;13(8):837-842.

132. Makita Z, Radoff S, Rayfield EJ, Yang Z, Skolnik E, Delaney V, et al. Advanced glycosylation end products in patients with diabetic nephropathy. N Engl J Med 1991;325(12):836-842.

133. Singh R, Barden A, Mori T, Beilin L. Advanced glycation end-products: a review. Diabetologia 2001;44(2):129-146.

134. Goldin A, Beckman JA, Schmidt AM, Creager MA. Advanced glycation end products: sparking the development of diabetic vascular injury. Circulation 2006;114(6):597-605.

135. Sajithlal GB, Chithra P, Chandrakasan G. The role of metal-catalyzed oxidation in the formation of advanced glycation end products: an in vitro study on collagen. Free Radic Biol Med 1998;25(3):265-269.

136. Bierhaus A, Hofmann MA, Ziegler R, Nawroth PP. AGEs and their interaction with AGE-receptors in vascular disease and diabetes mellitus. I. The AGE concept. Cardiovasc Res 1998;37(3):586-600.

137. Nagai R, Murray DB, Metz TO, Baynes JW. Chelation: a fundamental mechanism of action of AGE inhibitors, AGE breakers, and other inhibitors of diabetes complications. Diabetes 2012;61(3):549-559.

138. Giardino I, Edelstein D, Brownlee M. Nonenzymatic glycosylation in vitro and in bovine endothelial cells alters basic fibroblast growth factor activity. A model for intracellular glycosylation in diabetes. J Clin Invest 1994;94(1):110-117.

139. Cantero AV, Portero-Otín M, Ayala V, Auge N, Sanson M, Elbaz M, et al. Methylglyoxal induces advanced glycation end product (AGEs) formation and dysfunction of PDGF receptor-beta: implications for diabetic atherosclerosis. FASEB journal : official publication of the Federation of American Societies for Experimental Biology 2007;21(12):3096-3106.

140. Nass N, Vogel K, Hofmann B, Presek P, Silber RE, Simm A, et al. Glycation of PDGF results in decreased biological activity. Int J Biochem Cell Biol 2010;42(5):749-754.

141. Facchiano F, Lentini A, Fogliano V, Mancarella S, Rossi C, Facchiano A, et al. Sugar-induced modification of fibroblast growth factor 2 reduces its angiogenic activity in vivo. Am J Pathol 2002;161(2):531-541.

142. Portero-Otín M, Pamplona R, Bellmunt MJ, Ruiz MC, Prat J, Salvayre R, et al. Advanced glycation end product precursors impair epidermal growth factor receptor signaling. Diabetes 2002;51(5):1535-1542.

143. Giacco F, Brownlee M. Pathogenesis of Microvascular complications. In: Richard I G Holt; Cockram, Clive; Flyvbjerg, Allan; Goldstein, Barry J, editor. Textbook of Diabetes. 4 ed. Oxford, UK: John Wiley & Sons; 2011. p. 555-74.

144. Reigle KL, Di Lullo G, Turner KR, Last JA, Chervoneva I, Birk DE, et al. Non-enzymatic glycation of type I collagen diminishes collagen-proteoglycan binding and weakens cell adhesion. J Cell Biochem 2008;104(5):1684-1698.

145. Sengoelge G, Födinger M, Skoupy S, Ferrara I, Zangerle C, Rogy M, et al. Endothelial cell adhesion molecule and PMNL response to inflammatory stimuli and AGE-modified fibronectin. Kidney Int 1998;54(5):1637-1651.

146. Price DL, Rhett PM, Thorpe SR, Baynes JW. Chelating activity of advanced glycation end-product inhibitors. J Biol Chem 2001;276(52):48967-48972.

147. Nagai R, Nagai M, Shimasaki S, Baynes JW, Fujiwara Y. Citric acid inhibits development of cataracts, proteinuria and ketosis in streptozotocin (type 1) diabetic rats. Biochem Biophys Res Commun 2010;393(1):118-122.

148. Teixeira AS, Andrade SP. Glucose-induced inhibition of angiogenesis in the rat sponge granuloma is prevented by aminoguanidine. Life Sci 1999;64(8):655-662.

149. Teixeira AS, Caliari MV, Rocha OA, Machado RD, Andrade SP. Aminoguanidine prevents impaired healing and deficient angiogenesis in diabetic rats. Inflammation 1999;23(6):569-581.

150. Ozturk A, Fırat C, Parlakpınar H, Bay-Karabulut A, Kirimlioglu H, Gurlek A, et al. Beneficial effects of aminoguanidine on skin flap survival in diabetic rats. Exp Diabetes Res 2012;2012:721256.

151. Freidja ML, Tarhouni K, Toutain B, Fassot C, Loufrani L, Henrion D, et al. The AGE-breaker ALT-711 restores high blood flow-dependent remodeling in mesenteric resistance arteries in a rat model of type 2 diabetes. Diabetes 2012;61(6):1562-1572.

152. Wolffenbuttel BH, Boulanger CM, Crijns FR, Huijberts MS, Poitevin P, Swennen GN, et al. Breakers of advanced glycation end products restore large artery properties in experimental diabetes. Proc Natl Acad Sci U S A 1998;95(8):4630-4634.

153. Catrina SB, Okamoto K, Pereira T, Brismar K, Poellinger L. Hyperglycemia regulates hypoxia-inducible factor-1alpha protein stability and function. Diabetes 2004;53(12):3226-3232.

154. Botusan IR, Sunkari VG, Savu O, Catrina AI, Grünler J, Lindberg S, et al. Stabilization of HIF-1alpha is critical to improve wound healing in diabetic mice. Proc Natl Acad Sci U S A 2008;105(49):19426-19431.

155. Xiao H, Gu Z, Wang G, Zhao T. The possible mechanisms underlying the impairment of HIF-1α pathway signaling in hyperglycemia and the beneficial effects of certain therapies. Int J Med Sci 2013;10(10):1412-1421.

156. Ceradini DJ, Yao D, Grogan RH, Callaghan MJ, Edelstein D, Brownlee M, et al. Decreasing intracellular superoxide corrects defective ischemia-induced new vessel formation in diabetic mice. J Biol Chem 2008;283(16):10930-10938.

157. Altavilla D, Saitta A, Cucinotta D, Galeano M, Deodato B, Colonna M, et al. Inhibition of lipid peroxidation restores impaired vascular endothelial growth factor expression and stimulates wound healing and angiogenesis in the genetically diabetic mouse. Diabetes 2001;50(3):667-674.

158. Frank S, Hübner G, Breier G, Longaker MT, Greenhalgh DG, Werner S, et al. Regulation of vascular endothelial growth factor expression in cultured keratinocytes. Implications for normal and impaired wound healing. J Biol Chem 1995;270(21):12607-12613.

159. Linden T, Wenger RH. Iron chelation, angiogenesis and tumor therapy. Int J Cancer 2003;106(3):458-459.

160. Knowles HJ, Tian YM, Mole DR, Harris AL. Novel mechanism of action for hydralazine: induction of hypoxia-inducible factor-1alpha, vascular endothelial growth factor, and angiogenesis by inhibition of prolyl hydroxylases. Circ Res 2004;95(2):162-169.

161. Warnecke C, Griethe W, Weidemann A, Jürgensen JS, Willam C, Bachmann S, et al. Activation of the hypoxia-inducible factor-pathway and stimulation of angiogenesis by application of prolyl hydroxylase inhibitors. FASEB journal : official publication of the Federation of American Societies for Experimental Biology 2003;17(9):1186-1188.

162. Nangaku M, Izuhara Y, Takizawa S, Yamashita T, Fujii-Kuriyama Y, Ohneda O, et al. A novel class of prolyl hydroxylase inhibitors induces angiogenesis and exerts organ protection against ischemia. Arterioscler Thromb Vasc Biol 2007;27(12):2548-2554.

163. Gill SE, Parks WC. Metalloproteinases and their inhibitors: regulators of wound healing. Int J Biochem Cell Biol 2008;40(6-7):1334-1347.

164. Lobmann R, Ambrosch A, Schultz G, Waldmann K, Schiweck S, Lehnert H, et al. Expression of matrix-metalloproteinases and their inhibitors in the wounds of diabetic and non-diabetic patients. Diabetologia 2002;45(7):1011-1016.

165. Wall SJ, Sampson MJ, Levell N, Murphy G. Elevated matrix metalloproteinase-2 and -3 production from human diabetic dermal fibroblasts. Br J Dermatol 2003;149(1):13-16.

166. Fuller B. Anti-oxidants and anti-inflammatories. In: Draelos, ZD, editor. Cosmetic Dermatology. 2 ed. West Sussex, UK: John Wiley & Sons; 2015. p. 296.

167. Kar S, Subbaram S, Carrico PM, Melendez JA. Redox-control of matrix metalloproteinase-1: a critical link between free radicals, matrix remodeling and degenerative disease. Respir Physiol Neurobiol 2010;174(3):299-306.

168. Siwik DA, Chang DL, Colucci WS. Interleukin-1beta and tumor necrosis factor-alpha decrease collagen synthesis and increase matrix metalloproteinase activity in cardiac fibroblasts in vitro. Circ Res 2000;86(12):1259-1265.

169. Rundhaug JE. Matrix metalloproteinases and angiogenesis. J Cell Mol Med 2005;9(2):267-285.

170. Gibson DJ, Schultz GS. Molecular Wound Assessments: Matrix Metalloproteinases. Advances in wound care 2013;2(1):18-23.

171. Trengove NJ, Stacey MC, MacAuley S, Bennett N, Gibson J, Burslem F, et al. Analysis of the acute and chronic wound environments: the role of proteases and their inhibitors. Wound Repair Regen 1999;7(6):442-452.

172. Olmos JM, García MT, Amado JA, González-Macías J. Urine hydroxyproline increase in patients with diabetes mellitus. Diabet Med 1996;13(3):284.

173. Weihrauch D, Lohr NL, Mraovic B, Ludwig LM, Chilian WM, Pagel PS, et al. Chronic hyperglycemia attenuates coronary collateral development and impairs proliferative properties of myocardial interstitial fluid by production of angiostatin. Circulation 2004;109(19):2343-2348.

174. Jacobsen JA, Major Jourden JL, Miller MT, Cohen SM. To bind zinc or not to bind zinc: an examination of innovative approaches to improved metalloproteinase inhibition. Biochim Biophys Acta 2010;1803(1):72-94.

175. Mirastschijski U, Haaksma CJ, Tomasek JJ, Agren MS. Matrix metalloproteinase inhibitor GM 6001 attenuates keratinocyte migration, contraction and myofibroblast formation in skin wounds. Exp Cell Res 2004;299(2):465-475.

176. Agren MS, Mirastschijski U, Karlsmark T, Saarialho-Kere UK. Topical synthetic inhibitor of matrix metalloproteinases delays epidermal regeneration of human wounds. Exp Dermatol 2001;10(5):337-348.

177. Gooyit M, Peng Z, Wolter WR, Pi H, Ding D, Hesek D, et al. A chemical biological strategy to facilitate diabetic wound healing. ACS Chem Biol 2014;9(1):105-110.

178. Gao M, Nguyen TT, Suckow MA, Wolter WR, Gooyit M, Mobashery S, et al. Acceleration of diabetic wound healing using a novel protease-anti-protease combination therapy. Proc Natl Acad Sci U S A 2015;112(49):15226-15231.

179. Tong X, Peng H, Liu D, Ji L, Niu C, Ren J, et al. High-density lipoprotein of patients with Type 2 Diabetes Mellitus upregulates cyclooxgenase-2 expression and prostacyclin I-2 release in endothelial cells: relationship with HDL-associated sphingosine-1-phosphate. Cardiovasc Diabetol 2013;12(1):27.

180. Zhang H, Desai NN, Olivera A, Seki T, Brooker G, Spiegel S, et al. Sphingosine-1-phosphate, a novel lipid, involved in cellular proliferation. J Cell Biol 1991;114(1):155-167.

181. Spiegel S, Milstien S. Functions of the multifaceted family of sphingosine kinases and some close relatives. J Biol Chem 2007;282(4):2125-2129.

182. Venkataraman K, Thangada S, Michaud J, Oo ML, Ai Y, Lee YM, et al. Extracellular export of sphingosine kinase-1a contributes to the vascular S1P gradient. Biochem J 2006;397(3):461-471.

183. Hla T, Venkataraman K, Michaud J. The vascular S1P gradient—Cellular sources and biological significance. Biochim Biophys Acta 2008;1781(9):477-482.

184. Waeber, Christian. Sphingosine 1-Phosphate (S1P) Signaling and the Vasculature. In: Chun, Jerold; Hla, Timothy; Spiegel, Sara; Moolenaar, Wouter, editor. Lysophospholipid Receptors. 1 ed. John Wiley & Sons; 2013. p. 313-47.

185. Chae SS, Paik JH, Furneaux H, Hla T. Requirement for sphingosine 1-phosphate receptor-1 in tumor angiogenesis demonstrated by in vivo RNA interference. J Clin Invest 2004;114(8):1082-1089.

186. Paik JH, Chae Ss, Lee MJ, Thangada S, Hla T. Sphingosine 1-phosphate-induced endothelial cell migration requires the expression of EDG-1 and EDG-3 receptors and Rho-dependent activation of alpha vbeta3- and beta1-containing integrins. J Biol Chem 2001;276(15):11830-11837.

187. Skoura A, Hla T. Regulation of vascular physiology and pathology by the S1P2 receptor subtype. Cardiovasc Res 2009;82(2):221-228.

188. Inoki I, Takuwa N, Sugimoto N, Yoshioka K, Takata S, Kaneko S, et al. Negative regulation of endothelial morphogenesis and angiogenesis by S1P2 receptor. Biochem Biophys Res Commun 2006;346(1):293-300.

189. Liu Y, Wada R, Yamashita T, Mi Y, Deng CX, Hobson JP, et al. Edg-1, the G protein-coupled receptor for sphingosine-1-phosphate, is essential for vascular maturation. J Clin Invest 2000;106(8):951-961.

190. Allende ML, Proia RL. Sphingosine-1-phosphate receptors and the development of the vascular system. Biochim Biophys Acta 2002;1582(1-3):222-227.

191. Gaengel K, Niaudet C, Hagikura K, Laviña B, Muhl L, Hofmann J, et al. The sphingosine-1-phosphate receptor S1PR1 restricts sprouting angiogenesis by regulating the interplay between VE-cadherin and VEGFR2. Dev Cell. 2012;23(3):587-599.

192. Schaphorst KL, Chiang E, Jacobs KN, Zaiman A, Natarajan V, Wigley F, et al. Role of sphingosine-1 phosphate in the enhancement of endothelial barrier integrity by platelet-released products. Am J Physiol Lung Cell Mol Physiol 2003;285(1):L258-L267.

193. Feistritzer C, Riewald M. Endothelial barrier protection by activated protein C through PAR1-dependent sphingosine 1-phosphate receptor-1 crossactivation. Blood 2005;105(8):3178-3184.

194. Singleton PA, Dudek SM, Chiang ET, Garcia JGN. Regulation of sphingosine 1-phosphate-induced endothelial cytoskeletal rearrangement and barrier enhancement by S1P1 receptor, PI3 kinase, Tiam1/Rac1, and alpha-actinin. FASEB journal : official publication of the Federation of American Societies for Experimental Biology 2005;19(12):1646-1656.

195. Sanna MG, Wang SK, Gonzalez-Cabrera PJ, Don A, Marsolais D, Matheu MP, et al. Enhancement of capillary leakage and restoration of lymphocyte egress by a chiral S1P1 antagonist in vivo. Nat Chem Biol 2006;2(8):434-441.

196. Nofer JR, van der Giet M, Tölle M, Wolinska I, von Wnuck Lipinski K, Baba HA, et al. HDL induces NO-dependent vasorelaxation via the lysophospholipid receptor S1P3. J Clin Invest 2004;113(4):569-581.

197. Pchejetski D, Kunduzova O, Dayon A, Calise D, Seguelas MH, Leducq N, et al. Oxidative stress-dependent sphingosine kinase-1 inhibition mediates monoamine oxidase A-associated cardiac cell apoptosis. Circ Res 2007;100(1):41-49.

198. Geoffroy K, Wiernsperger N, Lagarde M, El Bawab S. Bimodal effect of advanced glycation end products on mesangial cell proliferation is mediated by neutral ceramidase regulation and endogenous sphingolipids. J Biol Chem 2004;279(33):34343-34352.

199. Kawanabe T, Kawakami T, Yatomi Y, Shimada S, Soma Y. Sphingosine 1-phosphate accelerates wound healing in diabetic mice. J Dermatol Sci 2007;48(1):53-60.

200. Sanchez T, Estrada-Hernandez T, Paik JH, Wu MT, Venkataraman K, Brinkmann V, et al. Phosphorylation and action of the immunomodulator FTY720 inhibits vascular endothelial cell growth factor-induced vascular permeability. J Biol Chem 2003;278(47):47281-47290.

201. Yin Z, Fan L, Wei L, Gao H, Zhang R, Tao L, et al. FTY720 protects cardiac microvessels of diabetes: a critical role of S1P1/3 in diabetic heart disease. PloS one 2012;7(8):e42900.

202. Mateo MC, Bustamante JB, Cantalapiedra MA. Serum, zinc, copper and insulin in diabetes mellitus. Biomedicine 1978;29(2):56-58.

203. Tobin J, Walsh G. Regulatory Strategy. In: Tobin, JJ; Walsh, G, editor. Medical Product Regulatory Affairs. Weinheim, Germany: John Wiley & Sons; 2011. p. 32-36.

204. Therapeutic Angiogenesis [Internet]. [updated 2015; cited 28 March 2016]. Available from: http://www.angio.org/learn/treatments/

205. Greer N, Foman N, Dorrian J, Fitzgerald P, MacDonald R, Rutks I, et al. Advanced Wound Care Therapies for Non-Healing Diabetic, Venous, and Arterial Ulcers: A Systematic Review. VA-ESP Project 2012;#09-009:1-177.

206. Alexiadou K, Doupis J. Management of diabetic foot ulcers. Diabetes therapy : research, treatment and education of diabetes and related disorders 2012;3(1):4.

207. Yu J, Moon A, Kim H. Both platelet-derived growth factor receptor (PDGFR)-alpha and PDGFR-beta promote murine fibroblast cell migration. Biochem Biophys Res Commun 2001;282(3):697-700.

208. Uhl E, Rösken F, Sirsjö A, Messmer K. Influence of platelet-derived growth factor on microcirculation during normal and impaired wound healing. Wound Repair Regen 2003;11(5):361-367.

209. Greenhalgh D, Sprugel K, Murray M, Ross R. PDGF and FGF stimulate wound healing in the genetically diabetic mouse. Am J Pathol 1990;136(6):1235-1246.

210. Senter L, Legrand E, Laemmerhirt K, Kiorpes T. Assessment of full-thickness wounds in the genetically diabetic mouse for suitability as a wound healing model. Wound Repair Regen 1995;3(3):351-358.

211. Rees RS, Robson MC, Smiell JM, Perry BH. Becaplermin gel in the treatment of pressure ulcers: a phase II randomized, double-blind, placebo-controlled study. Wound Repair Regen 1999;7(3):141-147.

212. Embil J, Papp K, Sibbald G, Tousignant J, Smiell J, Wong B, et al. Recombinant human platelet-derived growth factor-BB (becaplermin) for healing chronic lower extremity diabetic ulcers: an open-label clinical evaluation of efficacy. Wound Repair Regen 2000;8(3):162-168.

213. Smiell J, Wieman T, Steed D, Perry B, Sampson A, Schwab B, et al. Efficacy and safety of becaplermin (recombinant human platelet-derived growth factor-BB) in patients with nonhealing, lower extremity diabetic ulcers: a combined analysis of four randomized studies. Wound Repair Regen 1999;7(5):335-346.

214. Greco III J, Nanney LB. Growth factors - modulators of wound healing. In: Norman, GR; Streiner, DL, editor. Biostatistics. Shelton, CT: PMPH-USA; 2008. p. 389.

215. Papanas N, Maltezos E. Benefit-risk assessment of becaplermin in the treatment of diabetic foot ulcers. Drug safety 2010;33(6):455-461.

216. Govindarajan B, Shah A, Cohen C, Arnold R, Schechner J, Chung J, et al. Malignant transformation of human cells by constitutive expression of platelet-derived growth factor-BB. J Biol Chem 2005;280(14):13936-13943.

217. Lacci KM, Dardik A. Platelet-rich plasma: support for its use in wound healing. Yale J Biol Med 2010;83(1):1-9.

218. Regranex withdrawal of the marketing authorisation in the European Union [Internet]. [updated 2012; cited 29-11-13]. Available from: http://www.ema.europa.eu/docs/en_GB/document_library/Public_statement/2012/08/WC500130948.pdf

219. Slesaczeck T, Paetzold H, Nanning T, Reichel A, Barthel A, Bornstein S, et al. Autologous derived, platelet-rich plasma gel in the treatment of

nonhealing diabetic foot ulcer: a case report. Therapeutic advances in endocrinology and metabolism 2012;3(2):75-78.

220. Choi J, Minn K, Chang H. The efficacy and safety of platelet-rich plasma and adipose-derived stem cells: an update. Archives of plastic surgery 2012;39(6):585-592.

221. Bir SC, Esaki J, Marui A, Sakaguchi H, Kevil CG, Ikeda T, et al. Therapeutic treatment with sustained-release platelet-rich plasma restores blood perfusion by augmenting ischemia-induced angiogenesis and arteriogenesis in diabetic mice. J Vasc Res 2011;48(3):195-205.

222. Pietramaggiori G, Scherer SS, Mathews JC, Gennaoui T, Lancerotto L, Ragno G, Valeri CR, et al. Quiescent platelets stimulate angiogenesis and diabetic wound healing. J Surg Res 2010;160(1):169-177.

223. Saad Setta H, Elshahat A, Elsherbiny K, Massoud K, Safe I. Platelet-rich plasma versus platelet-poor plasma in the management of chronic diabetic foot ulcers: a comparative study. Int Wound K 2011;8(3): 307-312.

224. Driver VR, Hanft J, Fylling CP, Beriou JM. Autologel Diabetic Foot Ulcer Study Group. A prospective, randomized, controlled trial of autologous platelet-rich plasma gel for the treatment of diabetic foot ulcers. Ostomy Wound Manage 2006;52(6):68-70, 72, 74 passim.

225. Kakagia D, Kazakos K, Xarchas K, Karanikas M, Georgiadis G, Tripsiannis G, et al. Synergistic action of protease-modulating matrix and autologous growth factors in healing of diabetic foot ulcers. A prospective randomized trial. J Diabetes Complications. 2007;21(6):387-391.

226. Ribatti D, Baiguera S. Phase II angiogenesis stimulators. Expert Opin Investig Drugs 2013;22(9):1157-1166.

227. Alfranca A. VEGF therapy: a timely retreat. Cardiovasc Res 2009;83(4):611-612.

228. Cost of Developing a New Drug [Internet]. [updated 2014; cited 18 Sept 2015]. Available from: http://csdd.tufts.edu/files/uploads/Tufts_CSDD_briefing_on_RD_cost_study_-_Nov_18,_2014..pdf

229. DiMasi J, Grabowski H, Hansen R. Innovation in the pharmaceutical industry: new estimates of R&D costs. J Health Econ 2016;47:20-33.

230. Meier K, Nanney LB. Emerging new drugs for wound repair. Expert Opin Emerg Drugs 2006;11(1):23-37.

231. Repurposing Drugs [Internet]. [updated 2016; cited 6 May 2016]. Available from: https://ncats.nih.gov/preclinical/repurpose

232. Ashburn T, Thor K. Drug repositioning: identifying and developing new uses for existing drugs. Nat Rev Drug Discov 2004;3(8):673-683.

233. Tallarida RJ. Drug synergism: its detection and applications. J Pharmacol Exp Ther 2001;298(3):865-872.

234. Owens CM, Mawhinney C, Grenier JM, Altmeyer R, Lee MS, Borisy AA, et al. Chemical combinations elucidate pathway interactions and regulation relevant to Hepatitis C replication. Mol Syst Biol 2010;6:375.

235. Nelander S, Wang W, Nilsson B, She QB, Pratilas C, Rosen N, et al. Models from experiments: combinatorial drug perturbations of cancer cells. Mol Syst Biol 2008;4:216.

236. Jansen G, Lee AY, Epp E, Fredette A, Surprenant J, Harcus D, et al. Chemogenomic profiling predicts antifungal synergies. Mol Syst Biol 2009;5:338.

237. Sharma S, Mathur AG, Pradhan S, Singh DB, Gupta S. Fingolimod (FTY720): First approved oral therapy for multiple sclerosis. Journal of pharmacology & pharmacotherapeutics 2011;2(1):49-51.

238. Subissi A, Monti D, Togni G, Mailland F. Ciclopirox: recent nonclinical and clinical data relevant to its use as a topical antimycotic agent. Drugs 2010;70(16):2133-2152.

239. FDA approved drug products: Ciclopirox [Internet]. [updated 2016; cited 28 March 2016]. Available from: http://www.accessdata.fda.gov/scripts/cder/drugsatfda/index.cfm?fuseaction=Search.Overview&DrugName=CICLOPIROX

240. Tarawneh R, Hamdan I, Bani-Jaber A, Darwish R. Physicochemical studies on Ciclopirox olamine complexes with divalent metal ions. Int J Pharm 2005;289(1-2):179-187.

241. Linden T, Katschinski DM, Eckhardt K, Scheid A, Pagel H, Wenger RH, et al. The antimycotic ciclopirox olamine induces HIF-1alpha stability, VEGF expression, and angiogenesis. FASEB journal : official publication of the Federation of American Societies for Experimental Biology 2003;17(6):761-763.

242. Raghunath M, Lim SH and Kamm R. Compositions And Methods For Neovascularization. Patent 9446031. U.S. Patent and Trademark Office. 2013.

243. Richard D, Berra E, Gothié E, Roux D, Pouysségur J. p42/p44 mitogen-activated protein kinases phosphorylate hypoxia-inducible factor 1alpha (HIF-1alpha) and enhance the transcriptional activity of HIF-1. J Biol Chem. 1999;274(46):32631-32637.

244. Sang N, Stiehl D, Bohensky J, Leshchinsky I, Srinivas V, Caro J, et al. MAPK signaling up-regulates the activity of hypoxia-inducible factors by its effects on p300. J Biol Chem. 2003;278(16):14013-14019.

245. Hirota K, Semenza G. Regulation of angiogenesis by hypoxia-inducible factor 1. Crit Rev Oncol Hematol. 2006;59(1):15-26.

246. Grindlay JH, Waugh JM. Plastic sponge which acts as a framework for living tissue; experimental studies and preliminary report of use to reinforce abdominal aneurysms. AMA Arch Surg 1951;63(3):288-297.

247. Wang H, Gordon D, Olszewski B, Song YL, Kovesdi I, Keiser JA, et al. Rat sponge implant model: a new system for evaluating angiogenic gene transfer. Int J Mol Med. 2000;6(6):645-653.

248. Andrade S, Ferreira MAND. The Sponge Implant Model of Angiogenesis. In: Martin, S.; Murray, C., editor. Methods in Molecular Biology, Angiogenesis Protocols. 2 ed. Humana Press, a part of Springer Science + Business Media; 2009. p. 295-304.

249. Deskins D, Ardestani S, Young P. The polyvinyl alcohol sponge model implantation. J Vis Exp. 2012;:3885.

250. Dorsett-Martin WA, Wysocki AB. Rat models of skin wound healing. In: Conn, P Michael, editor. Sourcebook of Models for Biomedical Research. Totowa, New Jersey: Springer Science & Business Media; 2008. p. 633-34.

251. Staton C, Reed M, Brown N. A critical analysis of current in vitro and in vivo angiogenesis assays. Int J Exp Pathol. 2009;90(3):195-221.

252. Laitinen L. Griffonia simplicifolia lectins bind specifically to endothelial cells and some epithelial cells in mouse tissues. Histochem J 1987;19(4):225-234.

253. Benton R, Maddie M, Minnillo D, Hagg T, Whittemore S. Griffonia simplicifolia Isolectin B4 Identifies a Specific Subpopulation of Angiogenic Blood Vessels Following Contusive Spinal Cord Injury in the Adult Mouse. J Comp Neurol 2008;507(1):1031-1052.

254. Kirkeby S, Winter H, Goldstein I. Binding of Griffonia simplicifolia 1 isolectin B4 (GS1 B4) to alpha-galactose antigens. Immunol Cell Biol 2001;79:121-127.

255. Shiota M, Printz R. Diabetes in Zucker diabetic fatty rat. Methods Mol Biol 2012;933:103-123.

256. Diet evaluation study for the induction of type 2 diabetes in obese female ZDF rats [Internet]. [updated 2010; cited 4 April 2016]. Available from: http://www.criver.com/files/pdfs/rms/zdf/rm_rm_r_zdf_diet_eval_tech_sheet.aspx

257. Lee Y, Hirose H, Ohneda M, Johnson JH, McGarry JD, Unger RH, et al. Beta-cell lipotoxicity in the pathogenesis of non-insulin-dependent diabetes mellitus of obese rats: impairment in adipocyte-beta-cell relationships. Proc Natl Acad Sci U S A 1994;91(23):10878-10882.

258. Leonard B, Watson R, Loomes K, Phillips A, Cooper G. Insulin resistance in the Zucker diabetic fatty rat: a metabolic characterisation of obese and lean phenotypes. Acta Diabetol 2005;42(4):162-170.

259. Peterson R, Shaw W, Neel M, Little L, Eichberg J. Zucker diabetic fatty as a model for non-insulin dependent diabetes mellitus. Ilar News 1990;32:16-19.

260. Danis RP, Yang Y. Microvascular retinopathy in the Zucker diabetic fatty rat. Invest Ophthalmol Vis Sci 1993;34(7):2367-2371.

261. Vardaxis NJ, Brans TA, Boon ME, Kreis RW, Marres LM. Confocal laser scanning microscopy of porcine skin: implications for human wound healing studies. J. Anat 1997;190:601-611.

262. Chatzigeorgiou A, Halapas A, Kalafatakis K, Kamper E. The use of animal models in the study of diabetes mellitus. In Vivo 2009;23(2):245-258.

263. Wong VW, Sorkin M, Glotzbach JP, Longaker MT, Gurtner GC. Surgical approaches to create murine models of human wound healing. Journal of biomedicine & biotechnology 2011;2011:969618.

264. Davidson JM, Yu F, Opalenik SR. Splinting Strategies to Overcome Confounding Wound Contraction in Experimental Animal Models. Advances in wound care 2013;2(4):142-148.

265. James DW, Newcombe JF. Granulation tissue resorption during free and limited contraction of skin wounds. J Anat. 1961;95:247.

266. Abercrombie M, James DW, Newcombe JF. Wound contraction in rabbit skin, studied by splinting the wound margins. J Anat. 1960;94:170.

267. Kennedy DF, Cliff WJ. A systematic study of wound contraction in mammalian skin. Pathology 1979;11(2):207-222.

268. Wagner F. The diabetic foot. Orthopedics 1987;10:163-172.

269. Valero C, Javierre E, García-Aznar JM, Gómez-Benito MJ. Nonlinear finite element simulations of injuries with free boundaries: application to surgical wounds. International journal for numerical methods in biomedical engineering 2014;30(6):616-633.

270. Stashak TS, Theoret CL. Wounds of the distal extremeties. In: Stashak TS; Theoret CL, editor. Equine Wound Management. 2 ed. Iowa, USA: John Wiley & Sons; 2011. p. 428.

271. Biel NM, Lee JA, Sorg BS, Siemann DW. Limitations of the dorsal skinfold window chamber model in evaluating anti-angiogenic therapy during early phase of angiogenesis. Vascular cell 2014;6:17.

272. Junker J, Kamel R, Caterson E, Eriksson E. Clinical Impact Upon Wound Healing and Inflammation in Moist, Wet, and Dry Environments. Advances in wound care 2013;2(7):348-356.

273. D'Hemecourt P, Smiell J, Karim M. Sodium carboxymethylcellulose aqueous-based gel vs. becaplermin gel in patients with nonhealing lower extremity diabetic ulcers. Wounds 1998;10(3):69-75.

274. Guinta F, Di Salvo C, Rubino A, et al. Does choice of inhaled anesthetic agent matter? In: Leykin, Y; Brodsky, JB, editor. Controversies in the Anesthetic Management of the Obese Surgical Patient. Italia: Springer Science & Business Media; 2013. p. 201.

275. Kato Y, Iwata T, Morikawa S, Yamato M, Okano T, Uchigata Y, et al. Allogeneic Transplantation of an Adipose-Derived Stem Cell Sheet Combined With Artificial Skin Accelerates Wound Healing in a Rat Wound Model of Type 2 Diabetes and Obesity. Diabetes 2015;64(8):2723-2734.

276. Ruifrok A, Johnston D. Quantification of histochemical staining by color deconvolution. Anal Quant Cytol Histol 2001;23(4):291-299.

277. Clement P, Hanauske-Abel H, Wolff E, Kleinman H, Park M. The antifungal drug ciclopirox inhibits deoxyhypusine and proline hydroxylation, endothelial cell growth and angiogenesis in vitro. International journal of cancer 2002;100(4):491-498.

278. Rich L, Whittaker P. Collagen and Picrosirius red staining: A polarized light assessment of fibrillar hue and spatial distribution. Braz. J. morphol. Sci. 2005;22(2):97-104.

279. English D., Welch Z., Kovala A.T., Harvey K., Volpert O.V., Brindley D.N., et al. Sphingosine 1-phosphate released from platelets during clotting accounts for the potent endothelial cell chemotactic activity of blood serum

and provides a novel link between hemostasis and angiogenesis. FASEB J. 2000;14(14):2255-2265..

280. Kalhori V, Kemppainen K, Asghar M, Bergelin N, Jaakkola P, Törnquist K, et al. Sphingosine-1-Phosphate as a Regulator of Hypoxia-Induced Factor-1α in Thyroid Follicular Carcinoma Cells. PloS one 2013;8(6):e66189.

281. Luo Y, Zhou H, Liu L, Shen T, Chen W, Xu B, et al. The fungicide ciclopirox inhibits lymphatic endothelial cell tube formation by suppressing VEGFR-3-mediated ERK signaling pathway. Oncogene. 2011;30(18):2098-2107.

282. Tal R, Shaish A, Rofe K, Feige E, Varda-Bloom N, Afek A, et al. Endothelial-targeted Gene Transfer of Hypoxia-inducible Factor-1α Augments Ischemic Neovascularization Following Systemic Administration. Mol Ther. 2008;16(12):1927-1936.

283. Tal R, Shaish A, Bangio L, Peled M, Breitbart E, Harats D, et al. Activation of C-transactivation domain is essential for optimal HIF-1 alpha-mediated transcriptional and angiogenic effects. Microvasc Res 2008;76(1):1-6.

284. Zeng Y, Adamson RH, Curry FRE, Tarbell JM. Sphingosine-1-phosphate protects endothelial glycocalyx by inhibiting syndecan-1 shedding. Am J Physiol Heart Circ Physiol 2014;306(3):H363-H372.

285. Moon MH, Jeong JK, Lee YJ, Seol JW, Park SY. Sphingosine-1-phosphate inhibits interleukin-1β-induced inflammation in human articular chondrocytes. Int J Mol Med 2012;30(6):1451-1458.

286. Nielsen B, Rank F, López J, Balbin M, Vizoso F, Lund L, et al. Collagenase-3 expression in breast myofibroblasts as a molecular marker of transition of ductal carcinoma in situ lesions to invasive ductal carcinomas. Cancer Res 2001;61(19):7091-7100.

287. Desmoulière A, Chaponnier C, Gabbiani G. Tissue repair, contraction, and the myofibroblast. Wound Repair Regen 2005;13(1):7-12.

288. Hinz B, Mastrangelo D, Iselin CE, Chaponnier C, Gabbiani G. Mechanical tension controls granulation tissue contractile activity and myofibroblast differentiation. Am J Pathol 2001;159(3):1009-1020.

289. Valenzuela-Silva C, Tuero-Iglesias Á, García-Iglesias E, González-Díaz O, Del Río-Martín A, Yera Alos I, et al. Granulation response and partial wound closure predict healing in clinical trials on advanced diabetes foot ulcers treated with recombinant human epidermal growth factor. Diabetes Care 2013;36(2):210-215.

290. Carlson-Banning K, Chou A, Liu Z, Hamill R, Song Y, Zechiedrich L, et al. Toward repurposing ciclopirox as an antibiotic against drug-resistant Acinetobacter baumannii, Escherichia coli, and Klebsiella pneumoniae. PloS one. 2013;8(7):e69646.

291. Fleming J, Glass T, Lackie S, Wojciak J. A novel approach for measuring sphingosine-1-phosphate and lysophosphatidic acid binding to carrier proteins using monoclonal antibodies and the kinetic exclusion assay. The Journal of Lipid Research. 2016;57(9):1737-1747.

292. Wacker B, Scott E, Kaneda M, Alford S, Elbert D. Delivery of sphingosine 1-phosphate from poly(ethylene glycol) hydrogel. Biomacromolecules. 2006;7(4):1335-1343.

293. Murata N, Sato K, Kon J, Tomura H, Yanagita M, Kuwabara A, et al. Interaction of sphingosine 1-phosphate with plasma components, including lipoproteins, regulates the lipid receptor-mediated actions. Biochem Journal. 2000;352(2):809-815.

294. Fournie P, Galiacy S, Ranty M, Rico-Lattes I, Malecaze F, Quintyn JC, et al. Sphingosine-1 phosphate prevents ethanol-induced corneal epithelial apoptosis. Indian J Ophthalmol. 2012;60(2):115-118.

295. Kang K, Allen P, Bischoff J. Bioengineered human vascular networks transplanted into secondary mice reconnect with the host vasculature and re-establish perfusion. Blood. 2011;118(25):6718-6721.

296. Duvall C, Taylor W, Weiss D, Guldberg RE. Quantitative microcomputed tomography analysis of collateral vessel development after ischemic injury. Am Heart Circ Physiol. 2004;287(1):H302-H310.

297. Badea C, Panetta D. High-Resolution CT for Small Animal Imaging Resesarch. In: Brahme, A.; Bundiger TF, editor. Comprehensive Biomedical Physics. Amsterdam, Netherlands: Newnes; 2014. p. 234-35.

298. Cicco G, Giorgino F, Cicco S. Wound healing in diabetes: hemorheological and microcirculatory aspects. Adv Exp Med Biol 2011;701:263-269.

299. Nunan R, Harding KG, Martin P. Clinical challenges of chronic wounds: searching for an optimal animal model to recapitulate their complexity. Disease models & mechanisms. 2014;7(11):1205-1213.

300. Jeffcoate WJ, Harding KG. Diabetic foot ulcers. Lancet (London, England). 2003;361(9368):1545-1551.

301. Gould LJ, Leong M, Sonstein J, Wilson S. Optimization and validation of an ischemic wound model. Wound Repair Regen 2005;13(6):576-582.

302. Richard J, Sotto A, Lavigne J. New insights in diabetic foot infection. World journal of diabetes. 2011;2(2):24-32.

303. Becker DL, Thrasivoulou C, Phillips ARJ. Connexins in wound healing; perspectives in diabetic patients. Biochim Biophys Acta. 2012;1818(8):2068-2075.

304. Kopecki Z, Arkell R, Powell BC, Cowin AJ. Flightless I regulates hemidesmosome formation and integrin-mediated cellular adhesion and migration during wound repair. J Invest Dermatol. 2009;129(8):2031-2045.

305. Auerbach R. An overview of current angiogenesis assays: Choice of assay, precautions in interpretation, future requirements and directions In: Staton CA, Lewis C, Bicknel R, editor. *Angiogenesis Assays: A critical appraisal of current techniques*. John Wiley & Sons. 2006; p. 365.

306. Andrade SP, Ferreira MAND, Fan TP. Implantation of sponges and polymers. In: Staton CA, Lewis C, Bicknel R, editor. *Angiogenesis Assays: A critical appraisal of current techniques*. John Wiley & Sons. 2006; p.167-182.

307. Woessner JF Jr, Boucek RJ. Enzyme activities of rat connective tissue obtained from subcutaneously implanted polyvinyl sponge. J Biol Chem.1959; 234:3296–3300

308. Vogel HB, Berry RG. Chorioallantoic membrane heterotransplantation of human brain tumors. Int. J. Cancer.1975;15:401–408.

309. Gimbrone MA, Cotran RS, Leapman SB, Folkman J.Tumor growth and neovascularization: an experimental model using the rabbit cornea. J. Natl. Cancer Inst. 1974;52:413-427.

310. Algire GH. An adaptation of the transparent chamber technique to the mouse. J. Natl. Cancer Inst.1943;4:1–11.

311. Isogai S., Horiguchi M., Weinstein BM.The vascular anatomy of the developing zebrafish: an atlas of embryonic and early larval development. Dev. Biol. 2001; 230:278–301.

312. Hoffman RM. Green fluorescent protein imaging of tumour growth, metastasis, and angiogenesis in mouse models. Lancet Oncol. 2002; 3:546–556.

313. International Diabetes Federation. Diabetes Atlas, 6th edition, Brussels, Belgium: International Diabetes Federation, 2013.

314. King AJF. The use of animal models in diabetes research. Br J Pharmacol. 2012; 166:877-894.

315. Schäfer S, Steioff K, Linz W, Bleich M, Busch AE, Löhn M. Chronic vasopeptidase inhibition normalizes diabetic endothelial dysfunction. Eur J Pharmacol. 2004; 484(2-3):361-2.

316. Belin de Chantemèle EJ, Vessières E, Guihot AL, Toutain B, Maquignau M, Loufrani L, Henrion D. Type 2 diabetes severely impairs structural and functional adaptation of rat resistance arteries to chronic changes in blood flow. Cardiovasc Res. 2009; 81(4):788-96.

317. Lu X, Guo X, Karathanasis SK, Zimmerman KM, Onyia JE, Peterson RG, Kassab GS. Rosiglitazone reverses endothelial dysfunction but not remodeling of femoral artery in Zucker diabetic fatty rats. Cardiovasc Diabetol. 2010;19:9-19.

318. Scalia R, Gong Y, Berzins B, Zhao LJ, Sharma K. Hyperglycemia Is a Major Determinant of Albumin Permeability in Diabetic Microcirculation. Diabetes. 2007; 56: 1842-1849.

319. Kajiwara H, Luo Z, Belanger AJ, Urabe A, Vincent KA, Akita GY, Cheng SH et al. A hypoxic inducible factor-1 alpha hybrid enhances collateral development and reduces vascular leakage in diabetic rats. J Gene Med. 2009; 11:390-400.

320. Castracane VD, Henson MC. The Obese (ob/ob) Mouse and the Discovery of Leptin. In: Castracane VD, Henson MC, editor. *Leptin*. Springer US. p. 2007 1-9

321. Hummel KP, Dickie MM, Coleman DL. Diabetes, a new mutation in the mouse. Science. 1966; 153:1127–1128.
322. Kondo K, Nozawa K, Tomita T, Ezaki K. Inbred strains resulting from Japanese mice. Bulletin of the Experimental Animals 1957. 6:107–112.

323. Iwatsuka H, Shino A, Suzuoki Z. General survey of diabetic features of yellow KK mice. Endocrinol Jpn. 1970;17:23-35.

324. Melez KA, Harrison LC, Gilliam JN, Steinberg AD. Diabetes is associated with autoimmunity in the New Zealand obese (NZO) mouse. Diabetes.1980; 29:835-40.

325. Leiter EH, Reifsnyder PC. Differential levels of diabetogenic stress in two new mouse models of obesity and type 2 diabetes. *Diabetes*. 2004; 53:S4-11.

326. Allan MF, Eisen EJ, Pomp D.The M16 mouse: an outbred animal model of early onset polygenic obesity and diabesity. Obes Res. 2004;12:1397-1407.

327. Takahashi A, Tabuchi M, Suzuki W, Iizuka S, Nagata M, Ikeya Y, Takeda S et al. Insulin resistance and low sympathetic nerve activity in the Tsumura Suzuki obese diabetic mouse: a new model of spontaneous type 2 diabetes mellitus and obesity. Metabolism. 2006; 55:1664-1669.

328. Phillips MS, Liu Q, Hammond HA, Dugan V, Hey PJ, Caskey CJ et al. Leptin receptor missense mutation in the fatty Zucker rat. Nat Genet. 1996; 13:18–19.

329. Kawano K, Hirashima T, Mori S, Natori T. OLETF (Otsuka Long-Evans Tokushima Fatty) rat: a new NIDDM rat strain. Diabetes Res Clin Pract. 1994; 24:S317-20.

330. Russell JC, Koeslag DG. Jcr:LA-corpulent Rat: A Strain with Spontaneous Vascular and Myocardial Disease. ILAR J. 1990; 32: 27-32.

331. Michaelis OE, Hansen CT. The Spontaneous Hypertensive/NIH-corpulent Rat: A New Rodent Model for the Study of Non-insulin-dependent Diabetes Mellitus and Its Complications. ILAR J.1990; 32:19-22

332. Phillips RW, Panepinto LM, Spangler R, Westmoreland N. Yucatan miniature swine as a model for the study of human diabetes mellitus. Diabetes. 1982; 31:30–36.

333. Shafrir E, Ziv E, Kalman R. Nutritionally induced diabetes in desert rodents as models of type 2 diabetes: Acomys cahirinus (spiny mice) and Psammomys obesus (desert gerbil). ILAR J. 2006; 47:212-24.

334. Surwit RS, Kuhn CM, Cochrane C, McCubbin JA, Feinglos MN. Diet-Induced Type II Diabetes in C57BL/6J Mice. Diabetes. 1988; 37:1163-1167.

335. Frenkel G, Kraicer PF, Shani J. Diabetes in the sand-rat: diabetogenesis, responses to mannoheptulose and atriplex ash. Diabetologia. 1972;8:313-318.

336. Wise PH, Weir BJ, Hime JM, Forrest E. The diabetic syndrome in the tuco-tuco (Ctenomys talarum). Diabetologia. 1972;8:165-172.

337. Bremer AA, Stanhope KL, Graham JL, Cummings BP, Wang W, Saville BR, Havel PJ. Fructose-fed rhesus monkeys: A nonhuman primate model of insulin resistance, metabolic syndrome, and type 2 diabetes. Clin Transl Sci. 2011;4:243-52.

338. Karasawa H, Takaishi K, Kumagae Y. Obesity-induced diabetes in mouse strains treated with gold thioglucose: a novel animal model for studying β-cell dysfunction. Obesity (Silver Spring). 2011;19:514-521.

339. Lee MS, Song KD, Yang HJ, Solis CD, Kim SH, Lee WK. Development of a type II diabetic mellitus animal model using Micropig®. Lab Anim Res. 2012; 28:205-208.

340. Rohner-Jeanrenaud F, Jeanrenaud B. Consequences of Ventromedial Hypothalamic Lesions upon Insulin and Glucagon Secretion by Subsequently Isolated Perfused Pancreases in the Rat. J Clin Invest. 1980; 65(4): 902–910.

341. Kulkarni RN, Brüning JC, Winnay JN, Postic C, Magnuson MA, Kahn CR. Tissue-specific knockout of the insulin receptor in pancreatic beta cells creates an insulin secretory defect similar to that in type 2 diabetes. Cell. 1999;96:329-339.

342. Joseph JW, Koshkin V, Zhang CY, Wang J, Lowell BB, Chan CB, Wheeler MB. Uncoupling protein 2 knockout mice have enhanced insulin secretory capacity after a high-fat diet. Diabetes. 2002;51:3211-3219.

343. Yoshioka M, Kayo T, Ikeda T, Koizumi A. A novel locus, *Mody4*, distal to D7Mit189 on chromosome 7 determines early-onset NIDDM in nonobese C57BL/6 (Akita) mutant mice. Diabetes. 1997;46:887–894.

344. Mathews CE, Bagley R, Leiter EH. ALS/Lt: a new type 2 diabetes mouse model associated with low free radical scavenging potential. Diabetes. 2004; 53:S125-129.

345. Weksler-Zangen S, Yagil C, Zangen DH, Ornoy A, Jacob HJ, Yagil Y. The newly inbred cohen diabetic rat: a nonobese normolipidemic genetic model of diet-induced type 2 diabetes expressing sex differences. Diabetes. 2001;50:2521-2529.

346. Goto Y, Suzuki KI, Sasaki M, Ono T, Abe S. GK rat as a model of non-obese, non-insulin dependent diabetes: selective breeding over 35 generations. In: Shafrir E, Reynold AE, editor. *Lessons from Animal Diabetes II*. London: Libbey; 1988. p.301–303

347. M. Shinohara, T. Masuyama, T. Shoda et al., “A new spontaneously diabetic non-obese torii rat strain with severe ocular complications,” International Journal of Experimental Diabetes Research. 2000;1:89–100.

348. Rerup CC. Dugs producing diabetes through damage of the insulin secreting cells. Pharmacol Rev 1970; 22: 485-518.

349. Srinivasan K, Viswanad B, Asrat L, Kaul CL, Ramarao P. Combination of high-fat diet-fed and low-dose streptozotocin-treated rat: a model for type 2 diabetes and pharmacological screening. Pharmacol Res. 2005;52:313-320.

350. Ibanez-Camacho R, Meckes-Lozaya M, Mellado-Campos V. The hypoglucemic effect of Opuntia streptocanthe studied in different animal experimental models. J Ethnopharmacol 1983; 7:175-181.

351.Tamemoto H, Kadowaki T, Tobe K, Yagi T, Sakura H, Hayakawa T, Terauchi Y, Ueki K, Kaburagi Y, Satoh S. Insulin resistance and growth retardation in mice lacking insulin receptor substrate-1. Nature. 1994; 372:182–186.

352. Withers DJ, Gutierrez JS, Towery H, Burks DJ, Ren JM, Previs S, Zhang Y, Bernal D, Pons S, Shulman GI, et al. Disruption of IRS-2 causes type 2 diabetes in mice. Nature. 1998; 391:900–904.

353. Zisman A, Peroni OD, Abel ED, Michael MD, Mauvais-Jarvis F, Lowell BB, Wojtaszewski JF, Hirshman MF, Virkamaki A, Goodyear LJ, et al. Targeted disruption of the glucose transporter 4 selectively in muscle causes insulin resistance and glucose intolerance. Nat Med. 2000; 6:924–928.

354. Hevener AL, He W, Barak Y, Le J, Bandyopadhyay G, Olson P, Wilkes J, Evans RM, Olefsky J. Muscle-specific Pparg deletion causes insulin resistance. Nat Med. 2003; 9:1491–1497.

355. Guillam MT, Hümmler E, Schaerer E, Yeh JI, Birnbaum MJ, Beermann F, Schmidt A, Dériaz N, Thorens B. Early diabetes and abnormal postnatal pancreatic islet development in mice lacking Glut-2. Nat Genet. 1997; 17:327–330.

356. Araki E, Lipes MA, Patti ME, Brüning JC, Haag B, Johnson RS, Kahn CR. Alternative pathway of insulin signalling in mice with targeted disruption of the IRS-1 gene. Nature. 1994; 372:186–190.

357. Zhang YL, Tan XH, Xiao MF, Li H, Mao YQ, Yang X, Tan HR. Establishment of liver specific glucokinase gene knockout mice: a new animal model for screening anti-diabetic drugs. Acta Pharmacol Sin. 2004; 25:1659-1665.

358. Fox N, Schrementi J, Nishi M, Ohagi S, Chan SJ, Heisserman JA, Westermark GT, Leckström A, Westermark P, Steiner DF. Human islet amyloid polypeptide transgenic mice as a model of non-insulin-dependent diabetes mellitus (NIDDM). FEBS Lett.1993. 323:40-44.

359. Ahn ST and Mustoe TA: Effects of ischemia on ulcer wound healing: a new model in the rabbit ear. Ann Plast Surg. 1990; 24: 17.

360. Kim I, Mogford JE, Chao JD, and Mustoe TA: Wound epithelialization deficits in the transforming growth factor-alpha knockout mouse. Wound Repair Regen. 2001; 9: 386.

361. Falanga V, Schrayer D, Cha J, Butmarc J, Carson P, Roberts AB, and Kim SJ: Full-thickness wounding of the mouse tail as a model for delayed wound healing: accelerated wound closure in Smad3 knock-out mice. Wound Repair Regen. 2004; 12: 320.

362. Galiano RD, Zhao LL, Clemmons DR, Roth SI, Lin X, and Mustoe TA: Interaction between the insulinlike growth factor family and the integrin receptor family in tissue repair processes. Evidence in a rabbit ear dermal ulcer model. J Clin Invest. 1996; 98: 2462.

363. Carlson MA, Longaker MT, and Thompson JS: Wound splinting regulates granulation tissue survival. J Surg Res. 2003; 110: 304.

364. Yu F, Opalenik SR, Samson PC, Schaffer DK, Wikswo JP, and Davidson JM: A novel PDMS device to prevent contraction in rodent excisional wounds. Wound Repair Regen. 2010; 18: A43.

365. Aarabi S, Bhatt KA, Shi Y, Paterno J, Chang EI, Loh SA, Holmes JW, Longaker MT, Yee H, and Gurtner GC: Mechanical load initiates hypertrophic scar formation through decreased cellular apoptosis. FASEB J. 2007; 21: 3250.

366. Sorg H, Krueger C, and Vollmar B: Intravital insights in skin wound healing using the mouse dorsal skin fold chamber. J Anat. 2007; 211:810.

367. Apelqvist J, Agardh CD. The association between clinical risk factors and outcome of diabeticfoot ulcers. Diabetes Res Clin Pract. 1992; 1843- 1853.

368. Krock BL, Skuli N, Simon CM. Hypoxia-Induced Angiogenesis. Genes Cancer. 2011; 2:1117–1133.

369. Comoglio, P. & Boccaccio, C. The HGF receptor family: unconventional signal transducers for invasive cell growth. Genes Cells.1996; 1;347-354.

370. Ding S, Merkulova-Rainon T, Han Z, Tobelem G. HGF receptor up-regulation contributes to the angiogenic phenotype of human endothelial cells and promotes angiogenesis in vitro. Blood. 2003; 101: 4816-4822.

371. Rosen EM, Grant DS, Kleinman HK, Goldberg ID, Bhargava MM, Nickoloff BJ, Kinsella JL, Polverini P. Scatter Factor (Hepatocyte Growth-Factor) Is a Potent Angiogenesis Factor in-Vivo. Sym Soc Exp Biol. 1993;47:227–234

372. Morales-Ruiz M, Fulton D, Sowa G, Languino LR, Fujio Y, Walsh K, Sessa WC.Vascular Endothelial Growth Factor–Stimulated Actin Reorganization and Migration of Endothelial Cells Is Regulated via the Serine/Threonine Kinase Akt. Circ Res. 2000;86:892-896.

373. Murohara T, Witzenbichler B, Spyridopoulos I, Asahara T, Ding B, Sullivan A, Losordo DW, Isner JM.. Role of endothelial nitric oxide synthase in endothelial cell migration. Arterioscler Thromb Vasc Biol. 1999; 19:1156-1161.

374. Auerbach R., Morrissey LW, Sidky YA. Gradients in tumour growth. Nature. 1978; 274:697–699.

375. Kennedy DF, Cliff WJ. A systematic study of wound contraction in mammalian skin. Pathology. 1979; 11:207-222.

376. Ansell DM, Campbell L, Thomason HA, Brass A, Hardman MJ. A statistical analysis of murine incisional and excisional acute wound models. Wound Repair Regen. 2014; 22: 281-287.

377. Kwan RL, Zheng YP, Cheing GL. Clin Biomech (Bristol, Avon). 2010; 25: 601-605.

378. Achora S, Muliira JK. Thanka AN. Strategies to promote healing of split thickness skin grafts: an integrative review. J Wound Ostomy Continence Nurs. 2014; 41: 335-339.

379. Cullen B, Ivins N. Promogran & Promogran Prisma. Wounds International. 2010; 1: 1-6

380. 510(k) Summary [Internet]. [updated 2011; cited 31 March 2017]. Available from: https://www.accessdata.fda.gov/cdrh_docs/pdf11/K111578.pdf

381. Blume P, Driver VR, Tallis AJ, Kirsner RS, Kroeker R, Payne WG, Wali S, Marston W et al. Formulated collagen gel accelerates healing rate immediately after application in patients with diabetic neuropathic foot ulcers. Wound Repair Regen. 2011;19: 302-308.

382. Chang J, DeLillo Jr N, Khan M, Nacinovich Jr MR. Review of Small Intestine Submucosa Extracellular Matrix Technology in Multiple Difficult-to-Treat Wound Types. Wounds. 2013; 25:113-120.

383. GRAFTJACKET® Regenerative Tissue Matrix [Internet]. [updated 2017; cited 31 March 2017]. Available from: http://www.acelity.com/products/graftjacket-regenerative-tissue-matrix#tab_1

384. INTEGRA. Limit uncertainty. [Internet]. [updated 2017; cited 31 March 2017]. Available from: http://www.ilstraining.com/default.html

385. Lobmann R, Zemlin C, Motzkau M, Reschke K, Lehnert, H. Expression of matrix metalloproteinases and growth factors in diabetic foot wounds treated with a protease absorbent dressing. J Diabetes Complications. 2006; 20: 329-335.

386. Cullen B, Watt PW, Lundqvist C, Silcock D, Schmidt RJ, Bogan D, Light ND. The role of oxidised regenerated cellulose/collagen in chronic wound repair and its potential mechanism of action. Int J Biochem Cell Biol. 2002; 34:1544-1556.

387. Holmes C, Wrobel JS, Maceachern MP, Boles BR. Collagen-based wound dressings for the treatment of diabetes-related foot ulcers: a systematic review. Diabetes, metabolic syndrome and obesity : targets and therapy. 2013; 6: 17-29.

388. Hart CE, Loewen-Rodriguez A, Lessem J. Dermagraft: Use in the Treatment of Chronic Wounds. Adv Wound Care (New Rochelle). 2012;1:138-141.

389. Zaulyanov L, Kirsner RS. A review of a bi-layered living cell treatment (Apligraf ®) in the treatment of venous leg ulcers and diabetic foot ulcers. Clin Interv Aging. 2007; 2: 93–98.

390. Eisenbud D, Ngan F. Huang BS; Luke S, Silberklang M. Skin Substitutes and Wound Healing: Current Status and Challenges. Wounds. 2004;16:1-8

391. Summary of safety and effectiveness data [Internet]. [updated 2001; cited 1 June 2017]. Available from: https://www.accessdata.fda.gov/cdrh_docs/pdf/P010016b.pdf

392. Ortega-Zilic N, Hunziker T, Läuchli S, Mayer DO, Huber C, Baumann Conzett K, Sippel K et al. EpiDex® Swiss field trial 2004-2008. Dermatology. 2010; 221:365-372.

393. Murthy R, DeLong L, Chen S. Critical appraisal of pharmacoeconomic studies. In: Williams H, Bigby M, Diepgen T, Herxheimer A, Naldi L, Rzany B, editor. *Evidence-Based Dermatology.* USA: John Wiley & Sons; 2011. p.744.

394. Veves A, Sheehan P, Pham H. A randomized, controlled trial of Promogran (a collagen/oxidized regenerated cellulose dressing) vs standard treatment in the management of diabetic foot ulcers. Arch Surg. 2002; 137: 822-827.

395. Mansbridge J, Liu K, Patch R, Symons K, Pinney E. Three-dimensional fibroblast culture implant for the treatment of diabetic foot ulcers: metabolic activity and therapeutic range. Tissue Eng. 1998; 4: 403-414.

396. Debels H, Hamdi M, Abberton K, Morrison W. Dermal matrices and bioengineered skin substitutes: a critical review of current options. Plastic and reconstructive surgery. 2005; 3: e284.

397. 510(k) Summary Product Name: V.A.C. Therapy system [Internet]. [updated 2006; cited 1 June 2017]. Available from: https://www.accessdata.fda.gov/cdrh_docs/pdf6/K062227.pdf

398. Borgquist O, Ingemansson R, Malmsjö M. The influence of low and high pressure levels during negative-pressure wound therapy on wound contraction and fluid evacuation. Plast Reconstr Surg. 2011; 127: 551-559.

399. Mrozikiewicz-Rakowska B, Bucior E, Kania J, Nowak A, Chojnowski M, Krzymien J. Modern Alternative or First-line Treatment: How to Safely Use Negative Pressure Wound Therapy in Diabetic Foot Syndrome? Negative Pressure Wound Therapy Journal. 2014; 2:21-25.

400. Borgquist O, Anesäter E, Hedström E, Lee CK, Ingemansson R, Malmsjö M. Measurements of wound edge microvascular blood flow during negative pressure wound therapy using thermodiffusion and transcutaneous and invasive laser Doppler velocimetry. Wound Repair Regen. 2011; 19: 727-733.

401. Glass GE, Murphy GF, Esmaeili A, Lai LM, Nanchahal J. Systematic review of molecular mechanism of action of negative-pressure wound therapy. Br J Surg. 2014; 101:1627-1636.

402. Yang F, Hu D, Bai XJ, Zhang K, Li RJ, Xue CC. The influence of oxygen partial pressure change and vascularization of rabbit wound through negative pressure wound therapy. Zhonghua Wai Ke Za Zhi. 2012; 50: 650-654.

403. Li XQ, Hu DH, Liu Y, Wang YJ, Han F, Hu XL, Li N, Zhang Y, Bai XZ. Influence of negative pressure wound therapy on the angiogenesis of wounds in diabetic rats. Zhonghua Shao Shang Za Zhi. 2013; 29: 442-447.

404. Armstrong DG, Lavery LA, Diabetic Foot Study Consortium. Negative pressure wound therapy after partial diabetic foot amputation: a multicentre, randomised controlled trial. Lancet. 2005; 366: 1704-1710.

405. Kanakaris NK, Thanasas C, Keramaris N, Kontakis G, Granick MS, Giannoudis PV. The efficacy of negative pressure wound therapy in the management of lower extremity trauma: review of clinical evidence. Injury. 2007; 38: S9-18.

406. Mendonca DA, Cosker T, Makwana NK. Vacuum-assisted closure to aid wound healing in foot and ankle surgery. Foot & ankle international. 2005; 26: 761-766.

407. Clare MP, Fitzgibbons TC, McMullen ST, Stice RC, Hayes DF, Henkel L. Experience with the vacuum assisted closure negative pressure technique in the treatment of non-healing diabetic and dysvascular wounds. Foot & ankle international. 2002; 23: 896-901.

408. Health Quality Ontario. Negative pressure wound therapy: an evidence-based analysis. Ontario health technology assessment series. 2006; 6: 1-38.

409. MIST Therapy System Premarket Notification (510(k)) Summary [Internet]. [updated 2005; cited 1 June 2017]. Available from: https://www.accessdata.fda.gov/cdrh_docs/pdf5/K050129.pdf

410. Doan N, Reher P, Meghji S, Harris M. In vitro effects of therapeutic ultrasound on cell proliferation, protein synthesis, and cytokine production by human fibroblasts, osteoblasts, and monocytes. J Oral Maxillofac Surg. 1999; 57: 409-419.

411. Lai J, Pittelkow MR. Physiological effects of ultrasound mist on fibroblasts. Int J Dermatol. 2007; 46: 587-593.

412. Thawer HA, Houghton PE. Effects of ultrasound delivered through a mist of saline to wounds in mice with diabetes mellitus. J Wound Care. 2004; 13: 171-176.

413. Game F, Hinchliffe R, Apelqvist J. A systematic review of interventions to enhance the healing of chronic ulcers of the foot in diabetes. Diabetes Metab Res Rev. 2012; 28: 119-141.

414. Katsilambros N, Dounis E, Makrilakis K, Tentolouris N, Tsapogas P. Methods of ulcer healing. In: Katsilambros N, Dounis E, Makrilakis K, Tentolouris N, Tsapogas P, editor. *Atlas of the Diabetic Foot*. UK, West Sussex: John Wiley & Sons; 2010. p. 200-223.

415. Cianci P, Hunt T. Adjunctive hyperbaric oxygen therapy in the treatment of the diabetic foot. In: Bowker JH, Pfeifer MA, editor. *Levin and O'Neal's The Diabetic Foot*. Philadelphia: Elsevier Health Sciences; 2007. p. 339-359.

416. Thom SR. Hyperbaric oxygen: its mechanisms and efficacy. Plast Reconstr Surg. 2011; 127: 131S-141S.

417. Zhang Q, Chang Q, Cox RA, Gong X, Gould LJ. Hyperbaric oxygen attenuates apoptosis and decreases inflammation in an ischemic wound model. J Invest Dermatol. 2008; 128: 2102-2112.

418. Thom SR. Oxidative stress is fundamental to hyperbaric oxygen therapy. J Appl Physiol. 2009; 106: 988-995.

419. Margolis DJ, Gupta J, Hoffstad O, Papdopoulos M, Glick HA, Thom SR, Mitra N. Lack of effectiveness of hyperbaric oxygen therapy for the treatment of diabetic foot ulcer and the prevention of amputation: a cohort study. Diabetes Care. 2013; 36: 1961-1966.

420. Marsolais D, Rosen H. Chemical modulators of sphingosine-1-phosphate receptors as barrier oriented therapeutic molecules. Drug Discovery. 2009; 8: 297-307.

421. Omi H, Okayama N, Shimizu M, Okouchi M, Ito S, Fukutomi T, Itoh M. Participation of high glucose concentrations in neutrophil adhesion and surface expression of adhesion molecules on cultured human endothelial cells: effect of antidiabetic medicines. J Diabetes Complications. 2002; 16: 201-208.

422. Capaldo CT, Nusrat A. Cytokine regulation of tight junctions. Biochim Biophys Acta. 2009;1788: 864-871.